ISSN 0911-5730
UVSOR-16
April 1989

# UVSOR
# ACTIVITY REPORT
# 1988

**Ultraviolet Synchrotron Orbital Radiation Facility**
**Institute for Molecular Science**

# CONTENTS

## PREFACE

## LIGHT SOURCE

## BEAMLINES & EQUIPMENTS

## RESEARCH ACTIVITIES

## APPENDIX

## Preface

It is a great pleasure for me to have recently celebrated the fifth anniversary of the synchrotron radiation of the UVSOR Facility. During the last year, our light source has been quite regularly operated with an electron energy of 750 MeV. and the stored ring current has recently been increased from 100 mA to 120 mA. In UVSOR we now have four beam lines for in-house staff and ten beam lines available to general users for molecular science and its related fields.

In the following articles, the present situation of the light source is briefly described by T. Kasuga, and an outline of the beam lines available for joint studies is presented by M. Watanabe. The beam lines belonging to the in-house staff have been used as follows: photochemistry and fluorescence studies of molecules and molecular clusters (BL2A; Shobatake Group); photoionization/photoelectron studies of molecular clusters (BL2B2; Kimura Group); photoelectron photo-ion coincidence studies of ion-molecule reaction (BL3B; Koyano Group); angular-resolved photoelectron studies of organic solids (BL8B2; Inokuchi Group).

In the 1988 fiscal year, various studies have been performed under the following; three Special-Project Programs, fifteen Cooperative-Research Programs, and eighty Use-of-Facility Programs. Two symposia of different kinds have been held; one a users' meeting, the other a workshop on synchrotron light sources.

I would like to express my thanks to all the UVSOR staff for their great efforts and contributions to the UVSOR Facility. I would also like to thank many outside users for their various kinds of cooperation.

February 1989

Katsumi Kimura
Director of UVSOR

# LIGHT SOURCE

# OVERVIEW OF LIGHT SOURCE

Toshio KASUGA

The light source has been regularly used for the production of synchrotron radiation during 1988. The reliability of the accelerator system has been steadily improved for some years. A rate of unscheduled shutdown time is about 1 %. The operating schedule is unchanged in 1988; machine studies were carried out every monday and user's studies were from Tuesday through Friday. Electron beam was injected into the storage ring twice a day at 9:00 and 13:00 and the beam was dumped at 18:00.

The total operating time of the light source was 46 weeks in 1988. The usual initial current in the multi-bunch mode was 100 mA (120 mA from November ) and the beam lifetime was 3-3.5 h at that current. The single-bunch operation was performed at a rate of 1 week in 2 months. The initial current in the single-bunch mode was 10-13 mA and the normal impurity ( the electron number in non-assigned bucket/ the total electron number ) is less than $0.5 * 10^{-3}$. A total machine time of 3 weeks was allocated to the wiggler users, and the undulator in the straight section S 3 was regularly used through this year.

The beam quality in the light source has been observed and improved continuously. A passive damper for the longitudinal coupled-bunch instability was successfully tried. The bunch lengthening and widening in the single-bunch mode were observed. The longitudinal coupling impedance of the storage ring was estimated from the bunch lengthening measurement. Though the impedance is about twice as large as the designed value, it is not so large compared with existing storage rings. The beam current of the injector synchrotron was considerably improved with vertical steering coils which correct the injection orbit around the inflector and with a sextuple magnet which corrects the chromaticity.

The design parameters with achieved ones are tabulated in Table I.

## Table I Main Parameters of UVSOR

| | Designed | | Achieved | |
|---|---|---|---|---|
| **Linac** | | | | |
| Energy | 15 | MeV | | |
| Frequency | 2.856 | GHz | | |
| **Synchrotron** | | | | |
| Energy | 600 | MeV | 600 | MeV |
| Current | 50 | mA | 32 | mA |
| Circumference | 26.6 | m | | |
| Periodicity | 6 | | | |
| Bending Radius | 1.8 | m | | |
| Tune ($Q_H$, $Q_V$) | (2.25, | 1.25) | | |
| Harmonic Number | 8 | | | |
| Radio Frequency | 90.1 | MHz | | |
| Repetition Rate | 1-3 | Hz | 2.5 | Hz |
| **Storage Ring** | | | | |
| Energy | 600 | MeV | 750 | MeV |
| | (max. | 750 MeV) | | |
| Critical Wavelength | 56.9 | A | | |
| Current | | | | |
| Multi-bunch mode | 500 | mA | 500 | mA |
| Single-bunch mode | | | 71 | mA |
| Lifetime | 1 | hr | 3 | hr |
| | (500 | mA) | (100 | mA) |
| Circumference | 53.2 | m | | |
| Periodicity | 4 | | | |
| Bending Radius | 2.2 | m | | |
| Bending Field | 0.91 | T | | |
| Tune ($Q_H$, $Q_V$) | (3.25, | 2.75) | | |
| Harmonic Number | 16 | | | |
| Radio Frequency | 90.1 | MHz | | |
| RF Voltage | 75 | kV | | |
| Radiation Damping Time | | | | |
| Horizontal | 45.4 | ms | | |
| Vertical | 40.9 | ms | | |
| Longitudinal | 19.5 | ms | | |
| Emittance | | | | |
| Horizontal | $8\pi \times 10^{-8}$ | m.rad* | $<16\pi \times 10^{-8}$ | m.rad |
| Vertical | $8\pi \times 10^{-9}$ | m.rad* | | |
| Beam Size (at the Center of Bending Section) | | | | |
| Horizontal ($2\sigma_H$) | 0.64 | mm* | | |
| Vertical ($2\sigma_V$) | 0.46 | mm | | |
| Bunch Length ($2\sigma$) | 0.17 | ns | 0.4 | ns |

*10% coupling is assumed.

# Suppression of Longitudinal Coupled-Bunch Instability by Decoupling Method

T. KASUGA, H. YONEHARA, M. HASUMOTO and T. KINOSHITA

A longitudinal coupled-bunch instability in the UVSOR electron storage ring for synchrotron radiation research had been observed when routine operation of the ring was started. It was successfully damped with a longitudinal active damping system, which consists of sixteen independent feedback loops; each of them corrects the energy deviation of any one of sixteen bunches individually. However, a fault in the system was found in the regular operation, i.e. the feedback loops have to be finely adjusted according to parameters such as the beam current, the position of the RF cavity tuner and the acceleration voltage. For example, the synchrotron frequency depends on the beam current, because the imaginary part of the cavity impedance at both synchrotron sidebands are different ( the Robinson effect ). A programmed control of the feedback parameters may offer a solution to this problem. While we were designing the improved feedback system, we also tested a passive damper. Two kinds of passive damping systems have been reported: Landau cavity or harmonic cavity method and a decoupling method. The former makes use of the Landau damping by the synchrotron frequency spread due to the strong nonlinearity which is introduced into the effective acceleration voltage around the stable phase angle. In the latter method, the phase oscillation of individual bunches are decoupled by a spread in their synchrotron frequencies, which is induced externally by modulation of the acceleration voltage. We adopted the latter because the required RF voltage is much smaller than that of the former. Moreover, the wideband acceleration gap for the active damping system was easy to convert into the cavity for the latter. The coupled-bunch instability was damped with this method when the beam current was less than 80mA and the growth rate of the instability is not very fast. The limitation of this method is not in the principle but in the maximum applicable voltage across the acceleration gap.

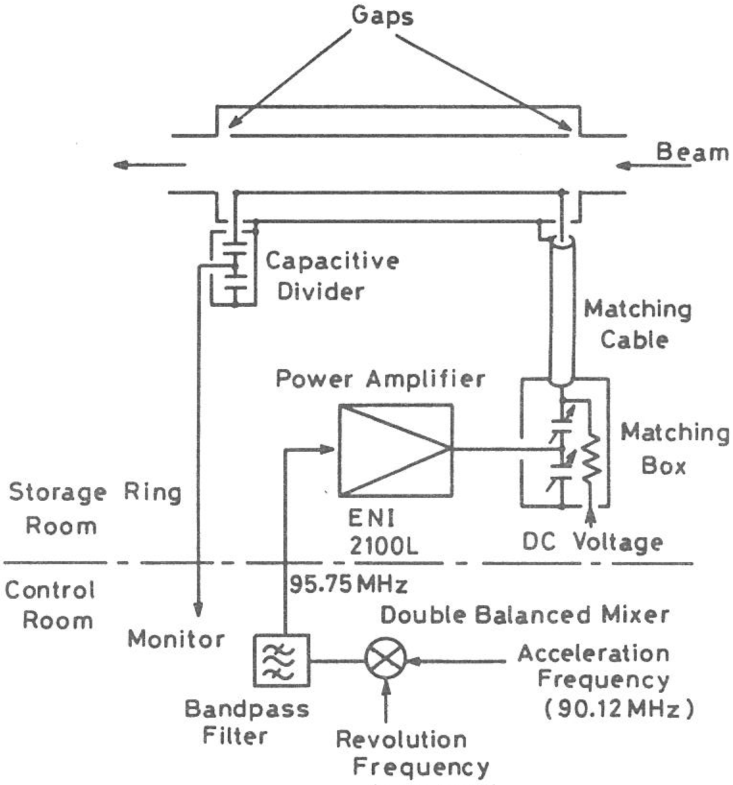

Fig. 1. A block diagram of the longitudinal passive damper.

# Bunch Lengthening in Single-Bunch Mode of UVSOR Storage Ring

Hiroto YONEHARA, Toshio KASUGA, Masami HASUMOTO
and Toshio KINOSHITA

Institute for Molecular Science, Myodaiji, Okazaki 444

The bunch lengthening and widening of the beam in the UVSOR ring were measured in the single-bunch mode. In the measurement certain thresholds were observed and the longitudinal coupling impedance of the ring was obtained with the threshold current.[1)]

The relation between the bunch lengthening and the longitudinal coupling impedance was theoretically studied[2-5)] and at low beam current the bunch lengthening due to the distortion of the acceleration potential by the beam pipe is described by

$$\left(\frac{\sigma_s}{\sigma_{s0}}\right)^3-\frac{\sigma_s}{\sigma_{s0}}-\frac{I\alpha e|Z/n|}{\sqrt{2\pi}\nu_{s0}^2E}\left(\frac{R}{\sigma_{s0}}\right)^3=0 \qquad (1)$$

where $\sigma_s$ is the standard deviation of the bunch length at the beam current of I, $\sigma_{s0}$ the natural bunch length, α the momentum compaction factor (0.026 for the UVSOR ring), e the electron charge, $|Z/n|$ the longitudinal coupling impedance, $\nu_{s0}$ the undisturbed phase oscillation wave number, E the beam energy and R the mean radius of the ring (16.9 m).[2)] Above a threshold current the bunch lengthening due to the microwave instability is described by Chao-Gareyte scaling law[6)]

$$\sigma_s^a \propto \frac{I\alpha}{\nu_{s0}^2E}. \qquad (2)$$

The synchrotron radiation emitted in a bending section was observed in order to measure the electron bunch length. The beam current dependence of the bunch length at the beam energy of 500, 600 and 750 MeV are shown in Fig. 1. We fitted the bunch length data using eq. (1) at low current and eq. (2) at high current to estimate a and $I_{th}$. The results are tabulated in Table I. We also measured the horizontal width of the beam to make sure of the change in the energy spread as shown in Fig. 2. The overall resolving power of the measurement is 0.8 in the same unit of the vertical scale in Fig. 2. The data in the case of the electron energy of 600 MeV shows that the width increses above the threshold current.

Table I. Bunch length and longitudinal coupling impedance.

| Beam Energy E (MeV) | 500 | | 600 | | 750 | |
|---|---|---|---|---|---|---|
| Undisturbed Phase Oscillation Wave Number $\nu_{s0}$ | $3.15\times10^{-3}$ | | $2.87\times10^{-3}$ | | $2.55\times10^{-3}$ | |
| Natural Bunch Length $\sigma_{s0}$ (ps) | 67.2 | | 88.4 | | 124.3 | |
| Estimated from | low current | threshold current | low current | threshold current | low current | threshold current |
| $\sigma_{s0}$ (ps) | 92.5 | 124 | 122.8 | 143 | 176.9 | |
| $\|Z/n\|$ (Ω) | 4.4 | 3.1 | 4.1 | 3.2 | 4.9 | |

We estimated the longitudinal coupling impedance of the UVSOR ring and it lies between 3.1 and 4.4 Ω. This value is about twice as large as the expected one of 2 Ω.[7)] The bunch widening is recognized above the threshold current in the case of the electron energy of 600 MeV, and it is consistent with the theory. However, it is difficult to discuss the widening quantitatively because of the insufficient resolution of the system.

The authors wish thank Y. Miyahara for his discussion of beam instabilities in electron storage rings. The assistance of K. Fukui in the use of the photon counting system is also acknowledged.

References

1) H. Yonehara, T. Kasuga, M. Hasumoto and T. Kinoshita: Jpn. J. Appl. Phys. 27 (1988) 2160.
2) A. Hofmann: CERN Intern. Rep. LEP-70/74 (1978).
3) A. W. Chao: AIP Conference Proceedings No. 105, Stanford, 1982(American Institute of Physics, New York, 1983) p.353.
4) F. J. Sacherer: IEEE Trans. Nucl. Sci. NS-24 (1977) 1393.
5) S. Hansen, H. G. Hereward, A. Hofmann, K. Hubner and S. Myers:IEEE Trans. Nucl. Sci. NS-22 (1975) 1381.
6) A. W. Chao and J. Gareyte: SLAC Intern. Rep. SPEAR-197, PEP-224(1976).
7) M. Watanabe, T. Kasuga, A. Uchida, O. Matsudo, M. Hasumoto, K. Sakai, H. Yamamoto, K. Takami, T. Katayama, K. Yoshida and M. Kihara: UVSOR Intern. Rep. UVSOR-9 (1982) 34.

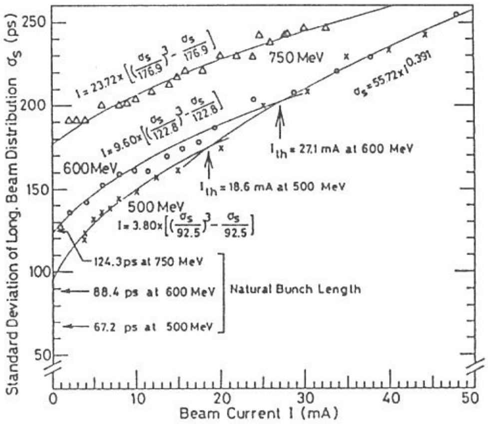

Fig. 1. The current dependence of the bunch length in the single-bunch operation. Triangles, circles and crosses show the measured values at the beam energy of 750, 600 and 500 MeV. Equations in this figure are obtained by fitting the data to eqs. (1) and (2).

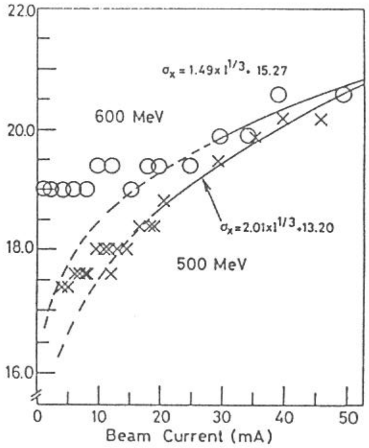

Fig. 2. The current dependence of the bunch width in the single-bunch operation. Circles and crosses show the widths at the beam energy of 600 and 500 MeV, respectively. Solid lines show the fittings above the thresholds (broken lines show the same fittings below the thresholds).

# Experimental Study of Free-Electron Laser at UVSOR Ring

Hiroto YONEHARA, Toshio KASUGA, Toshio KINOSHITA,
Masami HASUMOTO and Yoshikazu MIYAHARA*

Institute for Molecular Science, Myodaiji, Okazaki 444
* Institute for Solid State Physics, Univ. of Tokyo, Tokyo 106

Experimental studies of the Free-Electron Laser (FEL) are being carried out at the UVSOR, which is usually used as a synchrotron light source for the molecular science and its related fields. The wavelength within visible light, especially 488 nm, was chosen for simplicity of the optical system. In order to obtain the one-pass gain of 1 % at the electron beam current of 10 mA per one bunch, an undulator which has the period length of 74 mm, the number of the periods of 29 and the total length of 2.1 m was installed. The electron energy less than 270 MeV was necessary to achieve the wavelength of 488 nm with the undulator, however, the beam lifetime of 5 minutes at the energy was too short to align the optical system and to measure the one-pass gain. Therefore, the number of the periods was changed into 19 by arrangement of the magnet blocks. The beam lifetime increases to 50 minutes at the electron energy of 500 MeV. As the result, an expected one-pass gain is decreased to less than 0.1 %.

To measure the one-pass gain an Ar laser (10 mW) is used. The laser beam is enlarged and made pararrel beam by a laser beam expander (x3). The diameter of the laser beam is less than 2 mmϕ and about 2.5 mmϕ, at the inlet and outlet of the vacuum chamber for the FEL experiment. The size of the electron beam (standard deviation) is about 0.3 mmϕ at the center of the undulator. It is important to align the beams mutually in order to maximize the gain of the FEL. However, it is not esay to overlap these two beams at the undulator completely because these are very thin. An optical alignment system with TV cameras and beam splitters are installed to monitor the overlap as shown in Fig. 1. The profiles of the electron beam and the laser beam at the undulator are observed with the camera #2 with a telephoto lens. The images of these beams on the screens at the outlet of the vacuum chamber and at the point 6 m downstream from the undulator are monitored with the camera #1 and #3 respectively. The alignment of the two beams are tried with the monitoring system.

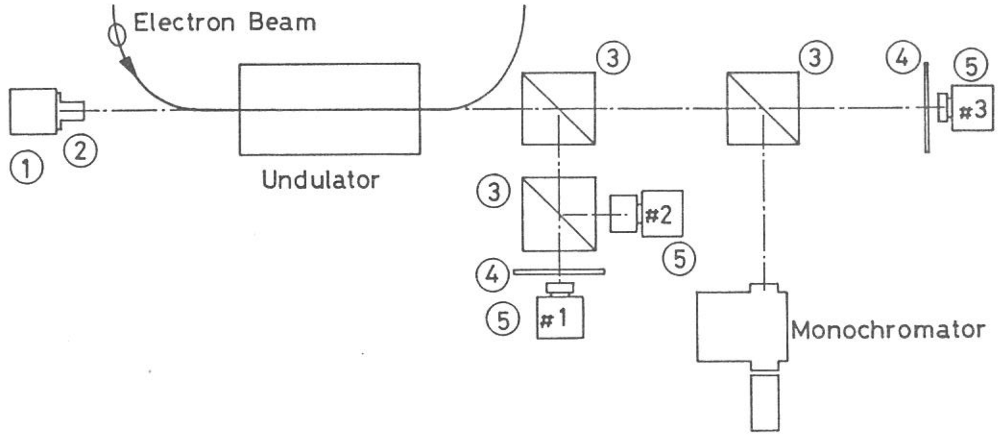

Fig. 1 Optical alignment system. 1) Ar laser, 2) laser beam expander, 3) beam splitter, 4) screen and 5) TV camera.

# BEAMLINES & EQUIPMENTS

# Overview of Beam Lines

M. Watanabe

UVSOR, Institute for Molecular Science, Myodaiji, Okazaki 444

There are fifteen beam lines at UVSOR Facility. They are listed in Table I. Four of them (BL2A, BL2B2, BL3B and BL8B2) are mainly used by in-house staffs of IMS, one of them (BL5B) is belonging to the Institute of Plasma Physics, Nagoya University and the others are opened to both inside and outside users of IMS. The front end of each beam line consists of a manual valve, a pneumatic valve, a fast closing valve and a beam shutter. It serves as the interface between the light source and monochromators. There exist four 1m Seya-Namioka, one 3m normal incidence, three plane grating, three grazing incidence and one double crystal monochromators for vacuum ultraviolet and soft x-ray, and one interferometer for far infrared. To these monochromators the equipments for absorption (reflection), fluorescence and photoelectron (photoion) measurements are attached. Standard DC detecting systems and counting systems are provided. Microcomputers are used individually. The date buses are both IEEE-488 and CAMAC. Two beam lines (BL3A1 and BL8A) are devoted to irradiation experiments of solid surfaces with and without gas atmosphere. Gas phase experiments have been carried out at BL2A, BL2B2 and BL3B. Solid state experiments have been made on BL6A1, BL6A2, BL7A, BL7B and BL8B2. At BL2B1 and BL8B1, both gas phase and solid state experiments were made. The lifetime studies of fluorescence were accomplished at BL1B, BL2A, BL3A1 and BL7B under single bunch operation for three weeks.

The numbers of joint studies are given in Appendix.

Table I Beam Lines at UVSOR

| Beam Line | Monochromator, Spectrometer | Wavelength Region | Acceptance Angle(mrad) | | Experiment |
|---|---|---|---|---|---|
| | | | Horiz. | Vert. | |
| BL1B | 1 m Seya-Namioka | 6500-300 A | 60 | 6 | Gas & Solid |
| BL2A | 1 m Seya-Namioka | 4000-300 A | 40 | 6 | Gas |
| BL2B1 | 2 m Grasshopper | 600-15 A | 10 | 1.7 | Gas & Solid |
| BL2B2 | 1 m Seya-Namioka | 2000-300 A | 20 | 6 | Gas |
| BL3A1 | None (Filter, Mirror) | | (U) 0.3 | 0.3 | Gas & Solid |
| BL3A2 | 2.2 m Constant Deviation Grazing Incidence | 1000-100 A | 10<br>(U) 0.3 | 4<br>0.3 | Gas & Solid |
| BL3B | 3 m Normal Incidence | 4000-300 A | 20 | 6 | Gas |
| BL5B | Plane Grating | 2000- 20 A | 10 | 2.2 | Calibration# |
| BL6A1 | Martin-Pupplet | 5 mm-50 μm | 80 | 60 | Solid |
| BL6A2 | Plane Grating | 6500-80 A | 10 | 6 | Solid |
| BL7A | Double Crystal | 15-8 A<br>15-2 A | 2<br>(W) 1 | 0.3<br>0.15 | Solid |
| BL7B | 1 m Seya-Namioka | 6500-300 A | 40 | 8 | Solid |
| BL8A | None (Filter) | | 25 | 8 | Irradiation, User's Instr. |
| BL8B1 | 2.2 m Rowland Circle Grazing Incidence | 440-20 A | 10 | 2 | Solid |
| BL8B2 | Plane Grating | 6500-80 A | 10 | 6 | Solid |

# : Institute of Plasma Physics, Nagoya University. U : with an undulator
W : with a wiggler.

## Molecular-beam photoionization apparatus on beamline BL2B2

Katsumi Kimura, Yohji Achiba,[a] and Haruo Shiromaru,[a]
Institute for Molecular Science, Okazaki 444, Japan

The final report on our beamline of molecular-beam photoionization experiments will soon be published in detail elsewhere [1]. In this paper we describe briefly the layout of our VUV beamline including a VUV monochromator and a molecular-beam photoionization apparatus. This beamline has been constructed for studying photoionization of molecular complexes such as van der Waals complexes or molecular clusters in supersonic jets by synchrotron radiation. Several SR studies have already been performed with this apparatus [2-3].

The layout of this beamline (BL2B2) is shown schematically in Fig. 1. The types of three pre-focusing mirrors ($M_1$, $M_2$, $M_3$) and a post-focusing mirror ($M_4$) are summarized in Table 1. The photon beam from the storage ring is separated by $M_1$ from the neighboring beamline (BL2B1), then reflected by $M_2$ to the upper, and further reflected by $M_3$ down toward the monochromator. The photon beam thus converged makes an image of 0.1mm (vertical) and 13mm (horizontal) on the monochromator entrance slit.

The 1-m Seya-Namioka monochromator used here covers the region 30-150 nm, its parameters being summarized in Table 2. A schematic drawing of the monochromator is shown also in Fig. 1. The monochromator maximum resolution ($\Delta E/E$) is $1\times10^{-4}$.

The molecular-beam apparatus consists of the beam source, the main chamber, and the beam catcher. The main chamber is separated from the beam source with a skimmer with a hole of 0.7 mm in diameter. A continuous molecular beam is ejected from a nozzle with a pin hole of 50-70 μm. The cooled molecular beam extracted through the skimmer crosses the SR beam. The stagnation pressure up to 10 atm is applicable.

Table 1. Pre-focusing and post-focusing mirrors.

| | | | |
|---|---|---|---|
| $M_1$ | Cylindrical (3064 cm, y) | $M_2$ | Spherical (2108 cm) |
| $M_3$ | Spherical (697 cm) | $M_4$ | Toroidal (179 cm, x; 6.5 cm, y) |

Table 2. Parameters of the 1-m Seya-Namioka monochromator.

| | |
|---|---|
| Incident beam | 10 mrad (vert.); 6 mrad (horiz.) |
| Wavelength region | 35-150 nm |
| Grating | 2400 lines/mm; Blaze 70 nm |
| Wavelength accuracy | <0.1 nm |
| Wavelength reproducibility | <0.005 nm |
| Resolution | 0.01 nm |
| Entrance slit | 20-240 μm (width); 2-16 mm (length) |
| Exit slit | 20-240 μm (width); 2-12 mm (length) |

---

[a] Present address: Department of Chemistry, Faculty of Science, Tokyo Metropolitan University, Setagaya, Tokyo 158.

**References** (1) K. Kimura, Y. Achiba, and H. Shiromaru, *Rev. Sci. Instrum.*, in press. (2) H. Shiromaru, Y. Achiba, K. Kimura and Y. T. Lee, *J. Phys. Chem.*, **91**, 17 (1987). (3) H. Shiromaru, H. Shinohara, N. Washida, H.-S. Yoo and K. Kimura, *Chem. Phys. Letters*, **141**, 7 (1987). (4) H. Shiromaru, H. Suzuki, H. Sato, S. Nagaoka, and K. Kimura, *J. Phys. Chem.*, in press.

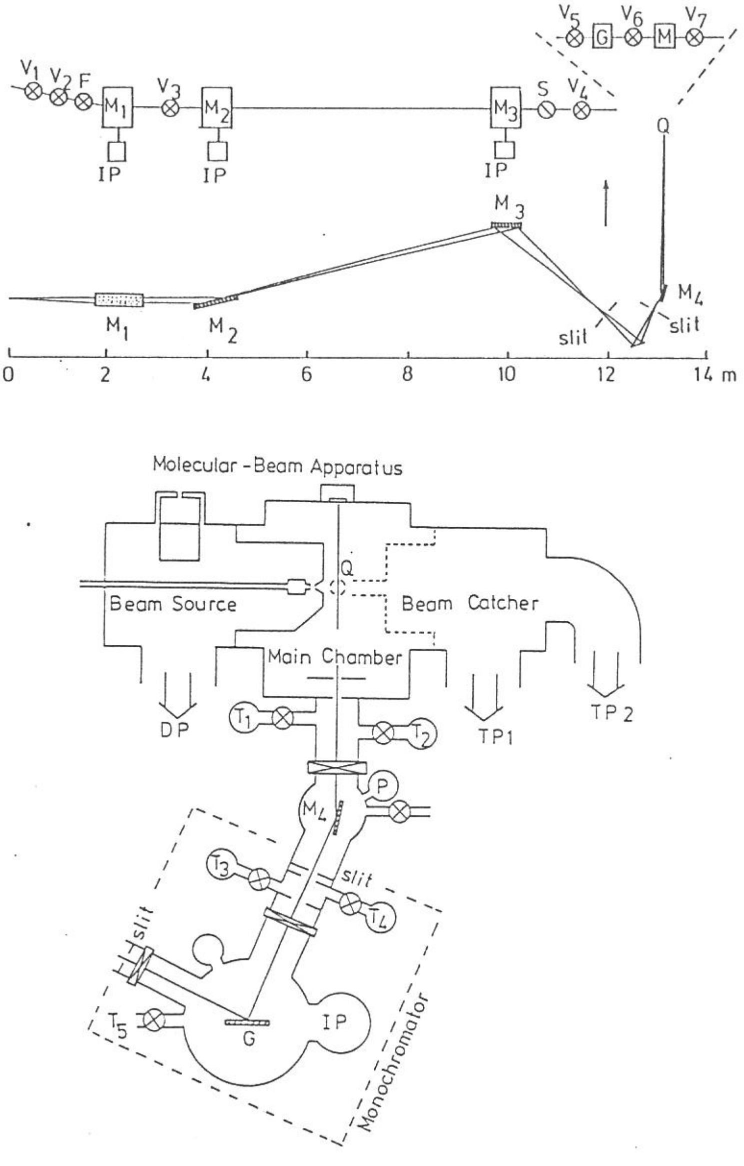

Fig. 1. Schematic layout and drawing of the Beamline BL2B2 at the UVSOR Facility, IMS.

# PERFORMANCE OF THE NEW PHOTOIONIZATION APPARATUS AT BL3A2

T. MASUOKA*, T. HORIGOME, and I. KOYANO

*Department of Applied Physics, Osaka City University Sumiyoshi, Osaka 558

Institute for Molecular Science, Myodaiji, Okazaki 444,

The new photoionization apparatus for angle and energy resolved measurements of photoelectrons and photoions[1)] is now in operation. New features of it include the main experimental chamber that is rotatable around the horizontal axis of incident photon beam, a 1m ion flight tube with a movable MCP detector in it to allow selection of any desired flight path lengths between 15 and 100 cm, an optical filter system in which any combination of two thin metal-film filters (out of five) can be chosen to remove higher order radiation, and a three-stage differential pumping system which reduces the pressure by a factor of $10^{-5}$ in a distance of ~70 cm. Figs. 1 and 2 show the mechanism for rotating the whole experimental chamber (which is attached to the rotatable cylinder) and the differential pumping system, respectively, while the section of the ion flight tube is shown in Fig. 3.

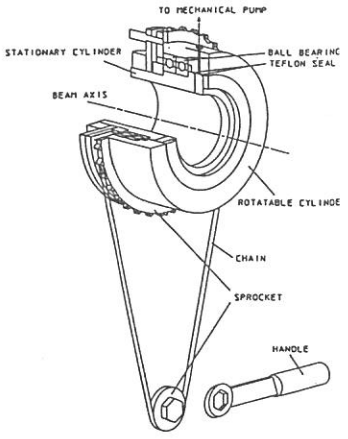

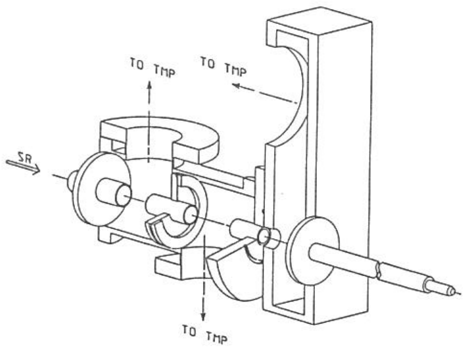

Fig. 2 Differential pumping system

Fig. 1 Mechanism for chamber rotation

All these new features have been tested and found to work satisfactorily. Fig. 4 shows that the pressure of the grating part of the monochromator is kept in the range of $10^{-9}$ Torr even when we work at the pressure as high as $1 \times 10^{-3}$ Torr in the main chamber. Tests also revealed that the vacuum deterioration during rotation of the chamber is negligibly small.

Ionization chamber and electron energy analyzers are set on a table which allows to adjust the chamber-analyzer axis both horizontally and vertically. This set is mounted on an XYZ manipulator in order to allign the set with the photon beam by visual inspection. By now, we have measured the TOF mass spectra and PIPICO spectra of several molecules in their double ionization region using a total electron detector. Coincidence experiments with energy-selected electrons are also in progress.

Reference

1) T. Masuoka, T. Horigome, and I. Koyano, UVSOR Activity Rept. 1987, 23

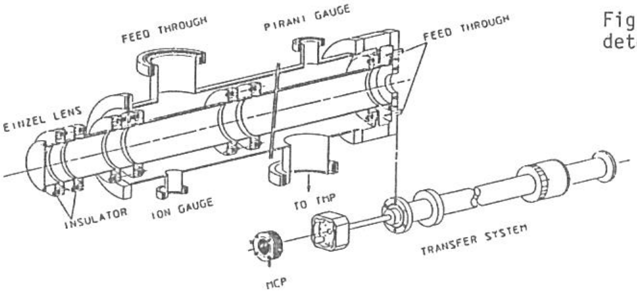

Fig. 3 Ion flight tube, MCP detector, and its manipulator

Fig. 4 Pressure relation showing performance of the differential pumping system

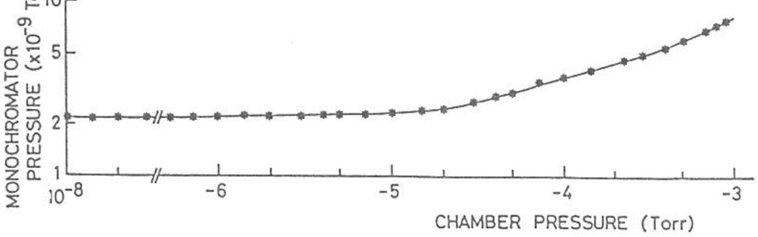

# PERFORMANCE OF A DODECAPOLE COLLISION CHAMBER FOR THE STUDY OF ION-MOLECULE REACTIONS USING SYNCHROTRON RADIATION

Shinzo Suzuki, Takashi Imamura, Inosuke Koyano,
and Kazuhiko Okuno*
Institute for Molecular Science, Myodaiji, Okazaki 444
*Department of Physics, Faculty of Science, Tokyo Metropolitan University, Setagaya-ku, Tokyo 158

For the study of state selected ion-molecule reactions using synchrotron radiation, the TEPSICO-II apparatus has been installed at the beam line BL3B of UVSOR.1) This apparatus incorporates a dodecapole ion-beam guide as a collision chamber to collect reactant and product ions completely over a wide range of collision energy and kinetic energy release.

Its performance has been examined utilizing the $Ne^+$ ions produced by photoionization of Ne at the $^2P_{3/2}$ threshold. Fig. 1 shows the change of the intensity of the primary ion $Ne^+(^2P_{3/2})$ as a function of the potential difference between the ionization region (fixed) and the center of the collision chamber (varied). It has been found that the ion intensity rises sharply as the potential difference reaches zero and then becomes almost constant at higher potential difference. This fact provides a favorable condition for the quantitative study, especially for the study of collision energy dependence, of ion-molecule reactions.

Fig. 2 shows an example of the TOF coincidence spectra for the primary ($Ne^+$) and secondary ($CO^+$, $S^+$) ions of the reaction $Ne^+$ + OCS, obtained at the threshold wavelength for $Ne^+(^2P_{1/2})$. The ratio $I(CO^+)/I(S^+)$ obtained from such measurements is 2.1±0.1 and 2.2±0.2 for $Ne^+(^2P_{3/2})$ and $Ne^+(^2P_{1/2})$, respectively, indicating that the spin-orbit state has no noticeable effect on this reaction. The present result differs from that reported previously on the branching ratio in the dissociation of $OCS^+$ ($C^2\Sigma^+$).2) The difference may stem from the difference in the vibrational state distribution in the $OCS^+(C^2\Sigma^+)$ state between ions produced by the two production modes.

REFERENCES

1) I. Koyano, K. Tanaka, T. Kato, and E. Ishiguro, UVSOR Activity Report 1984/85, p.31.

2) F. Carnovale, A. P. Hitchcook, J. P. D. Cook, and C. E. Brion, Chem. Phys., **66**, 249(1982)

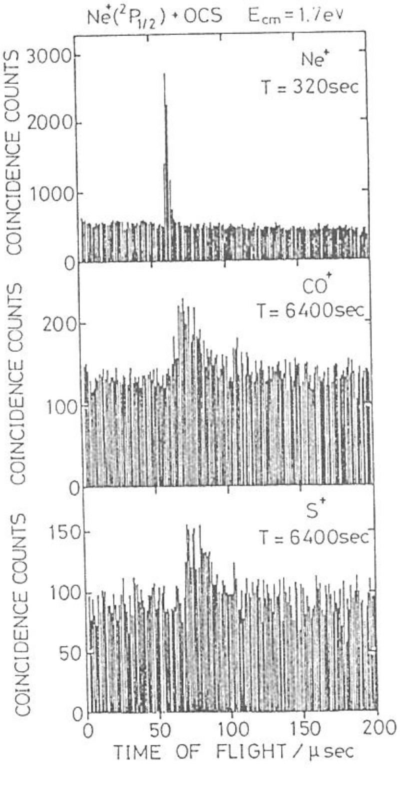

Fig. 2 TOF coincidence spectra for the primary and secondary ions of the reaction $Ne^+$ + OCS, obtained at the threshold wavelength for $Ne^+(^2P_{1/2})$ →

Fig. 1 The change of the intensity of the primary ion $Ne^+(^2P_{3/2})$ as a function of the potential difference (described in the text)

↓

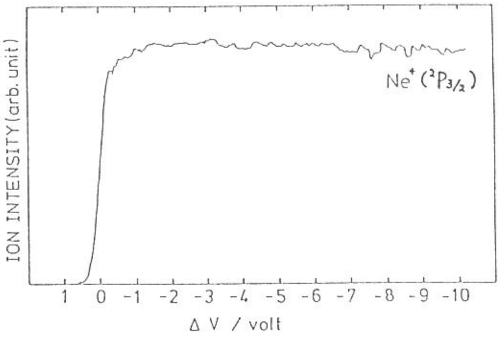

# Construction of a beam line for radiometric calibration

Makoto SAKURAI, Sigeru MORITA, Junji FUJITA, Hiroaki YONEZU,
Kazutoshi FUKUI*, Kusuo SAKAI*, Makoto WATANABE*,
Eiken NAKAMURA*, Eiji ISHIGURO**, and Koujun YAMASHITA***

Institute of Plasma Physics, Nagoya University, Nagoya 464-01
*Institute for Molecular Science, Myodaiji, Okazaki 444
**Faculty of Engineering, Osaka City University, Osaka 558
***Faculty of Science, Osaka University, Toyonaka 560

A new beam line for the radiometric calibration of plasma diagnostic devices has been constructed on BL5B. The beam line consists of a primary monochromator and a calibration chamber. The setup is shown in fig. 1. The primary monochromator (plane-grating monochromator, PGM) is designed to cover a wavelength range of 1.8 to 238 nm with moderate resolution. It has three holographic gratings ($G_1$ - $G_3$) and seven focusing mirrors ($M_{20}$ - $M_{26}$) which are interchangeable in vacuum.

The calibration chamber is equipped with a four-stage differential pumping system which enables to measure the absolute intensity by a rare gas ionization chamber and a photoelectron spectrometer without a gas seal. The suppression of the pressure rise at the monochromator due to a gas flow into the calibration chamber is $10^{-4}$. The chamber also contains a co-axial rotational stage for the characterization of optical components, detectors and spectrometers.

Fig.2 shows spectral distribution of the output from PGM for various grating-mirror combinations. It was measured by Al photo diode (fig. 2(a)) and rare gas ionization chamber (fig. 2(b)) at a slit width of 30μm. Photon number at 50 nm amounts to $2\times10^{10}$ photons/s, if secondary ionization effect is negligible. Fig.3 shows expanded absorption spectra near the core excitation regions. Photoelectron yield spectrum from a NaCl photocathode is shown in fig. 3(a). Exciton peaks near $Cl^-L_{2,3}$ edge was observed for $G_2$-$M_{21}$ combination. The structure in fig. 3(b), which was measured with ionization chamber for $G_3$-$M_{25}$, has been interpretted as Beutler autoionization lines of argon. From the FWHM of the progression, the resolving power is estimated at 800.

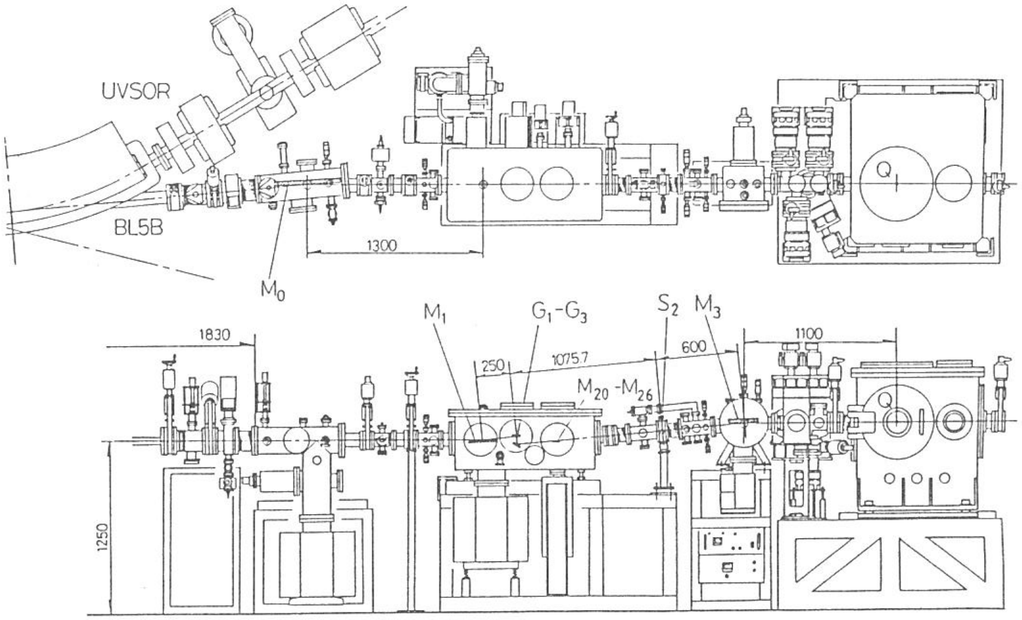

Fig.1. Schematic diagram of BL5B.

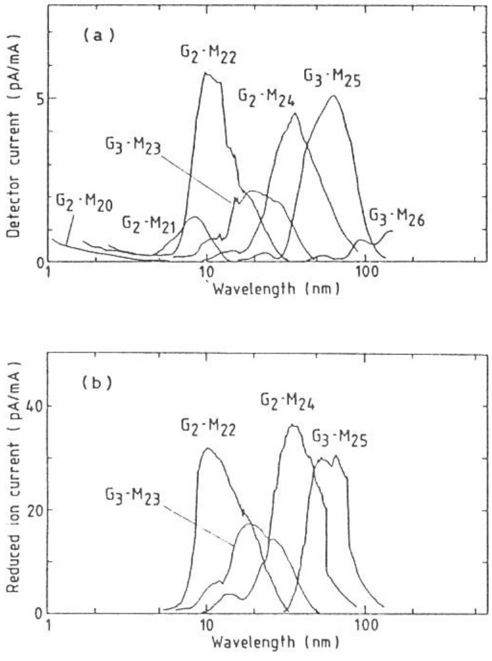

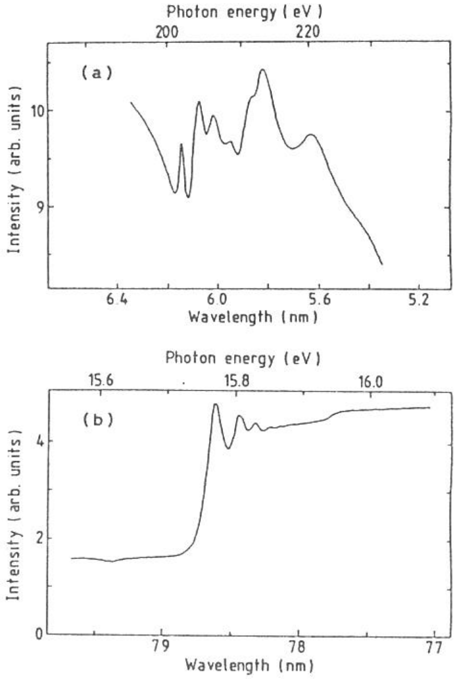

Fig.2. Spectral distribution of PGM measured by (a) Al photodiode and (b) ionization chamber.

Fig.3. Absorption spectra near (a) Cl $L_{23}$ and (b) Ar $M_{23}$ edges.

# DIAMOND ANVIL CELL FOR FAR INFRARED SPECTROSCOPY UNDER HIGH PRESSURE

Takao NANBA and Makoto Watanabe*

Department of Physics, Faculty of Science, Tohoku University, Sendai 980

* Institute for Molecular Science, Myodaiji, Okazaki 444

The study on the lattice vibration under high pressure has been widely made by laser Raman spectroscopy using a diamond anvil cell (DAC). However, Raman technique is not available for materials such as alkali halides which possess an inversion symmetry on the crystal structure because of the Raman inactive character of the optic phonon mode. In such case, direct transmission measurement in the far infrared region under high pressure is required. Up to now, such experiment has been hardly made using black body radiation because of the difficulty of obtaining narrow light beam with sufficient intensity which passes through a DAC. However, our experience at UVSOR proved that the high pressure experiment using a DAC becomes to be easily made because of the high brilliance of the synchrotron radiation in the far infrared region. At the beam line BL6A1, a so-called lever-arm type of DAC was fabricated and installed to the spectroscopic system$^{1)}$.

Fig. 1 shows a cross sectional view of the stainless-steel liquid helium cryostat containing the diamond anvil cell and its support structure. The DAC mounted on the bottom of the liquid helium tank is lifted by rotating the handle up to the level of the monochromator for the pressure measurement. The pressure induced in the DAC is monitored from the energy shifts of the R1 fluorescence line of a ruby chip which is immersed together with a sample in liquid paraffin which serves as a pressure transmitting material in the DAC. A stainless steel gasket is used. The thickness and diameter of the pinhole of the gasket are 0.2 and 1.0 mm for the usual measurement. Operation of the system at low temperature is on progress.

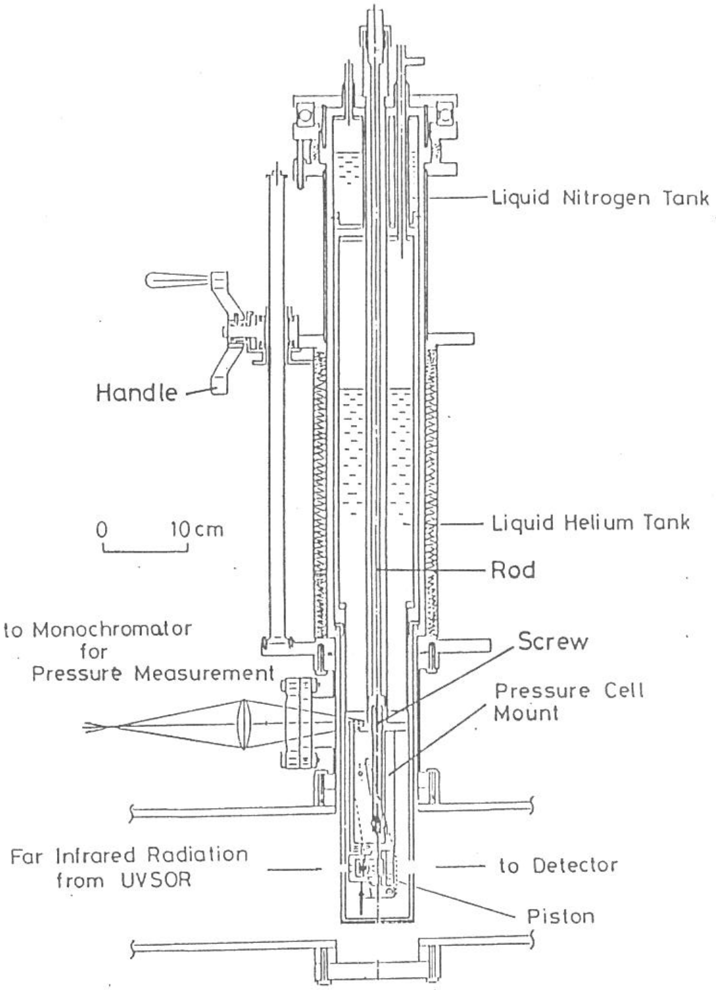

Fig. 1 Cross sectional view of the liquid helium cryostat containing the diamond anvil cell (DAC).

## References

1. T. Nanba; Rev. Sci. Instrum. in press (1989).

# Delay-time Modulation Spectroscopy Using a CW Mode-locked Nd:YAG Laser Synchronized with the SR Pulses

T. Mitani, H. Okamoto, Y. Takagi, M. Watanabe, and K. Fukui
Institute for Molecular Science, Myodaiji, Okazaki 444
S. Koshihara
Faculty of Science, University of Tokyo, Bunkyo-ku, Tokyo 113
C. Ito
Faculty of science, Nagoya University, Chigusa-ku, Nagoya 464

Synchrotron Radiation (SR) from an electron storage-ring can be utilized as a light source of pulses in a wide spectral region from the far-infrared to the soft X-ray. A high repetition rate of the pulse structure of the SR, whose frequency is 90 MHz (the multi-bunch mode) or 5.7 MHz (the single-bunch mode) with a duration time of 460 ps generated at the SR facility of the Institute for Molecular Science is quite suitable for the time-resolved fluorescence and excitation spectroscopies in the subnanosecond time domain.[1] In addition, a high stability of the time structure allows us to synchronize a CW mode-locked Nd:YAG laser (Quantronix 416, 10W) with the frequency of the SR pulses (90 MHz). A new system of the transient spectroscopy has been constructed for the first time by using a delay-time modulation technique. This system opens a unique possibility of expanding a measurable region of transient spectroscopy to infrared and far-infrared regions, where fast optical devices for detection have not been developed as yet.

The experimental instrumentation for the transient absorption measurements is schematically illustrated in Fig. 1. A typical number of monochromatic incident photons of the SR is $10^{2-3}$ photons/pulse with a spectral resolution of 0.1 %. A maximum averaged power of the laser (the pumping light) is 9.2 W, lasing at the fundamental wavelength (1064 nm), and 1.6 W at the second harmonic, which is contains $5\times10^{10}$ photons/pulse. The two synchronized beams are coaxially focused at the sample in a ca. 0.5 mm diameter spot using a small prism and mirrors. Using the tuning method of the laser pulses as shown in Fig. 1, a delay time of the laser pulses, $t_d$, measured from the peak position of the SR pulses can be modulated by applying an AC voltage (e.g. 200 Hz) with an amplitude of t. A change of the transmitted SR light induced by the modulated irradiation of the laser beam, which is sensitively dependent on $t_d$, is detected by a phase-sensitive lock-in amplifier as a modulation signal of the absorption coefficient. The resolution of time in this transient spectroscopy is limited by both of the rise time of the SR pulses and the pulse width of the laser, which was checked by the single-photon counting system[1] to be within 50 ps. These time characteristics of this system is in contrast to those obtained by the transient spectroscopy using a $N_2$-laser[2], in which the SR was used as a continuous light source, and by the two-photon absorption spectroscopy using the Q-switch Nd:YAG laser pulses with the pulse width of 15 ns, which were synchronized with one of the SR pulses at the frequency of 30 Hz[3]. In this sense, the present system is considered to have a high sensitivity and to be suitable for the two-step transient absorption measurements under a relatively low density of excitations in a short time period (0.05 - 11 ns). Furthermore, a spurious signal due to a thermal change of the sample by a shot of intensive laser pulse, which occasionally causes a serious problem in low frequency modulation spectroscopy in solids, may be removed from the modulation signals, since it would not follow the high repetition rate of pulses. As an experimental test of the ability of this system, the transient absorption spectra of R6G dye in an aqueous solution has been measured in the visible region. The results was almost in agreement with those obtained by standard laser spectroscopy. It is possible to expand the measurable energy region of this system to the infrared or vacuum ultra-violet region, which is now in progress.

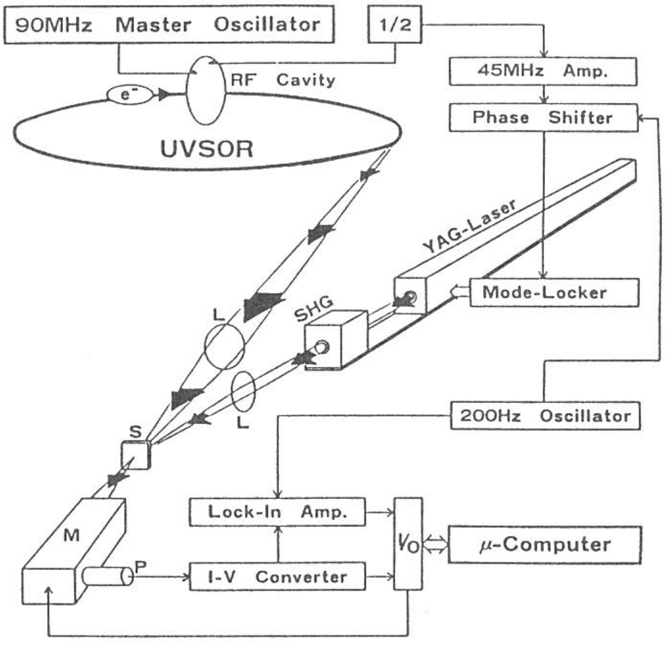

Fig. 1 Schematic diagram of the experimental setup for transient SR spectroscopy

1. T. Mitani, T. Yamanaka, M. Suzui, T. Horigome, K. Hayakawa, and I. Yamazaki, J. Luminescence 39, 313 (1988).
2. V. Saile, Appl. Opt. 19, 4115 (1980).
3. R. Pizzoferrato, M. Casalboni, R. Francini, U.M. Grassano, F. Amtonangeli, M. Piacentini, N. Zema, and F. Bassani, Europhys. Lett. 2, 571(1986).

# RESEARCH ACTIVITIES

# VACUUM-ULTRAVIOLET ABSORPTION SPECTRA OF $CBr_4$ AND RELATED MOLECULES

Ikuo TOKUE, Atsunari HIRAYA* and Kosuke SHOBATAKE*

*Department of Chemistry, Niigata University, Niigata 950-21*
**Institute for Molecular Science, Myodaiji, Okazaki 444*

The Rydberg transitions of methyl halides have been studied by several research groups[1]. The splitting of the lone-pair ionization potentials was either very small, as in methyl chloride, or very large, as in methyl iodide. On the other hand, the splittings in methyl bromides can be of intermediate size. In such a case, the Rydberg spectra are badly overlapped and assignments then become that much more difficult and tentative. In the present study, the photoabsorption cross sections (c.s.) and the fluorescence excitation spectra of $CH_3Br$, $CH_2Br_2$, $CHBr_3$ and $CBr_4$ in the vacuum ultraviolet (VUV) were measured.

Assignments of the Rydberg peak of methyl bromides have been given for the first and second bands by Robin[1]. However, we have found no previous study on the assignments of the

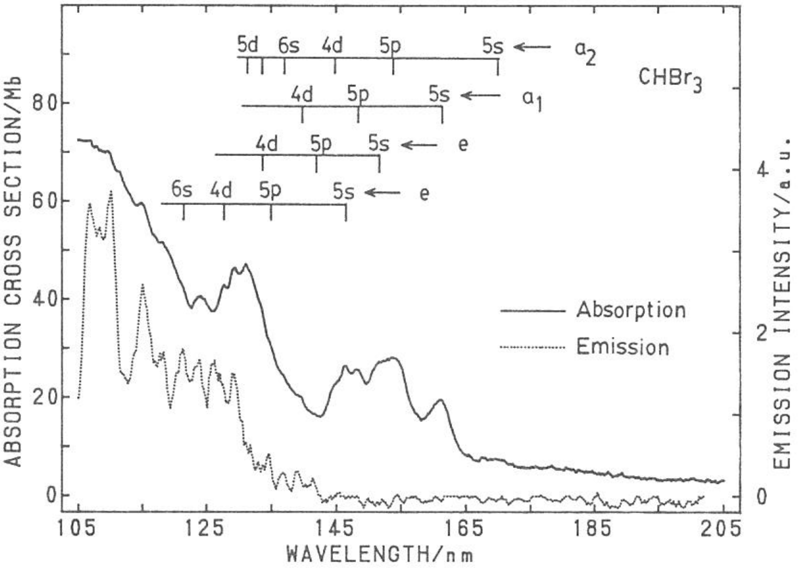

Fig. 1. Absorption and fluorescence excitation spectrum of $CHBr_3$ with the fwhm resolution of 1 nm.

higher Rydberg members. In this preliminary study, a number of peaks of methyl bromides have been assigned to the Rydberg series of the s, p and d types originating from the non-bonding orbitals of bromine. Fig. 1 shows the absorption and fluorescence excitation spectra of $CHBr_3$ using an apparatus at the BL-2A station of UVSOR. On the assumption that the electronic configuration of the valence shell of $CHBr_3$ is the same as that of $CHCl_3$, the valence shell configuration is expressed as $(3e'')^4(8e')^4(11a_1)^2(3a_2)^2$[2]. Lone-pair orbitals of bromine are of $a_2$, $a_1$, e and e symmetry, the ionization potentials (IP) of which are 10.44, 10.79, 11.25 and 11.66, respectively[3]. On the basis of these IP values and the quantum defects of Rb[4], the Rydberg transitions are assigned as shown in fig. 1. The quantum defects of the s, p and d type Rydberg transitions of bromine are estimated to be $2.90\pm0.03$, $2.61\pm0.03$ and $1.32\pm0.03$, respectively.

The onset for the emission from $CHBr_3$ is estimated to be $142.5\pm0.5$ nm ($8.71\pm0.03$ eV). The emission is attributable to the $CBr_2(\tilde{A}^1B_1-\tilde{X}^1A_1)$ transition[5]. Threshold for the fluorescence indicates the following process:

$$CHBr_3 \longrightarrow CBr_2(\tilde{A}^1B_1) + H + Br.$$

Quite weak emission was observed from $CBr_4$, whereas no emission from $CH_2Br_2$ and $CH_3Br$ was observed.

## References

[1] M. B. Robin, Higher excited States of Polyatomic Molecules, Vol. 1, (Academic, New York, 1974).

[2] K. Kimura et al., Handbook of HeI Photoelectron Spectra of Fundamental Organic Molecules, (Japan Sci. Soc., Tokyo, 1981).

[3] D. W. Turner et al., Molecular Photoelectron Spectroscopy, (John Wiley, London, 1970).

[4] A. A. Radzig and B. M. Smirnov, Reference Data on Atoms, Molecules and Ions, (Springer-Verlag, Berlin, 1985).

[5] V. E. Bondybey and J. H. English, J. Mol. Spectrosc. 79(1980)416.

# ABSORPTION AND FLUORESCENCE CROSS SECTIONS OF HEXACHLOROETHANE

**Toshio IBUKI, Atsunari HIRAYA* and Kosuke SHOBATAKE***
Institute for Chemical Research, Kyoto University, Uji, Kyoto 611
*Institute for Molecular Science, Myodaiji, Okazaki 444

Small chlorofluorocarbons are widely used and are known to be pollutants to the atmosphere and waters. Thus, photochemical information on the halogenated compounds is considered to be important.

Fig. 1 shows the absorption and fluorescence cross sections of $C_2Cl_6$ in the 105 - 200 nm region. The electronic configuration of $n_{Cl}$ of $C_2Cl_6$ is expressed as

$$(13e')^4(16a_1)^2(14e')^4(3e'')^4(17a_1)^2(3a_2)^2(4e'')^4(4a_2)^2$$

and their IPs have been determined [1]. Adopting the IP's and the term values for the Rydberg transitions of Cl atom [2], the photoabsorption bands of $C_2Cl_6$ molecule in Fig. 1 are assigned as the Rydberg excitations to 4*s*, *np* and *nd* levels.

The emitting species was identified as the $CCl_2(\tilde{A}^1B_1 \rightarrow \tilde{X}^1A_1)$ transition. The fluorescence yield starts at 160 nm and increases to $\Phi$ = 0.18 at 111.5 nm. From thermochemical considerations, the appreciable increase of quantum yield at 140 - 150 nm corresponds to the following reactions (1) and/or (2), and the steep increase at $\lambda$ < 120 nm is related to the atomic Cl releasing process (3).

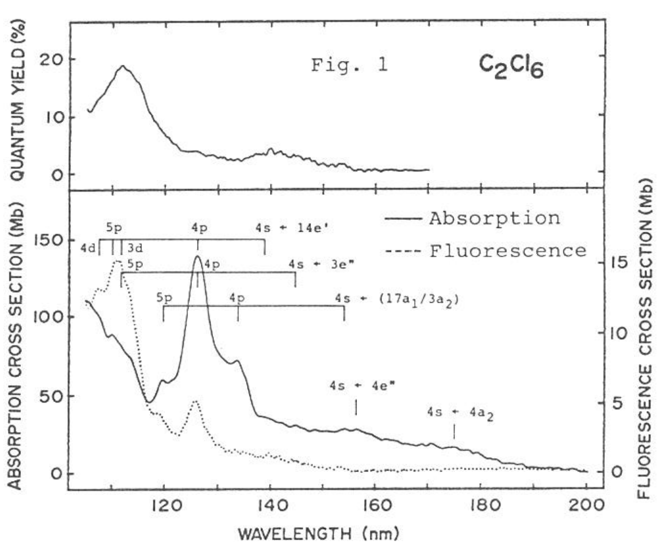
Fig. 1

$$C_2Cl_6 \rightarrow CCl_2(A) + CCl_3 + Cl, \quad \Delta H = 154 \text{ nm } (8.0 \text{ eV}) \quad (1)$$

$$C_2Cl_6 \rightarrow CCl_2(A) + CCl_2(X) + Cl_2, \quad \Delta H = 147 \text{ nm } (8.4 \text{ eV}) \quad (2)$$

$$C_2Cl_6 \rightarrow CCl_2(A) + CCl_2(X) + 2Cl, \quad \Delta H = 114 \text{ nm } (10.9 \text{ eV}) \quad (3)$$

---

[1] K. Kimura et al, "Handbook of He(I) photoelectron spectra of fundamental organic molecules" (Jpn. Sci. Soc. Press, 1981).

[2] C. E. Moore, "Atomic energy levels" (NSRDS-NBS 37, 1971).

# Formation of NH($c^1\Pi$) and NH($A^3\Pi$) in the VUV Photolysis of HNCO

Kenkichi UNO*, Takumi HIKIDA*,
Atsunari HIRAYA and Kosuke SHOBATAKE
*Department of Chemistry, Tokyo Institute of Technology, Meguroku, Ohokayama, Tokyo 152 Japan
Institute for Molecular Science, Myodaiji, Okazaki 444 Japan

In the VUV photolysis of HNCO at the wavelengths below 131nm Okabe has observed emissions from both NH($c^1\Pi$) and NH($A^3\Pi$) as well as from NCO($A^2\Sigma$) and NCO($B^2\Pi$).[1] It was at first proposed that the triplet NH($A^3\Pi$) should be formed by CO($a^3\Pi$) sensitization of NH($X^3\Sigma$), because the threshold excitation wavelength for the NH($A^3\Pi$) production measured at 131.4nm well corresponded to the threshold energy for the production of CO($a^3\Pi$) and NH($A^3\Pi$).[1] However time resolved measurements have shown that both the singlet and triplet NH radicals are formed immediately after the ns incident light pulse, indicating that both of the excited radicals are formed via direct photodissociation of HNCO.[2] In the present study we have measured the emission intensities of excited radicals formed in the photolysis of low pressure HNCO as a function of incident wavelength in the VUV region in order to clarify the mechanism for the primary photochemical processes involving spin-forbidden formation of NH($A^3\Pi$).

The fluorescence excitation spectra for NH($c^1\Pi$) observed at 325nm and for NH($A^3\Pi$) at 336nm are shown in Fig.1(a) and Fig.2(a), respectively. The threshold wavelength for the NH($c^1\Pi$) formation is found to be 141±1nm, which is in good agreement with the one reported by Okabe, 141.1±0.4nm. As is observed by Okabe, the emission intensity from NH($A^3\Pi$) does steeply increase with exciting photon energy starting at around 132nm (see Fig.2(a)). Our careful measurements have confirmed that triplet NH($A^3\Pi$) is certainly formed at wavelengths longer than 132nm and the emission extends to the region as long as 161nm or even longer.

Since the photo-excited state would be singlet, the formation of the triplet NH($A^3\Pi$) and ground state CO is a spin-forbidden process. It is worth noting that the spin-allowed process is more feasible than the spin-forbidden one by factors as high as six, below 132nm whereas the quantum yield for NH($A^3\Pi$) formation is comparable with that for NH($c^1\Pi$) at longer wavelengths than 132nm. Although the details are yet to be clarified the triplet NH($A^3\Pi$) radicals may be produced via triplet state formed by intersystem crossing from the photo-excited singlet state. Relatively long-lived excited states of up to 1ns lifetime may be involved in the photodissociation of HNCO.

## References

1) H. Okabe, J. Chem. Phys., **53**, 3507 (1970).

2) T. Hikida, Y. Maruyama, Y. Saito and Y. Mori, Chem. Phys. **121**, 63 (1988).

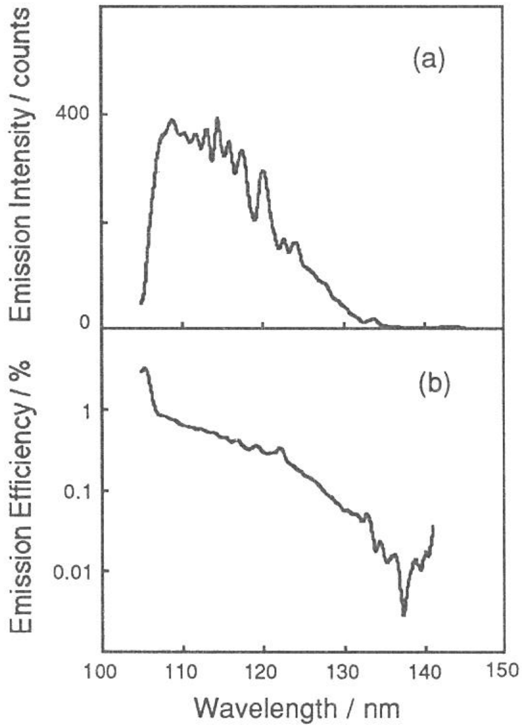

Fig.1. NH($c^1\Pi$) (a) $I_f$, (b) $\Phi_f$

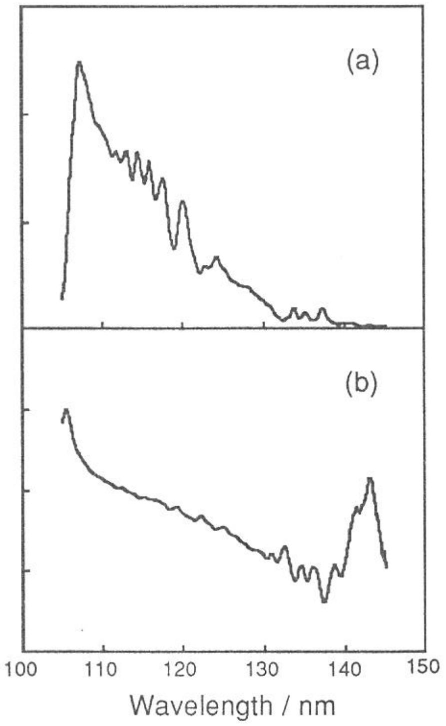

Fig.2. NH($A^3\Pi$) (a) $I_f$, (b) $\Phi_f$

# VUV PHOTOABSORPTION AND FLUORESCENCE EXCITATION SPECTRA OF GROUP IIb ORGANOMETALLICS

**Toshio IBUKI, Atsunari HIRAYA*, and Kosuke SHOBATAKE***

Institute for Chemical Research, Kyoto University, Uji, Kyoto 611
*Institute for Molecular Science, Myodaiji, Okazaki 444

Organometallics are widely used as the materials for microelectronic devices, and photons have positively employed for the growth of epitaxy or chemical vapor deposition. However, the photochemical knowledge of organometallics are quite limited.

The photoabsorption cross sections and fluorescence excitation spectra of $M(CH_3)_2$ (M = Zn, Cd and Hg) were simultaneously measured in the 106 - 270 nm region as shown in Fig. 1 in which the solid and the dotted curves indicate the absorption and fluorescence cross sections, respectively. The outer shell electronic configurations of $M(CH_3)_2$ are $(2e')^4(2e'')^4(3a_1')^2(2a_1'')^2$, and their ionization potentials (IP) have been determined by PES [1]. Using the term values of the Rydberg transitions for metal atoms [2] and the IP's [1], the absorption bands are accounted for in terms of Rydberg excitations of the valence shell electrons as indicated in Fig. 1. The emitting species are identified as $MCH_3(\tilde{A}^2E)$ radicals for M = Zn and Cd and $M(np\ ^3P^0)$ atoms for M = Cd and Hg. Especially the $Cd(^3P^0 \rightarrow {}^1S_0)$ emission in the middle panel shows the typical features of Rydberg series assigned as the $ns \leftarrow 3a_1'$ and $np \leftarrow 3a_1'$ transitions which are concealed in the absorption measurement. It is noticeable that the electronically excited $MCH_3(\tilde{A}^2E)$ radicals are formed through the Rydberg excitations of the C-H bonds (denoted by $2e'/2e''$), while $M(^3P^0)$ atoms are selectively produced through the Rydberg transitions of M-C bonds with $3a_1'$ and $2a_2''$ symmetries.

[1] J. C. Tse, G. M. Bancroft, and D. K. Creber, J. Chem. Phys. 74, 2097 (1981).

[2] C. E. Moore, *Atomic Energy Levels*, Vol. 2 and 3 (Nat. Stand. Ref. Data Ser., 35, Nat. Bur. Stand., Washington D.C. GPO, 1971).

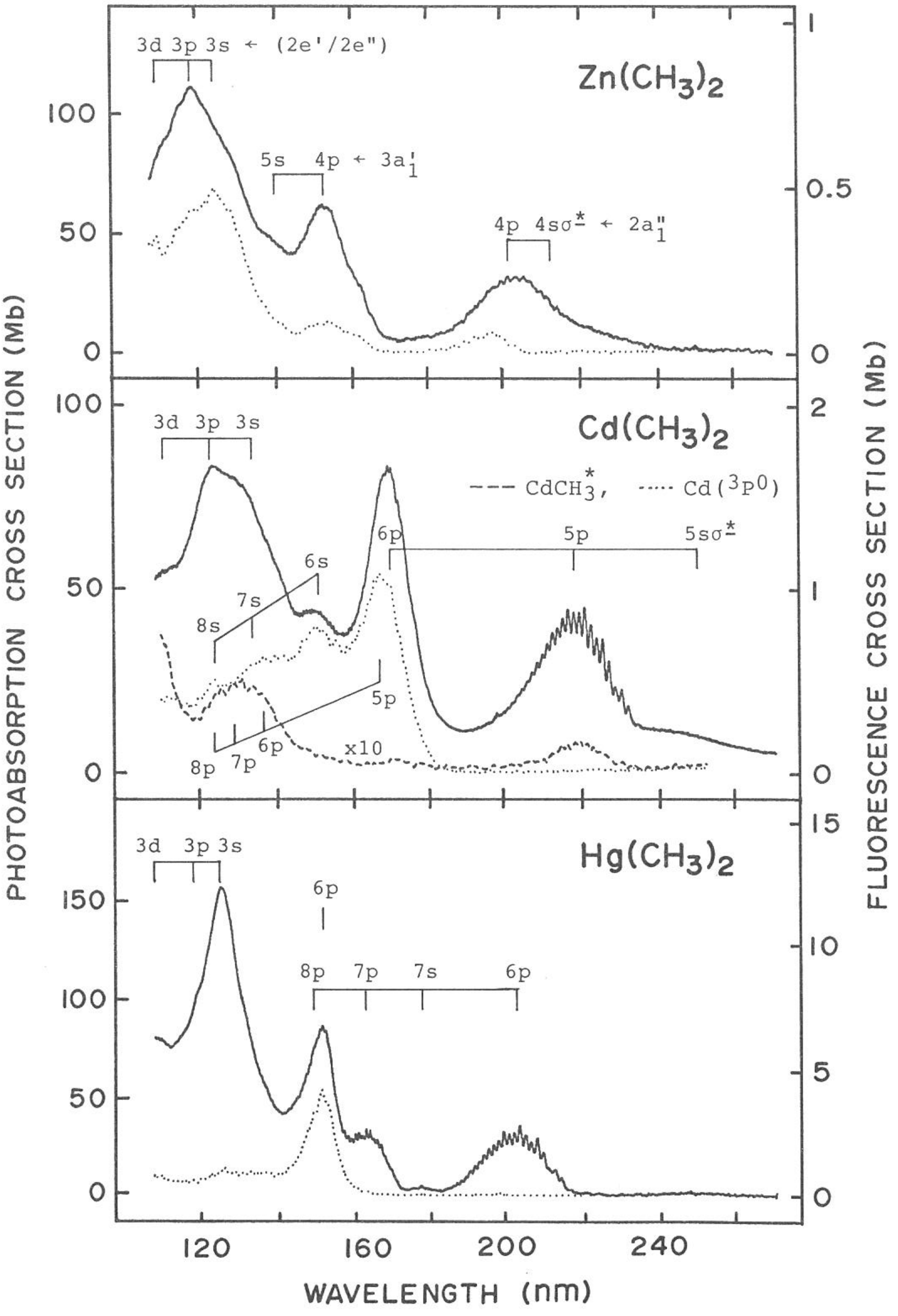

Figure 1. Photoabsorption and fluorescence excitation spectra of $M(CH_3)_2$.

# RYDBERG EXCITATIONS OF $M(CH_3)_3$ IN THE 106 - 270 nm REGION

Toshio IBUKI, Atsunari HIRAYA[*], Kosuke SHOBATAKE[*],
Yutaka MATSUMI[†] and Masahiro KAWASAKI[†]

Institute for Chemical Research, Kyoto Univ., Uji, Kyoto 611
*Institute for Molecular Science, Myodaiji, Okazaki 444
†Research Inst. of Appl. Electricity, Hokkaido Univ., Sapporo 060

Photolyses of $Ga(CH_3)_3$ and $In(CH_3)_3$ are one of the effective methods to form semiconductor film such as gallium arsenide, indium phosphide, gallium indium arsenide and so on.

Photoabsorption cross sections of $M(CH_3)_3$, M = Ga and In, were measured for the first time in the wavelength range of 106 - 270 nm. Broad bands were detected as shown in Fig. 1. The spectral resemblance suggests that the same type transitions take place in the $M(CH_3)_3$ photoexcitations.

Fig. 2 shows the PES of $Ga(CH_3)_3$ and $In(CH_3)_3$ measured at Hokkaido University. By the comparison with the previous PES of $B(CH_3)_3$ and $Al(CH_3)_3$ [1], the first biding energy at ~9 eV should be the ionization potential (IP) for the removal of a 3*e* electron forming M-C bond. The second broad band at around 13.5 eV is assigned as the superimposed IP's of $\sigma_{C-H}$ of $(2e')^{-1}$, $(3a')^{-1}$ and $(1e'')^{-1}$. Using the presently obtained IP's, the first 195 nm absorption peak of $Ga(CH_3)_3$ in Fig. 1 has the term value of 25600 $cm^{-1}$ with respect to the IP of 9.53 eV for $(3e')^{-1}$. This value is very close to that for the $5s \leftarrow 4p$ Rydberg transition of Ga(I) atom, that is, 23951 $cm^{-1}$ and the quantum defect of $\delta = 2.84$ [2]. Thus, we assign the 195 nm band as the $5s \leftarrow 3e'$ Rydberg transition of $Ga(CH_3)_3$ with $\delta = 2.93$. Adopting the similar term value concepts the absorption bands of $M(CH_3)_3$ are consistently assigned as the excitations to Rydberg orbitals as indicated in Fig. 1.

[1] G. K. Barker, M. F. Lappert, J. B. Pedley, G. J. Sharp, and N. P. C. Westwood, J. Chem. Soc. Dalton Trans. 1975, 1965.

[2] C. E. Moore, *Atomic Energy Levels*, Vol. 2 and 3 (Nat. Ref. Data Ser., NBS 35, Washington DC, 1971).

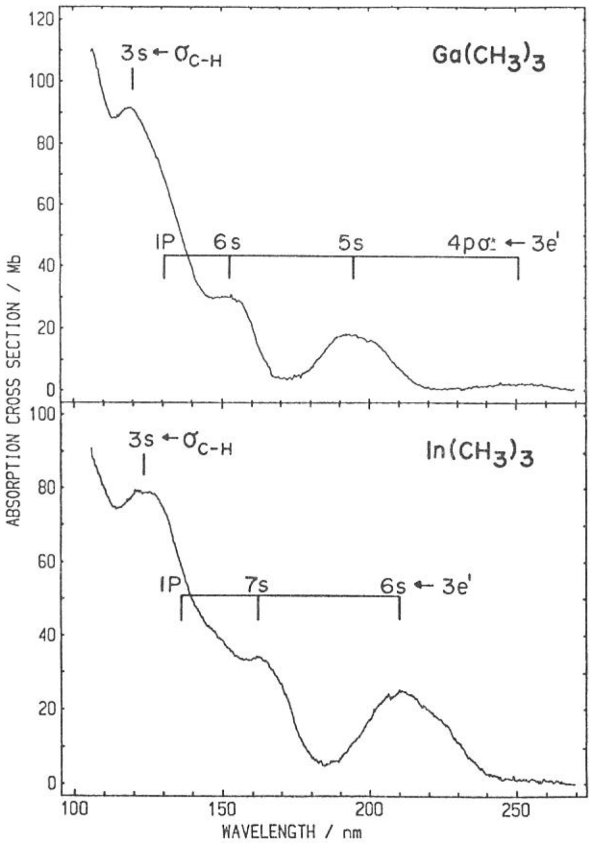

Fig. 1. Photoabsorption cross sections of $Ga(CH_3)_3$ and $In(CH_3)_3$. The Rydberg transitions are indicated.

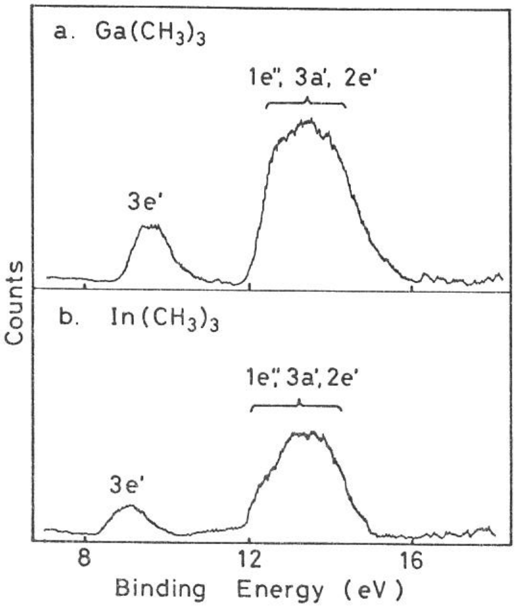

Fig. 2. He(I) PES of $Ga(CH_3)_3$ and $In(CH_3)_3$.

# IONIC FRAGMENTATION PROCESSES IN ORGANOMETALLIC MOLECULES OF GROUP II–V ELEMENTS FOLLOWING (n-1)*d* CORE PHOTOIONIZATION

Shin-ichi NAGAOKA, Shinzo SUZUKI, Umpei NAGASHIMA,
Takashi IMAMURA, and Inosuke KOYANO

Institute for Molecular Science, Myodaiji, Okazaki 444

In recent years, dynamic processes following core level excitation in molecules have been a topic of much interest. We have studied ionic fragmentation following photoionization from the shallowest *d* core orbital in organometallic molecules with a group II–V element [$ZnMe_2$, $GaMe_3$, $GeMe_4$, $SnMe_4$, $PbMe_4$, and $BiMe_3$ ($Me=CH_3$)] in the vapor phase.[1] The experiments were performed using the TEPSICO-II apparatus[2] installed at the BL3B beam line of UVSOR.

Photoionization from the (n-1)*d* core orbitals (n=4 for $ZnMe_2$, $GaMe_3$, and $GeMe_4$, n=5 for $SnMe_4$, and n=6 for $PbMe_4$ and $BiMe_3$) is identified in the threshold electron spectra of these molecules. The (n-1)*d* core-ionized state of the molecules with a group IV element ($PbMe_4$ and $SnMe_4$) is split into five sublevels owing to both the spin-orbit coupling and the electrostatic perturbation from the methyl groups (for example, see Fig. 1). By use of the threshold photoelectron - photoion coincidence (TPEPICO) technique, it is shown that, in the molecules studied in the present work (except $BiMe_3$), the excitation to the $[(n-1)d]^9$ hole-state opens dissociation paths quite different from those following valence photoionization (for example, see Fig. 2); the metal ions are predominantly produced following the excitation to the $[(n-1)d]^9$ hole-state. The monomethyl metal ions are likely to be produced following both the core and valence photoionization. The dimethyl and trimethyl metal ions are shown to originate from the valence-ionized states. The fragmentation processes following 5*d* core level ionization of $BiMe_3$ seem to be statistical (Fig. 3). The quintet splitting of the (n-1)*d* core-ionized states of the group IV organometallic molecules and their fragmentation patterns can be explained in terms of the crystal field theory and the hybrid orbitals constructed from the (n-1)*d*, n*s*, and n*p* atomic orbitals (Fig. 4).

References

1. S. Nagaoka, S. Suzuki and I. Koyano, Phys. Rev. Lett., 58, 1524 (1987); Nucl. Instrum. Methods, A266, 699 (1988); S. Nagaoka, S. Suzuki, U. Nagashima, T. Imamura and I. Koyano, Rev. Sci. Instrum., in press; J. Chem. Phys., submitted.
2. S. Suzuki, S. Nagaoka, I. Koyano, K. Tanaka and T. Kato, Z. Phys. D4, 111 (1986).

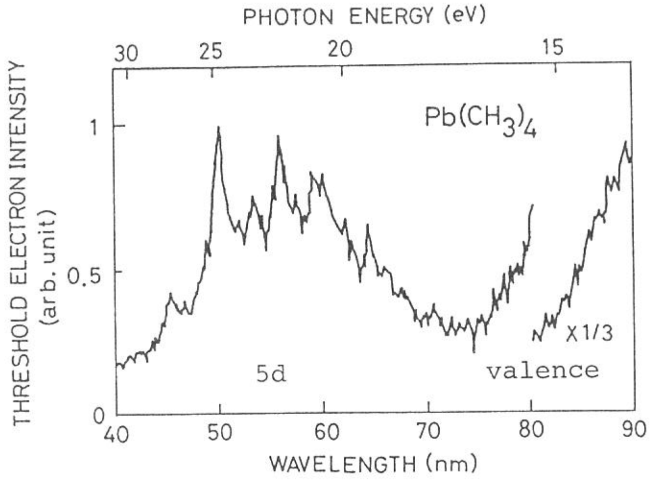

Fig. 1. Threshold electron spectrum of $PbMe_4$.

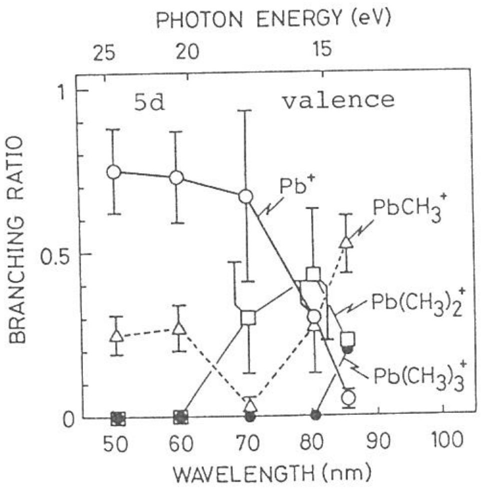

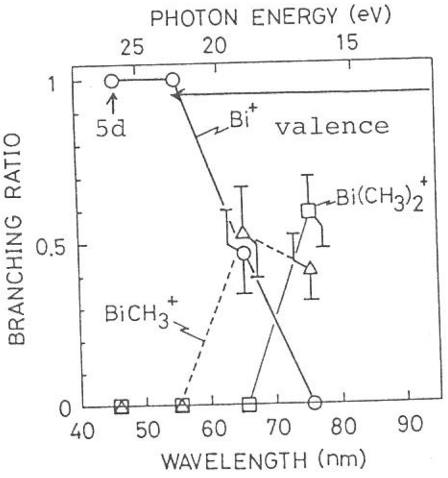

Fig. 2. Branching ratio of $PbMe_4$. Fig. 3. $BiMe_3$.

# Direct Absorption Spectrum of Benzene in a Free Jet

**Atsunari HIRAYA and Kosuke SHOBATAKE**

Institute for Molecular science, Myodaiji, Okazaki, 444 Japan

Direct absorption spectrum of benzene in a supersonic free-jet have been measured, for the first time, in the wavelength range of the $S_1$, $S_2$, $S_3$ states and up to the first ionization limit by using SOR as a light source on the supersonic free-jet apparatus constructed on a beam line BL2A. Figure 1 shows a direct absorption spectrum of jet-cooled benzene seeded in He. Absolute value of molar extinction coefficient (ε) was determined by normalizing the value at 200.1nm band of the $S_2$ state to that measured in room temperature vapor, assuming the invariance of absorption coefficient in both conditions for such broad band. In the $S_1$ region (230 - 260 nm), the vibrational progression of $6^1_0 1^n_0$ (n = 0 - 4) is clearly observed without any congestions arising from vibrational hot-bands. The maximum value of ε for the $S_1$ in the

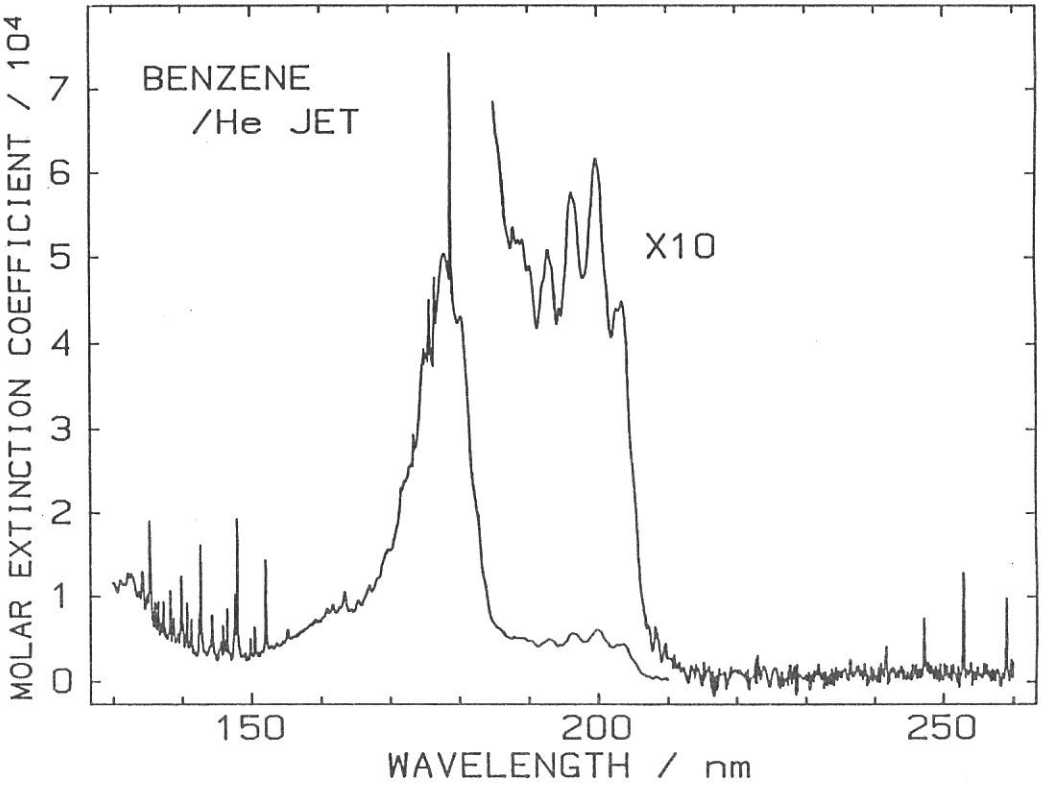

**Figure 1.** Absorption spectrum of benzene seeded in a He supersonic free-jet (total pressure 400torr). Spectral bandwidth is 0.065nm, nozzle temp. = 27°C.

**Table 1**

Absolute absorption intensity of the $6^1_0 1^n_0$ (n = 0,1,2,3,4) bands in the $^1B_{2u} \leftarrow {}^1A_{1g}$ transition in jet-cooled benzene. Experimental bandwidth is 0.065nm. Relative values are shown in brackets.

| | | this work | | | | Ref.[2] | | |
|---|---|---|---|---|---|---|---|---|
| | | (a) | | (b) | | (c) | | (d) |
| n | $\lambda_{vac}$(/nm) | ε | | f/$10^{-4}$ | | f/$10^{-4}$ | | |
| 0 | 258.99 | 980 | (1.00) | 1.37 | (1.00) | 0.88 | (1.00) | (1.00) |
| 1 | 252.95 | 1280 | (1.30) | 1.87 | (1.36) | 1.51 | (1.72) | (1.19) |
| 2 | 247.17 | 750 | (0.76) | 1.34 | (0.98) | 1.31 | (1.48) | (0.88) |
| 3 | 241.68 | 420 | (0.43) | 0.85 | (0.62) | 0.68 | (0.77) | (0.37) |
| 4 | 236.42 | 260 | (0.27) | 0.57 | (0.41) | 0.35 | (0.40) | — |
| total | — | — | — | 6.00 | — | 4.73 | | |

(a) peak value of ε at each vibronic bands.

(b) absolute oscillator strength of each band and total value.

(c) from Ref.[2], T = 25°C, resolution 0.08nm.

(d) relative integrated intensity, T = - 44°C, resolution 0.05nm.

jet (spectral bandwidth = 0.065nm) is found to be 1430 at 252.95nm ($6^1_0 1^1_0$), which is larger than that in room temperature vapor (<940). The oscillator strength of each band is obtained by integrating the quantity $0.432[\varepsilon(\lambda)/\lambda^2]d\lambda$ over the wavelength region with 0.5 nm width centered at each peak. By summing these values, the total oscillator strength induced by $\nu_6$ mode in the $^1B_{1u} \leftarrow {}^1A_{1g}$ transition are found to be $6.0 \times 10^{-4}$. This value in the present work is in good agreement with the theoretical value ($5.9 \times 10^{-4}$)[1] and also with the experimental value ($4.73 \times 10^{-4}$)[2] in room temperature vapor.

In the $S_2$ region, a shoulder is found at 205.2nm which have not been noticed in the spectrum measured in room temperature vapor. We tentatively assigned this band as the $S_2$ origin induced by a pseudo-Jahn-Teller effect. Two components at 203.6 and 202.7 nm in the first prominent band of the $S_2$ system are assigned as the $8^1_0$ and $6^1_0$ false origins, respectively. In this assignment it is assumed that the reduction of the vibrational frequency of the $\nu_8$ mode is caused by pseud-Jahn-Teller effect as in the $^3B_{1u}$ state. Second to fourth prominent bands are then assigned as the overlapped progressions of the $\nu_1$ mode each built on these two false origins. The $\nu_1$ progression built on the weak true origin is also identified.

[1] F. Mets, M.J. Robey, E.W. Shlag and F. Dorr, Chem. Phys. Lett. *51* (1977) 8.

[2] E. Pantos, J. Phillis and A. Bolobinos, J. Mol. Spectry. *72* (1978) 36.

# Absorption Spectra of Higher Electronic States of Benzene Clusters in a Free Jet

**Atsunari HIRAYA and Kosuke SHOBATAKE**

Institute for Molecular science, Myodaiji, Okazaki, 444 Japan

Extensive experimental works have been done on the first excited singlet state $S_1(^1B_{2u})$ of benzene clusters. In contrast only few attempts have been made to elucidate the spectroscopic and dynamical properties of benzene clusters in the higher electronic states. This is because good tunable UV - VUV light sources have not been available until recently. Moreover, benzene clusters undergo rapid dissociation in the higher excited or ionic states, making it difficult to detect the optically prepared states.

In the present study absorption spectra of benzene clusters in its $S_2$ and $S_3$ states have been observed, for the first time, in a supersonic free jet by using SOR as a light source on the free-jet apparatus constructed on a beam line BL2A. Figure 1 shows the absorption spectra of benzene in free jets under different conditions: (a) without carrier gas, (b) with 653 torr Xe as a carrier gas. The spectrum (a) obtained without carrier gas is almost similar to that measured in room temperature vapor. In the spectrum (b) obtained with Xe carrier gas, absorption starts to appear at longer wavelength (218nm) than the spectrum (a) and intensity increases monotonically toward shorter wavelength, while the spectrum (a) exhibits a rather flat region from 187 nm to 204 nm. The spectrum (b) can be regarded as the superposition of benzene monomer spectrum and those of benzene (or benzene-$Xe_n$) dimer and clusters. The spectrum (c) is obtained by subtracting spectrum (a) from spectrum (b) by multiplying an appropriate factor (0.84) to spectrum (a) in order to cancel out the vibrational structures of benzene monomer in spectrum (b). This difference spectrum (c) shows two broad absorption maxima at 186 and 207nm. The appearance of this broad feature is found to be quite sensitive to the nozzle temperature. At a higher nozzle temperature (70°C) these broad features disappear. There are two candidates for the species which gives these broad absorption bands in the difference spectrum: one is benzene clusters (and/or dimer) and the other is benzene-Xe clusters (and/or dimer). However, these two broad bands observed for Xe carrier gas are also found in the difference spectra for both He and Ar carrier gases with almost the same feature as that for Xe. Therefore, the observed two broad absorption bands are assigned, at least as the major species, to the *benzene clusters* and *not* to the *benzene-Xe clusters*. Both the energy difference between the two broad bands in spectrum (c) and their intensity ratio indicate that the lower and higher energy bands, respectively, correspond to the $S_2$ and $S_3$ systems of benzene monomer. The $S_2$ absorption of the benzene clusters starts at 218.5 nm and abruptly increases at about 215 nm toward shorter wavelength. In a thin film of benzene, the crystal-field-induced origin of the $S_2$ was observed weakly at 215 nm and strong false-origin was observed at 213nm. The spectral shift in crystal and that in clusters are almost the same (2100 $cm^{-1}$) for the $S_2$ absorption. On the contrary, the spectral shift of the $S_3$ system in clusters (178 $\rightarrow$186 nm $\approx$2400$cm^{-1}$) from monomer is much smaller than that in crystal (178 $\rightarrow$195 nm $\approx$4900$cm^{-1}$).

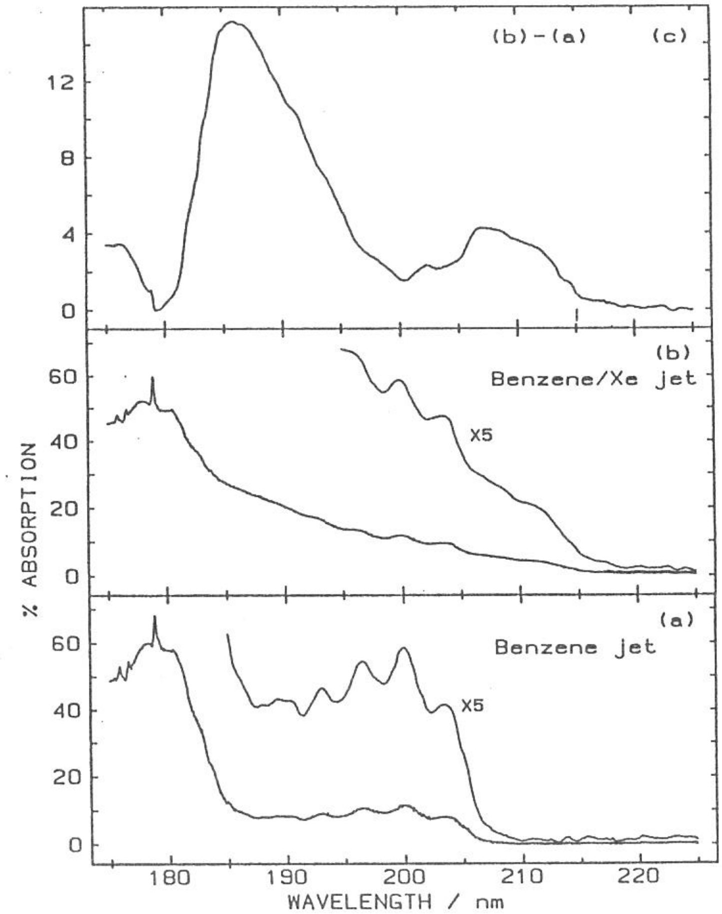

**Figure 1.** Absorption spectra of benzene and its clusters in a supersonic free-jet. Spectral bandwidth is 0.2nm: (a) 107 torr benzene without carrier gas, nozzle temperature = 20°C, (b) with 653 torr Xe gas (total 760 torr), nozzle temperature is 21.6°C. Difference spectrum (c) is obtained by subtracting spectrum (a) with scaling factor of 0.84 from spectrum (b).

# Experimental Studies on Photoionization Processes of Gaseous Clusters by a Threshold Electron-Photoion Coincidence Technique

Takato HIRAYAMA,* Shin-ichi NAGAOKA and Katsumi KIMURA
Institute for Molecular Science, Myodaiji, Okazaki, 444

We have designed and constructed a threshold-electron photoion coincidence (TEPICO) spectrometer for studying the photoionization processes of atomic and molecular clusters by synchrotron radiation. Application of the TEPICO technique to the cluster photoionization study is particularly useful, as the cluster system contains various kinds of cluster components with different masses.

The new spectrometer has been installed in the molecular beam apparatus of the beamline BL2B2 (with a 1m Seya-Namioka monochromator) of the UVSOR Facility. There are several methods for the threshold electron detection. In this study we have adopted an angular discrimination technique1) using a capillary array plate (HAMAMATSU PHOTONICS), in which each hole is 12$\mu$m in diameter and 1 mm in length.

A preliminary result of the threshold electron spectrum of $O_2$ in the wavelength region 65 - 89 nm is shown in Figure 1. The spectral features agree well with the previous measurements by the other groups.2,3) Vibrational bands of the $O_2^+$ were clearly observed.

Figure 2 shows a typical Time-of-Flight spectrum for $Ar_n$ clusters (n= 1,..,5) at the wavelength of 80 nm.

Coincidence experiments on the atomic and molecular clusters are in progress.

*Present address: Faculty of Science, Gakushuin University, 1-5-1,
Mejiro, Toshima-ku, Tokyo 171

References (1) R. Spohr, P. M. Guyon, W. A. Chupka and J. Berkowitz, *Rev. Sci. Instrum.* **42** (1971) 1872. (2) P. M. Guyon and I. Nenner, *Appl. Opt.* **19** (1980) 4068. (3) S. Suzuki, S. Nagaoka, I. Koyano, K. Tanaka and T. Kato, *Z. Phys.* **D4** (1986) 111.

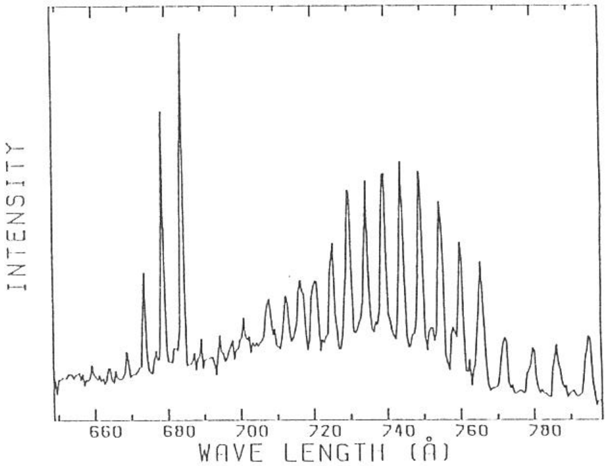

Fig. 1. Threshold electron spectrum of $O_2$ in the range 650-800 A.

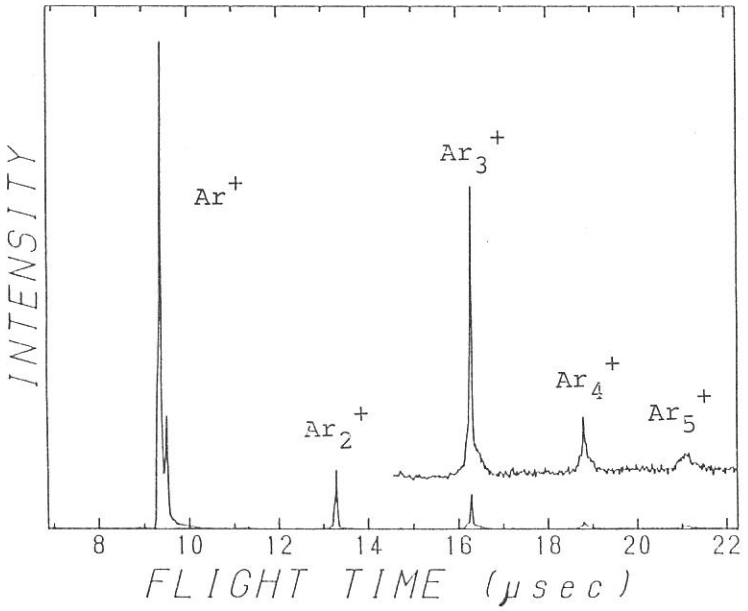

Fig. 2. TOF spectrum of Ar clusters at 800 A.

# AUTOIONIZATION OF SUPEREXCITED $(O_2)_2$, $(O_2)_3$, AND $O_2\cdot Ar$ CLUSTERS FOLLOWING VUV PHOTOEXCITATION

Masatoshi UKAI, Kosei KAMETA, Tetsu KAMOSAKI,
Kyoji SHINSAKA, and Yoshihiko HATANO
Department of Chemistry, Tokyo Institute of Technology, Meguro-ku, Tokyo 152
and
Takato HIRAYAMA, Shin-ichi NAGAOKA, and Katsumi KIMURA
Institute for Molecular Science,
Myodaiji, Okazaki 444, Japan.

Photoionization of mixed clusters offers an important oppotunity to investigate the influence of intermolecular forces on ionization processes; the difference between two distinct components of a cluster give rise to internal energy transfer processes such as intramolecule-intermolecular autoionization and intramolecular charge transfer: the dissociation of the clusters corresponds to the half collisions of ion-molecule reactions. Because electronic or atomic rearrangements are involved in these cases, an amount of detailed information is available about intramolecular potentials, coordination effects, and interpotential processes i.e., electronic transition probabitity or autoionization width. Although studies on mixed clusters are thus of increasing importance, only little work has hitherto been devoted to the photoionization of molecular clusters in the VUV-region.

In view of this situation, we report the photoionization of small molecular clusters, $(O_2)_2$, $(O_2)_3$, and $O_2\cdot Ar$, in the region of 50-100nm.

The experimental apparatus employed in the present experiment has been described previously$^{1)}$. The monochromatized VUV photon beam dispersed by a 1m Seya-Namioka monochromator of the beam line BL2-B2 intersects a supersonic nozzle beam at right angle. Ionic products are extracted perpendicularly to both of the photon and the molecular beams, and then mass-analyzed using a quadrupole mass-analyzer. Van der Waals clusters are produced in expansion of 1:1 gas mixture of $O_2$ and Ar via a 50$\mu$m$\phi$ nozzle at -100°.

A typical mass pattern is presented in fig.1 obtained at 50nm excitation under the back pressure of 5atm. Monomer region is not shown. The relative intensities of single component peaks for $(O_2)_2^+$, $(O_2)_3^+$, or $Ar_2^+$ are about one order of magnitude larger than those for mixed clusters such as $Ar\cdot O_2^+$, $Ar\cdot(O_2)_2^+$, or $Ar_2\cdot O_2^+$.

Vibrational structures due to Rydberg bands observed in the photoion yield spectrum of $O_2^+$ are almost completely diminished in the spectra of $(O_2)_2^+$, $(O_2)_3^+$ (see ref.2), and $O_2\cdot Ar^+$ in the region of 65-100nm; however, the characteristic window at 59nm due to the $c^4\Sigma_g^-\cdot 3s\sigma_g$ Rydberg state is clearly observed in fig.2. The ionization threshold for the dissociative product $O_2\cdot O^+$ is at a wavelength of 75nm, longer by 10nm than the $O^+$ threshold[2); the threshold for $Ar\cdot O^+$ is at almost the same position as that for $O^+$. The observation suggests that the effect of molecular rearrangement is depressed in the dissociative photoionization of $O_2\cdot Ar$.

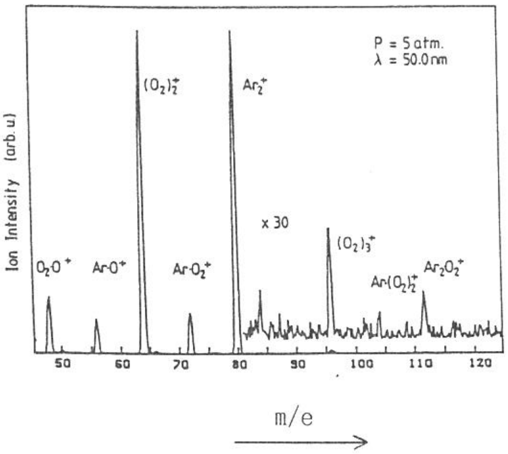

fig.1 *Typical mass pattern.*

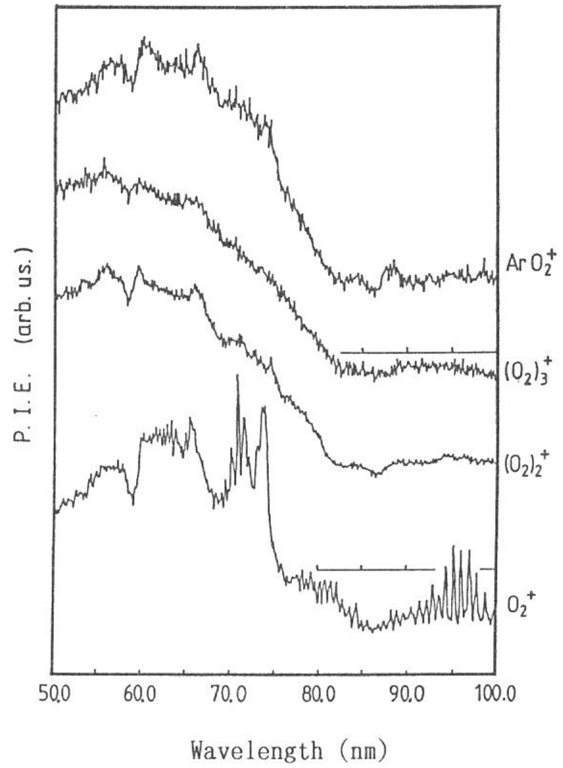

fig.2 *Photoion yield spectra.*

REFERNCES
1 H.Shiromaru et al *Chem. Phys. Lett.*, 141, 7(1987).
2 S.H.Linn et al *J.Chem. Phys.*, 74, 3348(1981).

# Absorption Specra of Quantum Well Exciton in Alkali Halide Multilayer Structures

Arisato Ejiri and Kazumichi Nakagawa

Dept. of Pure and Applied Sciences, University of Tokyo, 3-8-1
Komaba, Meguro-ku, Tokyo 153.

On the absorption spectra of KCl-KBr multilayers, KBr bulk-exciton-peaks are disappeared and new sharp peaks (spikes) having much steeper rise and locating above the respective bulk-exciton-peak are observed. This phenomenon was previously found by the present authors[1] for the first time and interpreted with terms of quantum size effects (QSE) in the longitudinal direction (one dementional confinement). It was also suggested in the work that the interface-mixture formed in the multilayer structures played important role in the QSE.

The present studies intend to observe the QSE in other alkali halides multilayers and performed absorption measurements for several kinds of multilayer structures at BL-1B and 8B equiped 1m Seye-Namioka monochromator. These specimens are alternatively deposited with vacuum evaporation on LiF single crystal substrate. It can be surely said from diffraction examinations with trasmission-electron-microscope that each layer of the multilayers is polycrystalline. Interesting absorption spectra obtained at 80 K for KCl-KI series, namely, curve 1; a single KI 200A layer (denoted SL), 2: a 2.5 periods of KCl 200A-KI 100A (A-ML), 3: KCl 150A plus 3 periods of KI 50A-KCl 100A (B-ML), and 4: KCl 120A plus 5 periods of KI 30A-KCl 80A, are shown in Fig. 1. On the SL spectrum, a large peak at the lowest photon energy is due to one of the KI spin-orbit-splitted bulk-exciton, and a next rise is corresponded to interband threshold. It should be noted that, on the respective spectrum of the multi-layers, the bulk-exciton peak persists its energy position and splitted into doublet with a separation of about 0.05 eV. On the other hand, 80 K spectra obtained for KBr-KI series, namely, 2.5 periods of KBr 150A-KI 100A and 3.5 periods of KBr 150A-KI 50A, are shown in Fig. 2 together with KI 200A single layer spectrum. On the KI 100A multilayer spectrum, a blue-shifted spike (by 0.06 eV) is observed contrary to the KCl-KI series. This might be explained with terms of the interface-mixture because of KCl and KI are hard to mix each other[2], whereas KBr and KI are easely mixed as in the cases of KCl-KBr series[1]. Origin of the peak-splitting on the KCl-KI series is not known in this moment.

1. A. Ejiri and K. Nakagawa: submitted to Phys. Rev. B.
2. H. Mahr : Phys. Rev. 125, 1510 (1962).

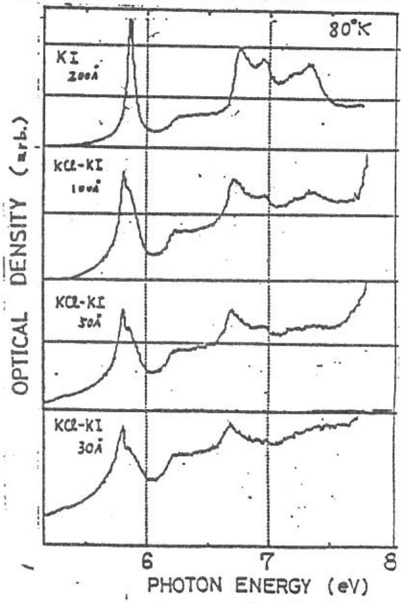

Fig. 1. Absorption spectra of the KCl-KI series. Top curve; SL, 2nd; A-ML, 3rd; B-ML, and 4th; C-ML.

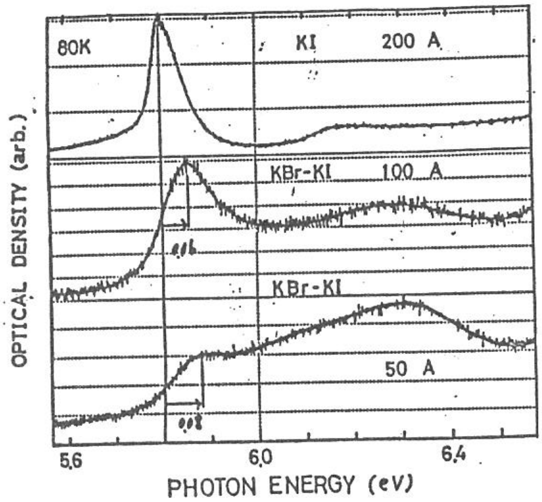

Fig. 2. Absorption spectra of the KBr-KI series. Top curve; SL, 2nd; 2.5 periods of KBr150A -KI 100A, 3rd; 3.5 periods of KBr 150A-KI 50A.

# Reflection Spectra of Silica Glass at low temperature in the VUV Region

Jun MATSUOKA, Michel COURBIERE, Hiroshi YAMANAKA,
Hiroshi YAMASHITA, Junji HAYAKAWA

Government Industrial Research Institute, Osaka

Refractive index (n) of silica glass (a-$SiO_2$) is a function of wavelength and temperature. It increases as wavelength goes down or temperature glows up. Moreover, its temperature coefficient (dn/dT) reaches at $10x10^{-6}$/K around 248 nm, which is about twice the value at 546 nm.1)

Present paper reports on the reflection spectra of silica glass at room and low temperatures in the vacuum ultra-violet region in order to know why the refractive index of the glass increases with temperature. We aimed to observe peak shifts of 1st and 2nd bands by decreasing temperature, which are located at 10.3 and 11.6 eV at room temperature,respectively.2) Crystalline quartz, which has the same chemical formula as the silica glass ($SiO_2$) but has a larger thermal expansion coefficient ($\alpha$=131and $74x10^{-7}$/K) than the glass($\alpha=4x10^{-7}$/K), was also measured for comparison. Informations about the silica glass and quartz will give us further insights into the refractive index properties of optical glasses which are composed of several modifier elements added to the glass forming $SiO_2$.

The glass samples were made by Verneuil(VN), soot(ST) and sol-gel(SG) methods. Light source was a SOR (Synchrotron Orbital Radiation) at Institute for Molecular Science, UVSOR facility. The VUV light was dispersed by a 1m Seya-Namioka monochromator whose Rowland circle was vertically arranged to conserve the degree of polarization of SOR. A thin plate of LiF crystal was inserted in front of a sample chamber to remove 2nd and higher order lights and to get wavelength reproducibility by using sharp cut-off property of the crystal. The wavelength reproducibility was estimated to be better than ±5 meV.

The reflection spectra obtained at room temperature (299 K) are in good agreement with the previous report.2) At low temperature (82 K), the 1st band of glass samples shows a high energy shift by about 50 meV as shown in Fig.1. There were no clear distinctions between the glasses made by different methods, and the spectra of VN are shown in the figure as a representative. Spectra of quartz are consisted of ordinary (o; $E\perp c$) and extra-ordinary (e; $E\parallel c$) components. The 1st bands show high energy shift by about 80 meV and 40 meV for o- and e-components, respectively, at 82 K (Fig.1). The 2nd bands of the glass and crystal show high energy shift, but they are too broad to say the shift energy quantitatively.

The refractive index at the low energy side adjacent to the reflection peak becomes high as a result of dispersion relation. Therefore, the dispersion curve (n versus photon energy) should shift, with some approximations, to high energy side by the same energy as that of reflection peak shift.

Fig.2 shows a comparison between the experimental dn/dT curve1) and theoretical one which is calculated from two dispersion curves displaced each other by 50 meV. Agreement is fairly good nevertheless the rough approximation adopted here. Due to the roughness of approximation, mismatch between the curves is larger in the long wavelength region than in the short one. Therefore, it is safe to say that dn/dT of silica glass is caused,mainly, by energy shift of the 1st and 2nd bands in the VUV region.

For crystalline quartz, thermal expansion effects must be taken into account besides the peak shift ones, because the $\alpha$'s of quartz are about 30 times larger than that of the glass. The thermal expansion effects will result in decrease of the VUV reflectivity as a whole. And the reflectivity decrease will bring out decrease of the refractive indices. For this reason, the dn/dT of quartz[3] is of positive sign in the UV regions where the slope of dispersion curve is steep, while it is of negative sign in the visible regions where the slope is slow and expansion effect is dominant. This explanation is also in accordance with our empirical data that glasses with $\alpha$ more than $80\times10^{-7}$/K have, in general, negative values of dn/dT in visible or near IR regions.

1) T.Kitaoka et al, Annual meeting of Japn. Ceramics Soc. May (1988)
2) L.Pasanova, Czech. J. Phys. B19 p1265 (1969)
3) F.J. Micheli, Ann. Physik, 4 p7 (1902)

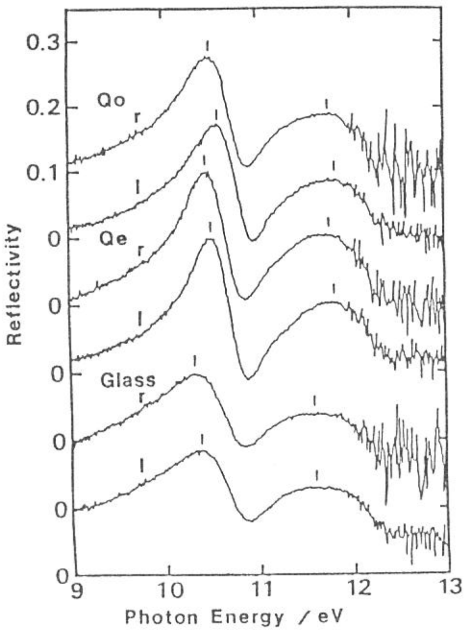

Fig.1 Reflection spectra of silica glass and quartz at room (r) and low (l) temperatures.

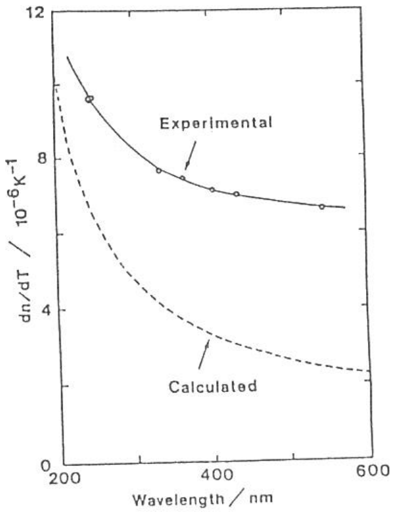

Fig.2

Comparison of dn/dT between experimental and calculated values for silica glass.

# VUV OPTICAL PROPERTIES OF $SiO_2$ FILMS DEPOSITED BY DIRECT PHOTO-EXCITATION CVD

Masanori OKUYAMA, Kohji INOUE, Masakazu NAKAMURA and Yoshihiro HAMAKAWA

Department of Electrical Engineering, Faculty of Engineering Science,
Osaka University, Toyonaka 560

Optical properties of $SiO_2$ thin films have been studied in VUV light region of photon energy between 6 and 25eV. The $SiO_2$ films were deposited on Si or $MgF_2$ from $Si_2H_6$ and $O_2$ by photo-induced CVD(chemical vapor deposition) using $D_2$ lamp or rare-gas resonance lamp.

VUV reflectances of the $SiO_2$ films on Si were measured in the region from about 8 to 25eV. Figure 1 shows reflectances of the film oxidized thermally at 1000°C and the photo-CVD films deposited at 25 and 177°C. These reflectance data can not be analyzed directly with Kramers-Kronig dispersion relation, as there are large interference oscillations in the reflectance spectra. Therefore, refractive indices, n, and extinction coefficient, k, have been obtained by comparison of the measured reflectance with calculated reflectance which is analyzed from modified k with the Kramers-Kronig relation[1,2] The modified k were calculated by giving reduction, broadening and tail to k of fused quartz,[3] and refractive indices were calculated also from the modified k with the Kramers-Kronig relation. The calculated reflectances give good agreement with the experimental reflectances within errors of several percents. Figure 2 shows the obtained n and k spectra of fused quartz film and the photo-CVD films deposited at 25 and 177°C. n of the photo-CVD films extrapolated to 6328Å agree well with n measured with ellipsometric analysis. The k values of the photo-CVD film deposited at 177°C are much close to those of the quartz. But those at 25°C are much lower than those of the quartz, and are broadened pretty. These facts show that density of the photo-CVD film becomes large with increase of the substrate temperature.

Absorption coefficient spectra were obtained from the transmittance of the $SiO_2$ films on $MgF_2$ near the fundamental edge to study localized levels. Figure 3 shows the absorption coefficient spectra, $\alpha$, of quartz and the films. $\alpha$ shift to lower energy region with decrease of the deposition temperature. This is why the film density increases and Urbach tail reduces with increase of the substrate temperature. A absorption peak is found around 7.6 eV in the films deposited at high temperature, especially at 280°C. This peak has been estimated to oxygen-deficient defect, but shows different substrate-temperature dependences from those of the other physical parameters such as infrared absorption intensities of SiH or SiOH, fixed oxide charge density and ratio of ESCA peak intensity of Si to that of O.

## References

1) K. Inoue, M. Nakamura, M. Okuyama and Y. Hamakawa: The Institute of Electronics, Information and Communication Engineers (IEICE) Technical Report SDM88-126, Vol. 88, No.309 (1988) 37-41 (in Japanese).

2) K. Inoue, M. Okuyama and Y. Hamakawa: to be published in Appl. Surf. Sci.

3) H. R. Philipp: Handbook of Optical Constants of Solids, ed. by E. D. Palik, Academic Press, Inc., 1985.

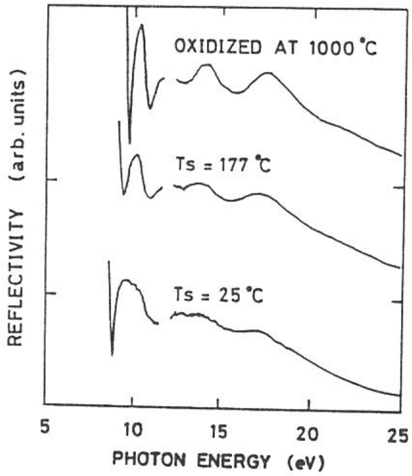

Fig. 1. Reflectance spectra of $SiO_2$ films oxidized at 1000 °C and deposited at 25 and 177°C.

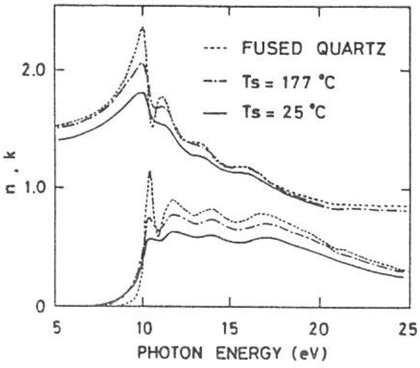

Fig. 2. n and k spectra of quartz and photo-CVD films.

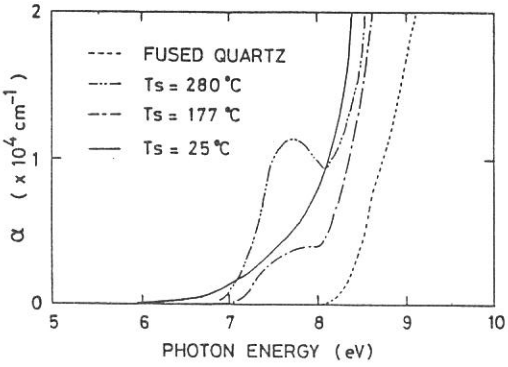

Fig. 3. Absorption coefficient spectra of quartz and photo-CVD films.

# Exciton Luminescence In LiBr Crystals

Koji FUJIWARA, Hitoshi NISHIMURA, Masaaki NAKAYAMA,
Teruo KOMATSU* and Satoshi HASHIMOTO**

Department of Applied Physics, Osaka City University,
Sumiyoshi, Osaka 558
* Department of Physics, Osaka City University, Sumiyoshi,
Osaka 558
** Kyoto University of Education, Fukakusa, Fushimi, Kyoto 612

The luminescence associated with self-trapped excitons (STE's) in alkali halides has extensively been studied over the past ten years.1),2) In LiBr, however, there have been few studies on the luminescence for the reasons that the first exciton-absorption peak lies in the VUV region, and the crystals are highly hygroscopic. In 1970 Pooley and Runciman first observed the luminescence spectra in LiBr using x-ray for excitation and concluded that there appear two luminescence bands associated with the STE's: one is lying at 5.30 eV, short-lived, and due to the singlet state, and the other is at 3.95 eV, long-lived, and due to the triplet state. On the other hand, in the alkali halides consisting of a large radius anion and a small radius cation, e.g., LiI, LiCl, NaI and NaBr, the singlet band is unobservable or overlaps with the triplet band4) for the reason that the STE's in these crystals are less localized and the exchange energy leading to the energy separation between the singlet and triplet exciton states is very small. For the same reason, it is expected for LiBr that the singlet band separated from the triplet band is absent.

In the present study, a specially designed cryostat to cleave the highly hygroscopic LiBr crystals in the site at 6 K and in a high vacuum ($<10^{-8}$ Torr) is used. The luminescence spectra of LiBr at 6 K measured using the BL7B beam line of UVSOR are shown in Fig. 1. Before the cleavage, the sample emits three luminescence bands peaking at 5.30, 3.95 and ~ 2.8 eV [Fig. 1 (a)]. However, by the cleavage, the 5.30 eV band becomes negligible and the 2.8 eV band completely disappears [Fig. 1(b)]. Therefore, it is concluded that both 5.30 and 2.8 eV bands are extrinsic, i.e., the singlet band is absent in LiBr, and that only the triplet band peaking at 3.95 eV appears as an intrinsic luminescence in LiBr.

The intensity of the 5.30 eV impurity band abruptly decreases above 10 K, while the intensity of the 3.95 eV intrinsic band increases instead (Fig. 2). This result may be attributed to the self-trapping of the free excitons (FE's). From this assumption, the potential barrier height for self-trapping is obtained to be about 7 meV by using an Arrhenius plot to the data of the 5.30 eV band.

The 5.30 eV impurity band is excited in the band-to-band transition region as much as in the exciton band region. This suggests that the holes in LiBr are metastable at low temperatures and recombine with electrons to form FE's whose energies transfer to impurities.

## References

1) M. N. Kabler, Phys. Rev. 136, A1296 (1964)
2) M. Ikezawa and T. Kojima, J. Phys. Soc. Jpn. 27, 1551 (1969)
3) D. Pooley and W. A. Runciman, J. Phys. C: Solid State Phys. 3, 1815 (1970)
4) K. Kan'no et al., unpublished

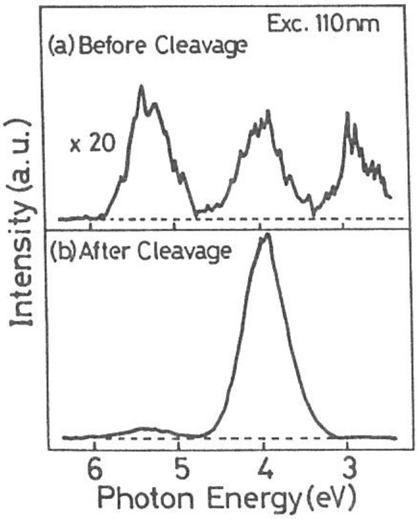

FIG.1.
Luminescence spectra of LiBr at 6 K: (a) before cleavage and (b) after cleavage in a high vacuum condition.

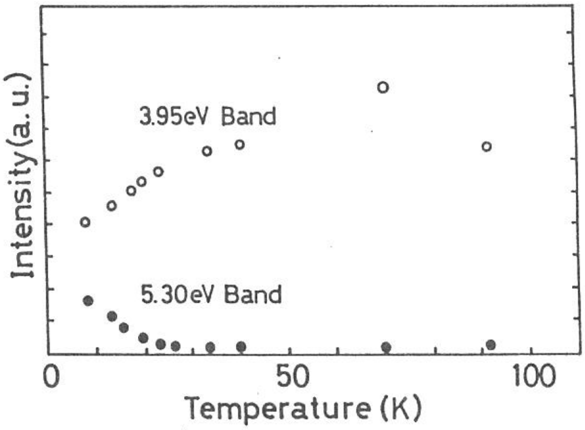

FIG.2.
Temperature dependence of the 3.95-eV band intensity (open circle) and the 5.30-eV one (closed circle) of cleaved LiBr.

# A New Aspect of Intrinsic Luminescence in NaBr and NaI

Ken-ichi KAN'NO, Koichiro TANAKA, Hideo KOSAKA, Takuya MUKAI, Yoshio NAKAI, Minoru ITOH,[a] Takeshi MIYANAGA,[b] Kazutoshi FUKUI,[c] and Makoto WATANABE[c]

Department of Physics, Kyoto University, Kyoto 606
a) Department of Applied Science, Shinshu University, Nagano 380
b) Department of Physics, Faculty of Education, Wakayama University, Wakayama 640
c) UVSOR, Institute for Molecular Science, Myodaiji, Okazaki 444

In many alkali halides, intrinsic luminescence consists of two broad bands, called $\sigma$ and $\pi$ emission according to its polarization. The $\sigma$ emission, which has not been observed in four crystals KCl, RbCl, NaBr and NaI, appears at higher energy with short lifetime less than 10 ns, and has been attributed to the allowed transition from the excited singlet state ${}^1\Sigma_u^+(2s\sigma_g)$ of a self-trapped exciton (STE). The $\pi$ emission appearing at lower energy with much longer lifetime has been attributed to the spin-forbidden transition from the lowest triplet state ${}^3\Sigma_u^+(1s\sigma_g)$. That is, it has been believed so far that it is not uncommon for alkali halides to exhibit only $\pi$ emission but that $\sigma$ emission never occurs alone. There has remained unsolved the question why one or two emission bands occur in a particular crystal, nor can the energies at which emission occurs be adequately explained.

In the present study, decay behavior of the $\sigma$ and/or $\pi$ emission of nine crystals, NaCl, KCl, RbCl, NaBr, KBr, RbBr, NaI, KI and RbI, was measured systematically under the single bunch operation of UVSOR, using the combination of a Seya-Namioka type monochromator at BL1B and a time-correlated single-photon counting system. The results obtained in the crystals except NaBr and NaI were essentially the same as those of previous studies by Kabler and Patterson[1)] and by Blair et al.[2)] In contrast with the $\pi$ emission (2.26 eV) in KBr, the $\pi$ emission in NaBr, which appears at exceptionally high energy (4.65 eV), was found to consist not only of the long-lived phosphorescent component but also of a fast decay component (fluorescence), as shown in Fig. 1(A). Very similar situation was confirmed to be the case also for the $\pi$ emission (4.24 eV) in NaI (Fig. 1(B)). Time-resolved measurements of these emission bands revealed that both decay components have almost the same spectral shape. This evidenced that both of them come from the exchange pair of the singlet state and the triplet state having the same electronic orbital.

In view of big difference in both the decay behavior and the peak energy of $\pi$ emission between in NaBr and in KBr, emission spectra and their decay curves were investigated in various systems of NaBr$_{1-x}$- KBr$_x$ $(0 \leqq x \leqq 1)$ mixed crystal. The $\pi$ emission peak in NaBr was found to be connected not to the $\pi$ emission peak in KBr but to the $\sigma$ emission peak (4.40 eV) in changing x. As shown in Fig. 2, the long-lived triplet component decreases with increase in x, and the singlet one has grown into the $\sigma$ emission of KBr.

From these evidences, we conclude that the $\pi$ emission in NaBr does not belong to the family of so-called $\pi$ emission in other crystals but to that of $\sigma$ emission and should be attributed to the radiative decay from 2s-STE states $^{1,3}\Sigma_u^+(2s\sigma_g)$. The situation will be the case in NaI.

1) M.N.Kabler and D.A.Patterson: Phys.Rev.Lett. 19 (1967), 652.
2) I.M.Blair, D.Pooley and D.Smith: J.Phys.C, Solid State Phys. 5 (1972), 1537.

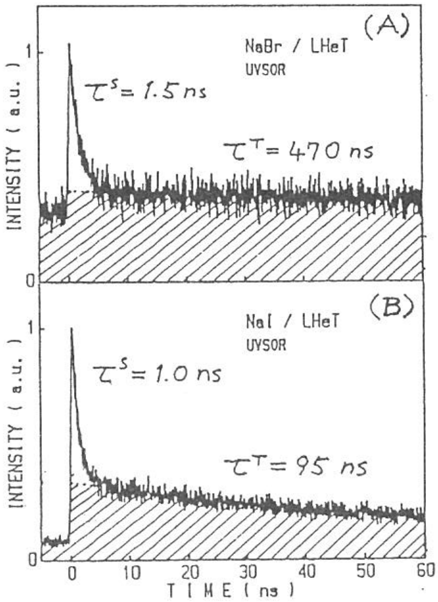

Fig. 1

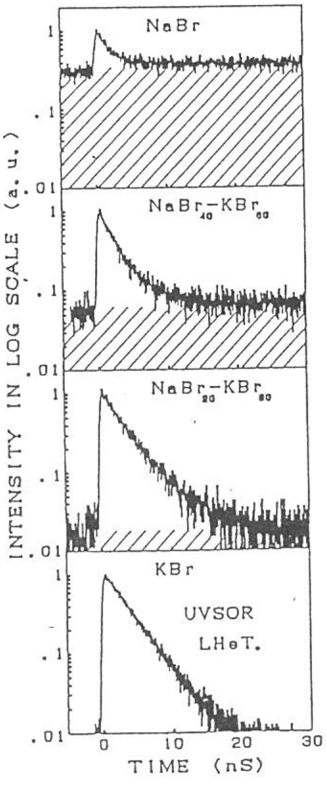

Fig. 2

Fig. 1 (A) Decay curve of $\pi$ emission in NaBr (4.65 eV) and (B) in NaI (4.24 eV) at 7 K.

Fig. 2. Change in decay curve of ~4.6 eV emission in NaBr-KBr mixed crystals.

# New Luminescence Bands in Alkali Chlorides Excited with Undulator Radiation at Low Temperature

Kazutoshi FUKUI, Toshiki DEGUCHI[1], Masami FUJITA[2], Takeshi MIYANAGA[3],
Hideyuki NAKAGAWA[1], Hiroaki MATSUMOTO[1] and Makoto WATANABE

*Institute for Molecular Science, Myodaiji, Okazaki 444*
[1] *Department of Electronics, Fukui University, Fukui 910*
[2] *Maritime Safety Academy, Wakaba, Kure 737*
[3] *Department of Physics, Faculty of Education, Wakayama University, Sakaedani, Wakayama 640*

Luminescence measurements of alkali chlorides (NaCl, KCl and RbCl) have been made at low temperature using non-monochromatized undulator light as the strong excitation light of VUV. The characteristics of the undulator light are given in Table I. A Jobin-Yvon HR-320 monochromator was used to measure the emission spectra. The lifetime measurements were carried out by the TAC method under the single bunch operation in which one can utilize the pulsed light of 450 ps width with 178 ns interval.

Figure 1 shows the emission spectra of NaCl, KCl and RbCl at 12 K. The emission band of NaCl from 3 to 4 eV and those of KCl and RbCl from 2 to 3 eV are well known π emission bands. In KCl the π emission band seems to have two peaks. This is due to the reabsorption of F-center at 2.3 eV. The reabsorption of F-center can also be seen in spectrum of RbCl at about 2 eV. Around 5 eV, one can find the emission band (5eV emission band) in each spectrum. This band of NaCl is σ emission. However, 5 eV emission bands of KCl and RbCl have not been known. Figure 2 shows the decay curves of higher and lower energy parts of 5 eV emission band in KCl. The fact that the lifetimes of the two curves are different indicate that 5 eV emission band consists of two emission bands. The lifetime of the lower energy part is about 1.8 ns which is quite similar to the lifetime of the emission due to the dimers of bromine impurity in KCl. The lifetime of the higher energy part is about 2.5 ns. The luminescence with the lifetime of 2.5 ns has not been known. The 5 eV emission band in RbCl is more complicated than in KCl. The 5 eV emission band in RbCl consists of more than 2 bands as shown in Figure 1. Figure 3 shows the decay curves of higher and lower energy parts of 5 eV emission band in RbCl. It is not unique to deconvolute the curve into components. However, the lower energy part of this band may consist of 3 components (< 0.5 ns, ~4 ns and ~130 ns) and the higher energy part may consist of 3 components (~2 ns, ~7 ns and ~40 ns). The component with 130 ns lifetime may be the emission due to the dimer of iodine impurity in RbCl.

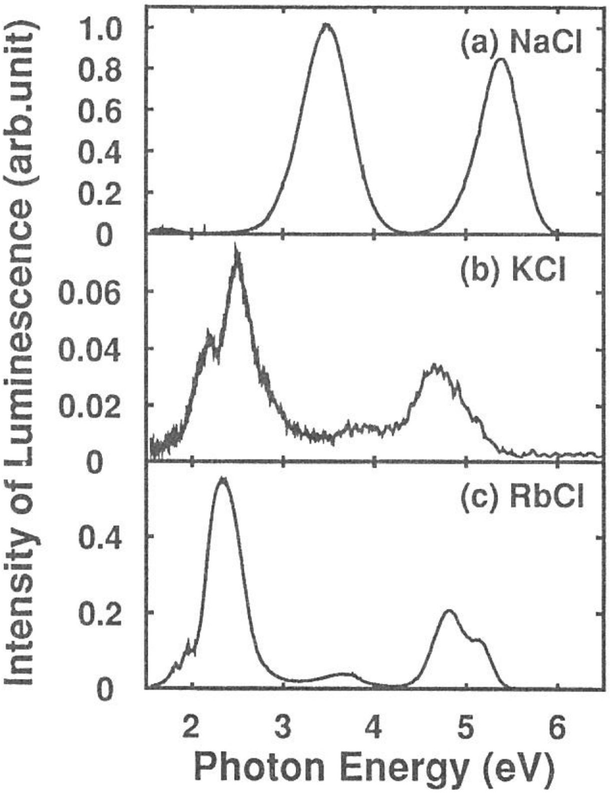

Fig. 1. Emission spectra of (a) NaCl, (b) KCl and (c) RbCl at 12 K

Table I.
Characteristics of undulator radiation

| | |
|---|---|
| peak wavelength | ~ 30 nm |
| bandwidth | ~ 5 % |
| baem spot † | ~ 1 mmϕ |
| number of photons †‡ | ~ $10^{14}$ /s |

† at the sample position
‡ with about 1500A thick Al film

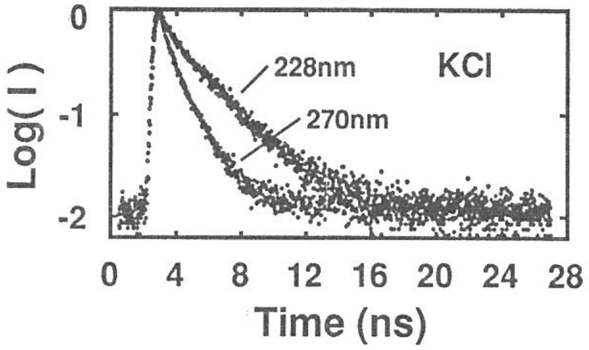

Fig. 2.
Decay curves at higher (228 nm) and lower (270 nm) parts of the 5 eV emission band in KCl.

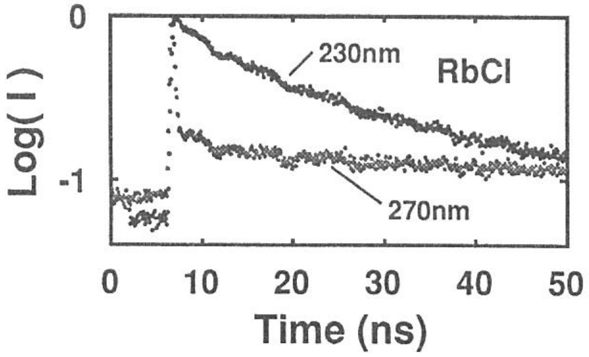

Fig. 3.
Decay curves at higher (230 nm) and lower (270 nm) parts of the 5 eV emission band in RbCl.

# THE LIFETIMES OF THE AUGER-FREE LUMINESCENCE FROM CsF, CsCl, CsBr, AND RbF

Shinzou KUBOTA,(1) Satoshi HASHIMOTO,(2) Minoru ITOH(3), Jian-zhi RUAN(GEN),(1) and Shiro SAKURAGI(4)

(1) Rikkyo University, Nishi-Ikebukuro 3, Tokyo 171
(2) Kyoto University of Education, Fushimi-ku, Kyoto 612
(3) Department of Applied Science, Faculty of Engineering, Shinshu University, Nagano 380
(4) Union Material Inc., Tone-machi, Kitasoma, Ibaraki 270-12

We have reported the first direct evidence of the luminescence due to interatomic radiative transition of valence band electrons to outermost-core-hole states in CsF, CsCl, CsBr, and RbF, of which the band gap energy $E_g$ is larger than the energy difference $E_{vc}$ between the top of the valence band and the outermost-core-hole state($E_g > E_{vc}$). We have proposed the term "Auger-free luminescence", emphasizing that this transition emits photons without ejecting Auger electrons.[1]

In this experiment the lifetimes of Auger-free luminescence from CsF, CsCl, CsBr, and RbF were measured by using 5.632 MHZ UVSOR single bunch and by a single-photon counting method. Energy resolved luminescence photons were detected by a MCP photomultiplier (Hamamatsu R1564U-030). The trigger pulse from this photomultiplier was used to start a time-to-amplitude converter, while UVSOR rf signals were used as stop pulses.

Figure 1 shows the typical decay curve of 385 nm band in CsF under 21.4 eV photon-excitation. Solid curve shows the best fitted calculation of convoluted decay curve to the experimental points by using the system response curve. Figure 2 shows typical decay curve of the 250 nm band in CsBr under 21.4 eV photon-excitation. Time response of the scattering light is also shown for comparison.

The measured decay times are 2.9 ± 0.1 ns (CsF), 0.9 ± 0.2 ns (CsCl), 0.10 ± 0.05 ns (CsBr), and 1.3 ± 0.1 ns (RbF) at room temperature. The emission arises from allowed transitions, the measured lifetimes were not surprising except the lifetime for CsBr.

The temperature dependence of the lifetime and of the luminescence intensity for 250 nm band in CsBr were measured in the temperature region of 77 - 300K. The results are shown in Fig. 3. The lifetime was observed to be 1.34 ± 0.05 ns at 77 K and the lifetime decreases with increasing temperature. The decrease in the intensity was also observed with increasing temperature and the intensity at 300 K was 1/100 of that at 77 K. These decreases will be explained with (i) activation of Auger electron emission at higher temperatures because of a reduction in $E_g$ of the order of 0.2 eV on increase in temperature, and/or (ii) activation of high-temperature hopping diffusion of cation self-localized holes and their transfer to states at which radiative recombination was hindered.[2]

References

1. S.Kubota et al.Phys. Rev. Lett. 60 (1988) 239.
2. Yu.M.Aleksandrov et al. Sov. Phys. Solid State 29 (1987)587.

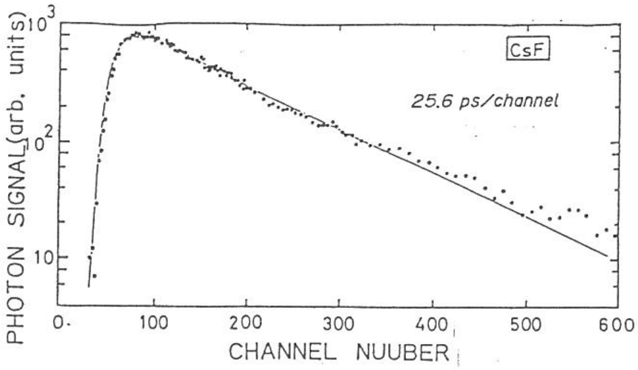

Fig. 1. Time dependence of the 385 nm band in CsF excited by 21.4 eV photons. A solid line shows the best fitted curve to the experimental points.

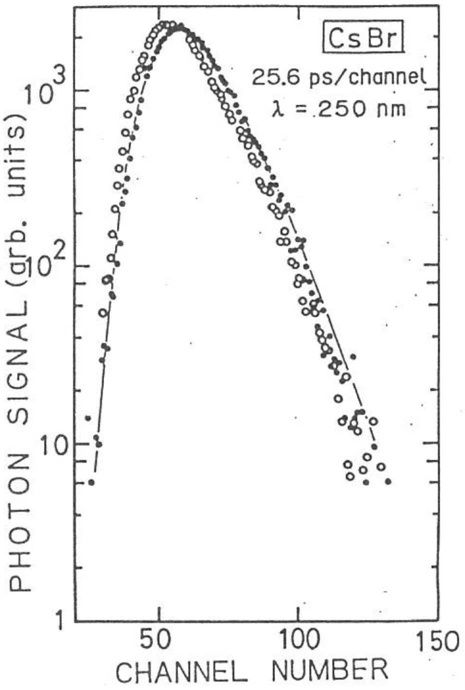

Fig. 2. Time dependence of the 250 nm band in CsBr excited by 21.4 eV photons( ● ). A solid line shows the best fitted curve to the experimental points. Time response of the scattered light is also shown for comparison (○).

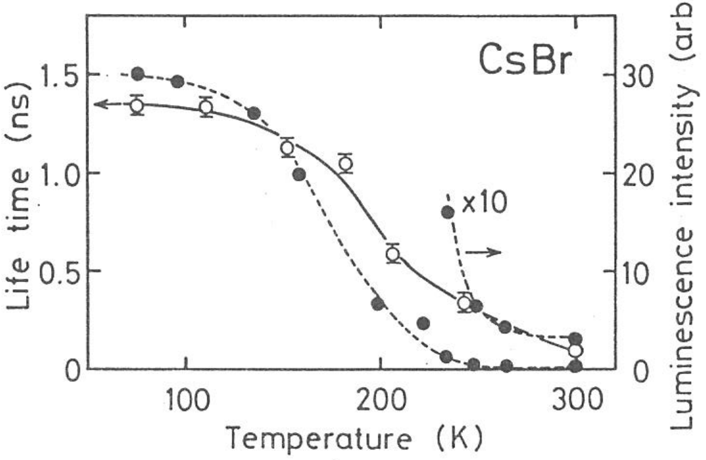

Fig.3. Temperature dependence of the lifetime and the luminescence intensity for 250 nm band in CsBr.

# Threshold Energy for Photogeneration of Self-Trapped Exciton in $SiO_2$

K. Tanimura, C. Itoh and N. Itoh

Department of Physic, Faculty of Science, Nagoya University,
Chikusa, Nagoya 464-01

and

M. Itoh

Department of Applied Science, Faculty of Engineering,
Shinshu University, Nagano 380

The response of $SiO_2$ to ionizing radiation is a topic of considerable current interest from both fundamental and practical view points.1,2) There are abundant experimental results suggesting that the blue luminescence around 2.8 eV is due to radiative recombination of self-trapped excitons. However, the composite properties of the luminescence band3) prevented us to obtain clear and direct experimental evidence. We have characterized each component of the blue luminescence by measuring polarization and time-resolved properties, and shown that only the emission band, which is peaked at 2.73 eV and polarized along the z axis, is intrinsic.4,5) The purpose of the present investigation is to measure the excitation spectrum and to determine the threshold energy of photogeneration of this luminescence component.

In Fig.1 is shown the obtained excitation spectrum of the 2.73-eV luminescence in $SiO_2$ at 80 K. The threshold energy of 8.3 eV seen in the figure agrees with the fundamental optical absorption edge,6) indicating that the band is intrinsic and is related to exciton. Thus we have proven that the luminescence peaking at 2.73 eV is due to the radiative recombination of the self-trapped excitons. It has been shown

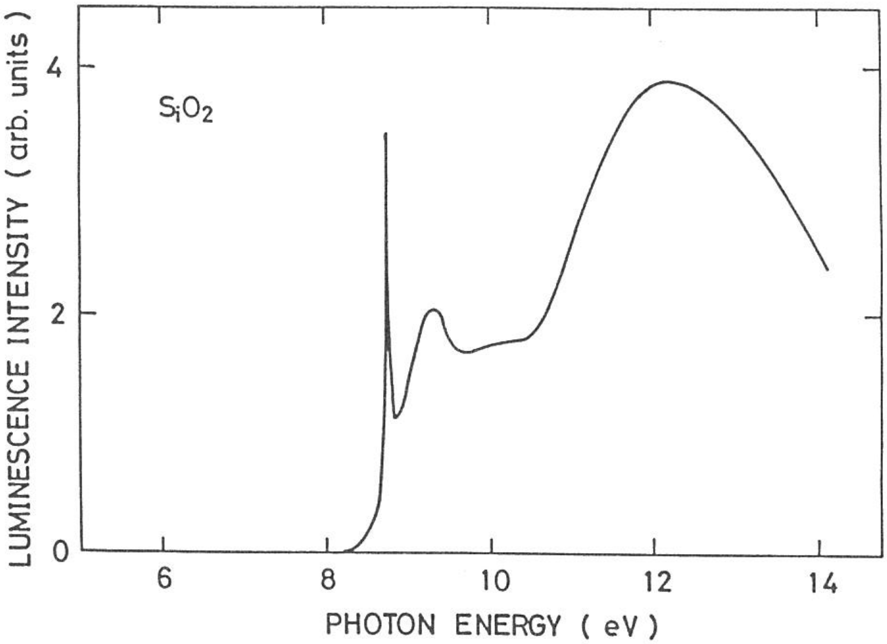

Fig.1 Excitation spectrum for the 2.73-eV luminescence in $SiO_2$ measured at 80 K

that the hole in $SiO_2$ is not self-trapped.[7] Thus electron-phonon and hole-phonon interactions are considered to make additive contributions in exciton self-trapping in $SiO_2$.

## References

1) N. Itoh, Proceedings of the International Conference on Defects in Insulating Crystals, edited by F. Luty(Gordon and Breach, New York, 1985).

2) E. A. Gerber and A. Ballato, "Precision Frequency Control" (Academic Press, New York, 1985).

3) P. L. Mattern, K. Lengweiler and P. W. Levy, Radiat. Eff. 26, 237(1975).

4) K. Tanimura and L. E. Halliburton, Phys. Rev. B34, 2933(1987).

5) C. Itoh, K. Tanimura and N. Itoh, J.Phys. C21, 4693(1988).

6) I. T. Godmains, A. N. Trukhin and K. Hubner, Phys. Status Solidi, B116, 279(1983).

7) W. Hayes and T. J. L. Jenkin, J. Phys. C19, 3211(1986).

# VUV EXCITED LUMINESCENCE OF CUBIC BORON NITRIDE

Yoshiki Wada, Koh Era and Osamu Mishima

National Institute for Research in Inorganic Materials, Tsukuba 305

Cubic boron nitride (cBN) is the widest band gap (>6.4 eV) semiconductor material having both p- and n-type. Recently, ultraviolet light-emitting diode (LED) action of cBN has been established as to pn junctions [1]. This suggests potentialities of cBN as new optoelectronic materials. However, few studies have been made on the fundamental electronic properties of cBN. In order to elucidate light-emitting mechanisms of the LED, we have measured luminescence spectra of cBN under VUV excitation using UVSOR light.

Crystals were prepared by a flux method under high pressure [2]. Intentionally doped p- and n- type crystals and non doped crystals were used for luminescence measurement. Luminescence from crystals cooled to liquid nitrogen temperature was excited by the UVSOR light monochromized by a 1 m Seya-Namioka type monochromator. Since the luminescence was very weak, it was measured by single photon counting method.

Luminescence spectra of these three kinds of crystals excited by 12.6 eV light seem similar to one another, having bands around 270 nm, 440 nm and longer than 550 nm. Luminescence spectra of n-type crystal are shown in Fig. 1-(a) ($E_{ex}$=9.5 eV), -(b) ($E_{ex}$=12.6 eV) and -(c) ($E_{ex}$=23.7 eV). ($E_{ex}$ is energy of excitation light. Fine structure is due to noise.) It is clearly seen that the relative intensity of the 270 nm band indicated by arrows decreases with increasing excitation energy. This band corresponds to the main luminescence band of the LED emission [3]. The band was not observed under cathode-ray excitation of 25 keV, but a band corresponding to the one longer than 550 nm was [3]. These facts are understood by assuming that the excitation process of the LED corresponds to the low energy (near the band gap energy) light excitation and that of the cathode luminescence to the high energy light excitation.

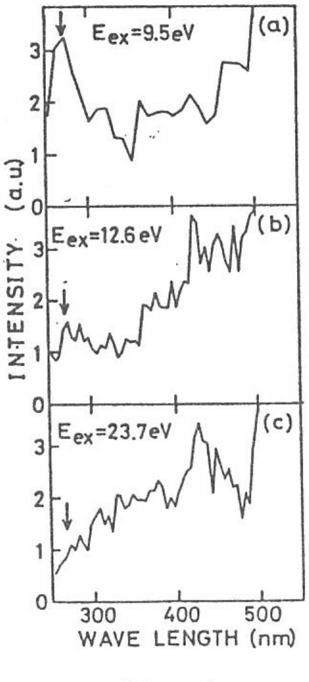

Fig. 1

[1] O. Mishima et. al., Appl. Phys. Lett. 53, 962 (1988).
[2] O. Mishima et. al., J. Appl. Phys. 61, 2822 (1987).
[3] K. Era et. al., Proc. Intnl. Workshop on EL, Tottori, 1988 (Springer, 1989) inpress.

# MECHANISM OF LUMINESCENCE FROM $CeF_3$

Shinzou KUBOTA,(1) Satoshi HASHIMOTO,(2) Jian-zhi RUAN(GEN),(1)
and Shiro SAKURAGI(3)

(1) Rikkyo University, Nishi-Ikebukuro 3, Tokyo 171
(2) Kyoto University of Education, Fushimi-ku, Kyoto 612
(3) Union Material Inc., Tone-machi, Kitasoma, Ibaraki 270-12

Very recently, Anderson,1) and Moses and Derenzo2) independently reported that $CeF_3$ is a fast, heavy scintillator which would be useful for applications to medical imaging and to high-energy physics. In order to study mechanism of luminescence from $CeF_3$, excitation spectra in the 5 - 40 eV region and decay times for $CeF_3$ have been measured.

Figure 1(a) shows the emission spectrum of $CeF_3$ excited by 21.4 eV incident photons, which excite the $Ce^{3+}$ 5p core to localized 5d states. For comparison, the emission spectrum of $CeF_3$ excited by 511 keV photons from $^{22}Na$ source is also shown in Fig. 1(b), together with the spectrum reported in Ref.1 shown in Fig.1(c). Luminescence bands having peak positions at 290 nm and 390 nm are observed.

According to Ref.3 a broad-band luminescence in the region 270 - 450 nm in $CeF_3$ under 5 eV photon-exciation is attributed to transitions from the localized 5d states of $Ce^{3+}$ to the 4f states. Figure 2 shows the excitation spectrum for 290 nm band together with the absorption spectrum and the reflectance spectrum from Ref.4. Five distinct excitation bands A through E are evident. The first peak A and the second peak B correspond to the direct excitaion of the localized 5d and 6s states of $Ce^{3+}$.3) The excitation band C results from excitation from the $F^-$ 2p valence-band to $Ce^{3+}$ 5d and 6s conduction bands, which terminates in the 4f states. The excitation band D which occur above 20 eV is assigned as the luminescence originating from the transitions of $Ce^{3+}$ $5p \rightarrow 5d$ type localized on $Ce^{3+}$ ions. Finally, transitions of 5p electrons to the conduction bands give the weak excitation band E.

Figure 3 shows typical decay curve of the 290 nm band in $CeF_3$ under 21.4 eV incident photon excitation. The exponential decay component with lifetime of 4 ± 1 ns is observed in the region of 77 - 300 K.

A difference between our measured emission spectrum and the reported spectra in Refs. 1 - 3 is that our crystal has luminescence band at 390 nm. The excitation spectrum for the 390 nm band was the same as that for 290 nm band but it's lower threshold energy of 0.1 eV. No fast component was observed from 390 nm band. No explanation is given for the origin of this band, and further study for this problem is required.

In conclusion, we expect that the radiative transition $5d \rightarrow 4f$ of $Ce^{3+}$ should also occur in $CeCl_3$, $CeBr_3$ and $CeI_3$. We intend to study the luminescence from these materials and look forward to develop of new-scintillators.

References

1. D.F.Anderson, IEEE Trans. on Nucl. Sci. Vol. NS-36 (1989) in press.
2. W.W.Moses and S.E.Derenzo, IEEE Trans. on Nucl. Sci. Vol. NS-36 (1989) in press.
3. L.R.Elias, Wm.S.Heaps, and W.M.Yen, Phys. Rev. 8 (1973) 4989.
4. C.G.Olson, M.Piacentini, and D.W.Lynch, Phys. Rev.18(1978)5740.

Fig.1. Measured emission spectra under 21.4 eV photon excitation (a), and under $\gamma$-ray excitation(b). The emission spectrum from Ref.1 is shown in (c). The excitation is 4.9 eV photons.

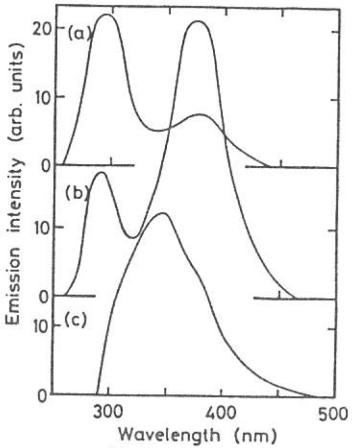

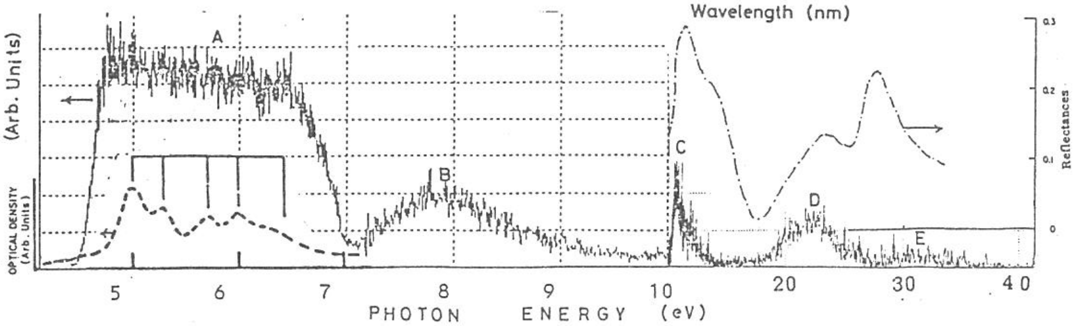

Fig.2. Excitation spectrum taken at 290 nm for $CeF_3$. Optical density and reflectance from Ref.6 are shown. Note the change of energy scale at 10 eV.

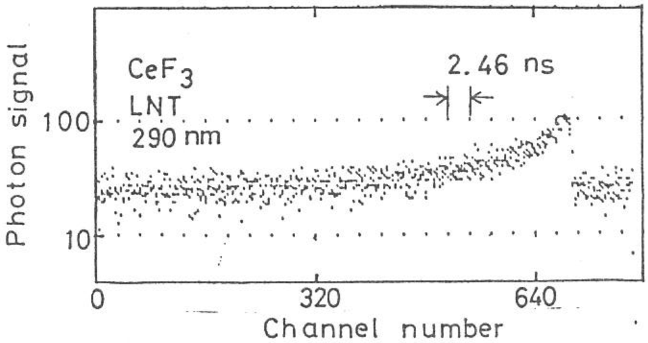

Fig.3. Time dependence of the 290 nm band in $CeF_3$ at liquid-nitrogen temperature. The excitation photon energy was at 21.4 eV. The data points are fitted to exponental decay of 4 ± 1 ns lifetime with 30 background

# Core Absorption Spectra of Amorphous and Crystalline GeTe Films

Kazutoshi FUKUI, Jun-ichiro YAMAZAKI, Tadaaki SAITO*, Shin-ichi KONDO*
and Makoto WATANABE

*Institute for MolecularScience, Okazaki 444*
**Department of Applied Physics, Fukui University, Fukui 910*

GeTe is one of the degenerate IV-VI semiconductors. As-deposit GeTe film (evaporated at room temperature) is known to be amorphous and becomes crystalline by annealing above 420 K. The resistivity shows an abrupt decrease from the order of 10 Ωcm (amorphous phase) to $10^{-3}$ Ωcm (crystalline phase) at the transformation temperature. 1) This transformation is irreversible. Core absorption spectra of Ge 3d level and Te 4d level of GeTe in both amorphous phase and crystalline phases were measured at BL2B1 equipped with a Grasshopper monochromator. GeTe samples were evaporated on the thin aluminum film (about 100 nm) at room temperature using electron beam gun. After that they were once exposed to air to be set on the cold end of a cryostat. At first we measured on the as-deposit films (amorphous phase) at 80 K. Secondly we annealed them *in situ* at 460 K and measured again on the annealed films (crystalline phase) at 80 K.

Figure 1 shows the absorption spectra of both amorphous and crystalline phase of GeTe in energy region from 27 to 37 eV. The gray solid line represents the spectrum in the amorphous phase and black one represents the spectrum in crystalline phase. This energy region corresponds to the transition from Ge 3d core level to the conduction band. In amorphous phase, a broad peak with a shoulder is observed. After crystallization, the broad peak in the amorphous phase changes into sharp doublet peaks. Figure 2 shows in energy region from 37 to 49 eV and the transition from Te 4d core level can be seen. After crystallization, the doublet structure in the amorphous phase becomes broad with several shoulders.

The structure due to the transition from Ge 3d core level in the amorphous phase is broad and it may reflect the density of state (DOS) of the conduction band. In the crystalline phase, the intensity ratio between the first and the second peaks of the Ge 3d sharp doublet at around 30 eV is about 2:3 which is different from the ratio of statistical weights between $M_V$ and $M_{IV}$ levels (3:2). This means the hole of Ge 3d core level become to have a strong exchange interaction with the electron. Therefore the doublet is due to excitonic transition. The doublet structure in the amorphous phase around 42 eV seems to correspond to the transition from the $N_V$ and $N_{IV}$ levels of the Te 4d core level, because the separation of the doublet is almost the same value as the spin-orbit splitting of the Te 4d level, 1.5 eV. After crystallization, the line shape becomes broad and this broad structure may reflect DOS of the conduction band. It is in contrast with the case of the transition from Ge 3d core level in which the structure in the amorphous phase may reflect the DOS. In previous work2), we measured the absorption spectrum of both amorphous and crystalline of another IV-VI semiconductors, SnTe. The line shapes of the structures due to the transition from Te 4d level are in good agreement with this result. On the other hand, the structures due to the transition from Sn 4d level are excitonic in both amorphous and crystalline phases, while the structure due to the transition from Ge 3d level i the crystalline is only excitonic and that in the amorphous phase is DOS-like.

Reference

1) S. K. Bahl and K. L. Chopra : J. Appl. Phys. **41** (1970) 2196.

2) K. Fukui, J. Yamazaki, T. Saito, S. Kondo and M. Watanabe : J. Phys. Soc. Jpn. **56** (1987) 4196.

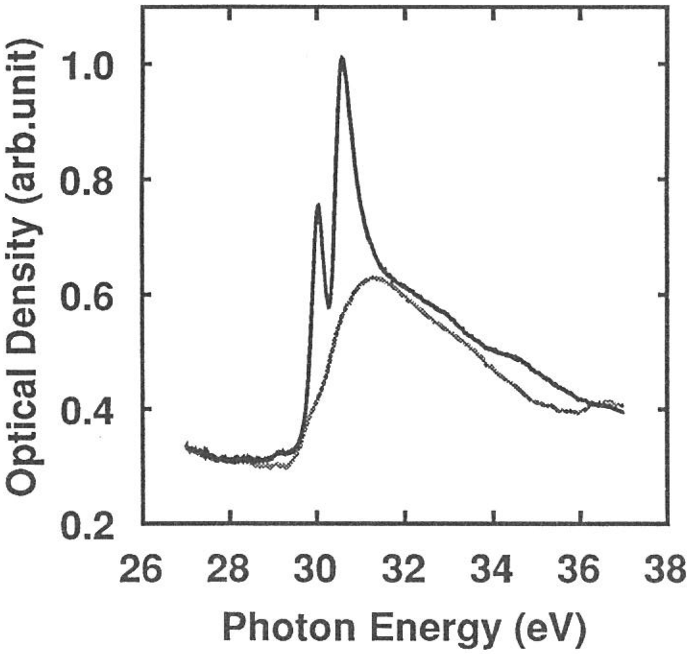

Fig. 1.
Absorption spectra of GeTe film at 80 K in the energy region 27 - 37 eV. Gray solid line represents the spectrum in the amorphous phase and black solid line, crystalline phase.

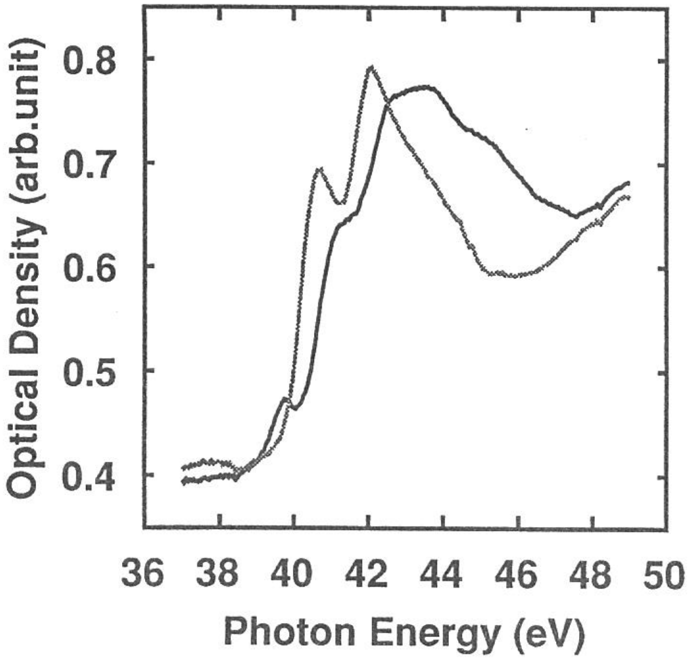

Fig. 2.
Absorption spectra of GeTe film at 80 K in the energy region 37 - 49 eV. Gray solid line represents the spectrum in the amorphous phase and black solid line, crystalline phase.

# EXAFS and XANES Studies of Light Elements using a New Soft X-ray Monochromator on BL7A

I. H. Munro*, T. Matsukawa+, T. Murata++, S. Naoe+++, M. Henderson**,
S. Marshall*, S. Gurman***

\+ College of General Education, Osaka University
++ Kyoto University of Education
+++ College of Arts & Science, Kanazawa University
* Daresbury Laboratory, Warrington WA4 4AD, UK
** Geology Department, Manchester University, UK
*** Physics Department, Leicester University, UK

A new, soft x-ray, two-crystal monochromator has been designed and installed for use on BL7A both in conjunction with Wiggler radiation and with radiation from a dipole magnet. Under the latter condition the monochromator has been used for experiments on a variety of sample materials, by making XANES and EXAFS type measurements at the edges of Na, Mg, Si, S, Cl. The monochromator design permits convenient and rapid interchange between different pairs of crystals and allows limited 'in situ' alignment. Beryl (2d = 1.5965 nm) and InSB (2d = 0.7481 nm) crystals are used to cover the ranges 800 eV to 3000 eV. The absolute energy (angle) calibration of the crystal monochromator is achieved by making a K-edge absorption measurement on thin Al foil.

XANES and EXAFS measurements were made by the total photo-electron yield method. The photo-electrons from the sample were detected using a 20-stage electron multiplier and picoammeter. Samples (usually ~100 mg quantities) were finely ground with about 20% graphite in a mortar and pestle to minimise sample charging effects. A thin layer of this sample powder mixed with acetone was then 'painted' onto the front surface of the first BeCu dynode of the electron multiplier. The reference signal was obtained from a clean BeCu first dynode and all signals were normalised using a ring current monitor. Data was collected locally on disc (PC-9800 micro-computer) and subsequently transferred to magnetic tape for processing at Daresbury Laboratory using the EXBACK and EXCURVE programmes. Measurements were made on 15 crystalline and glassy samples of silicate glasses at the Mg edge (1303 eV) and on 7 samples at the Na-edge (1071 eV). The accessible data range for EXAFS analysis was restricted to around 240 eV by the presence of aluminium absorption (1560 eV) associated with the Beryl crystal.

Measurements were made on the Cl edge (2833 eV) of $Fe((OC_2H_2OCH_2CO_2)(H_2O)_2Cl)$ and also on the S-edge (2472 eV) on a specimen derived from a single crystal of NiS. First results show a Ni-S EXAFS (see Fig.1) distance of 2.25Å using EXCURVE calculated phase shifts which is significantly below that determined from crystallographic data (2.39Å).

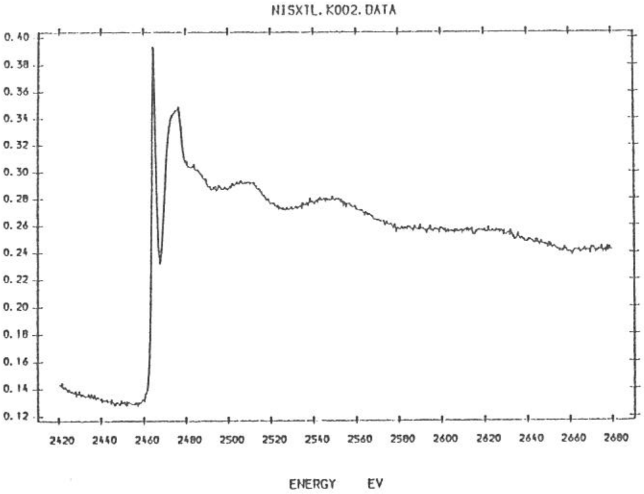

Figure 1
Nickel sulphide (NiS)
(sulphur edge data)

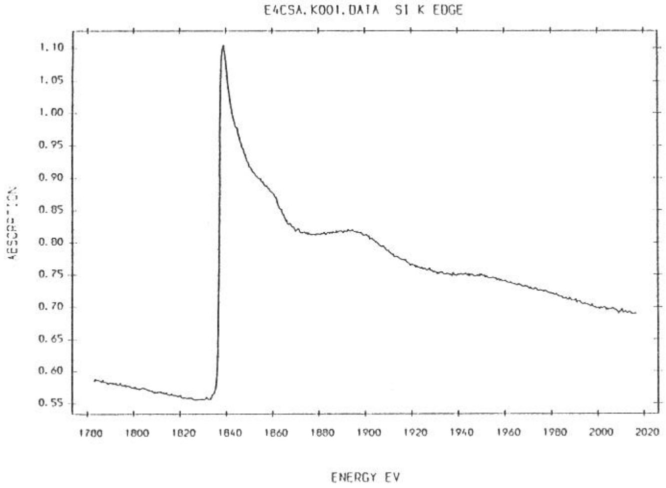

Figure 2
Thin film of
Cd/Si/As
(silicon edge data)

Finally, a series of absorption measurements were also made, in transmission, on Si (1839 eV) near-edge and EXAFS spectra for a range of thin film samples. Approximately 2 μm layers of various Cd/Si/As mixtures were supported on ~30 μm thick Be substrate (~70% transmitting). The composition of the films was $(Cd\,As_2)_xSi_{1-x}$ where x was varied from 0.5 to 0.2. An example is given in Figure 2.

# TOTAL YIELD SPECTRA OF PHOTOELECTRONS FROM L-EDGE OF GERMANIUM

Shun-ichi NAO-É, Takatoshi MURATA*, Kazutoshi FUKUI**
and Tokuo MATSUKAWA***,

Department of Physics, College of General Education, Kanazawa University,
Marunouchi, Kanazawa 920
*Department of Physics, Kyoto University of Education, Fushimi-ku,
Kyoto 612
**Institute for Molecular Science, Myodaiji, Okazaki 444
***Department of Physics, College of General Education, Osaka University,
Machikaneyama, Toyonaka 560

We have constructed a system for the measurement of total yield (TY) of emission of photoelectrons excited with soft X-ray at BL-7A of the UVSOR. Photoelectrons are detected with Hamamatsu R-595 electron multiplier with dc mode. In order to make the measurement electronics simple, the electric potential of the sample is set equal to that of the first dinode of the multiplier. For that purpose, the sample holder was insulated from the body of cryostat. Measurements were done in the vacuum of about $10^{-10}$ Torr.

Figure 1 shows a comparison of two spectra of Na K-edge of NaCl taken with a conventional transmission mode and with TY of photoelectrons at room temperature. As shown in the figure, two spectra are almost identical with each other. Sample used in the TY measurement was a single crystal cleaved in air. No apparent effect due to differences in surface condition of the sample and to charging-up were observed, which may be due to the large penetration depth of the X-ray.

In Fig. 2 are shown absorption and TY spectra of L-edge of Ge. Absorption measurement was made for evaporated thin film which may correspond to amorphous state, while the TY spectra was taken for the single crystal. In the TY spectrum, fine structure is observed in the $L_2$ and $L_3$ edge regions. A structure of $L_1$ edge is clearly observed in both spectra which is similar in shape with K-edge absorption spectrum.1) The background absorption at the $L_2$ and $L_3$ edge regions may be understood as a matrix element effect.2)

The spectra in the edge region in an expanded scale are shown in Fig. 3. Fine structures are clearly observed in the TY spectrum (curve b). The structure may be interpreted in relation to the electronic band structure of Germanium.3) Detailed discussion will be done elsewhere.

References

1) M.G.Proietti et al., Springe Proc. Phys. 2 26 (1984).

2) F.C.Brown, SOLID STATE PHYSICS ed. by H. Ehrenreich, F. Seitz and D. Turnbull (Academic Press, New York) 29 48 (1974).

3) T.M.Donovan and W.E.Spicer, Phys. Rev. Lett. 21 1572(1968)
W.E.Rudge and F.Herman, J. Non Cryst. Solids 8-10 653 (1972).

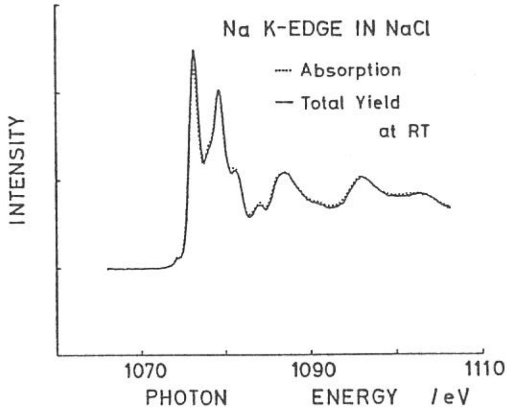

Fig. 1
Total yield (solid line) and absorption (dots) spectra of Na K-edge of NaCl at room temperature.

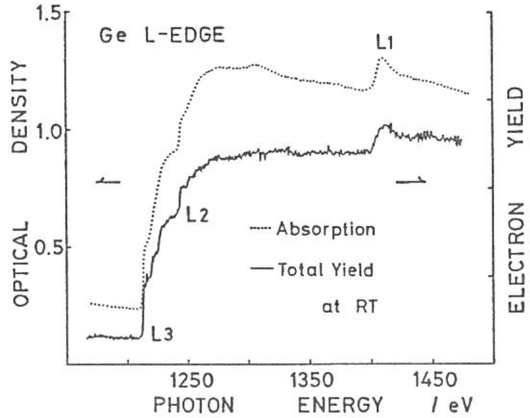

Fig. 2
Total yield (solid line) and absorption (dots) spectra of L-edge of Ge at room temperature.

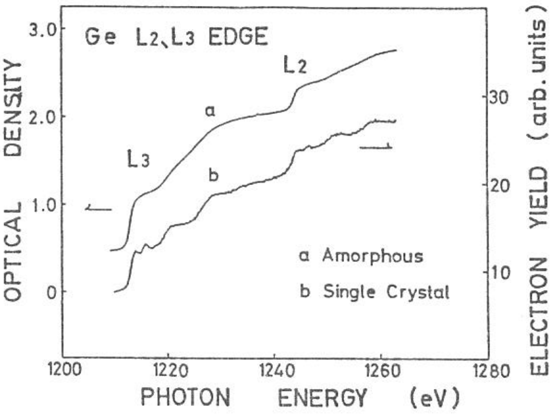

Fig. 3
Absorption (a) and total yield (b) spectra at edge region of Ge at room temperaure.

# K-edge Absorption Spectroscopy of Mg Bearing Minerals

I H Munro*, T Matsukawa, T Murata, S Naoe,
Institute for Molecular Science, Myodaiji, Okazaki 444.
*Visiting Scientist from Jan - May 1987

G N Greaves, M Henderson, J Charnock,
Daresbury Laboratory, Warrington WA4 4AD, Cheshire.

Magnesium is one of the "major elements" occurring in silicate materials, mainly in basic and ultrabasic rock types which form the bulk of the earth's crust and mantle. Radius ratio considerations of Mg and O suggest that the coordination of Mg should be 6 and this is the case in MgO (periclase), olivine (eg forsterite, $Mg_2SiO_4$) and pyroxene (eg diopside $CaMgSi_2O_6$). Such malic minerals usually exist as complete solid solutions between Mg and $Fe^{2+}$ end-members, ie ferromagnesian silicates. Mg is particularly interesting chemically in that it can enter smaller and larger coordinated sites. Thus in spinel ($MgAl_2O_4$) Mg is mainly 4- and Al 6-coordinated, while in pyrope garnet ($Mg_3Al_2Si_3O_{12}$) Mg is 8- while Al is again 6-coordinated. A total of 15 crystalline and glassy materials were studied by x-ray absorption spectroscopy using the soft x-ray monochromator on BL7A in April 1987. Crystallographic information taken from (1) and a summary of x-ray-determined bond lengths from a preliminary EXAFS survey for the materials studied are presented below. The raw data from UVSOR were analysed at Daresbury Laboratory using EXBACK and EXCURVE programmes.

MgO (periclase) was pure, synthetic MgO. Cubic 'rock salt' structure; space group Fm3m. Regular octahedral coordination; cell parameter a = +.211Å; Mg-O = 2.105Å.

$Mg_2SiO_4$ (Forsterite; mineral solid solution 90% forsterite; 10% feyalite ($Fe_2SiO_4$).) Structure based on separate $(SiO_4)^{4-}$ tetrahedra bonded by Mg (and $Fe^{2+}$) in octahedral sites, orthorhombic; Pbnm; a = 4.7534, b = 10.1902, c = 5.9783Å; Mg-O, Average 2.094 ± 0.029Å; 3 X-O distances : 2 x O1 2.0838 : 2 x O2 2.0678; 2 x O3 2.1311Å.

Pyrope ($Mg_3Al_2Si_3O_{12}$; solid solution mineral containing about 70% pyrope molecule.)
Structure based on separate $(SiO_4)^{4-}$ tetrahedral groups bonded by Mg in 8-coordination and Al in 6-coordination. Cubic; Ia 3 d; a = 11.459Å; Average Mg-O, 2.270 ± 0.078Å; 4 x O1 = 2.197, 4 x O2 = 2.343Å.

$MgAl_2O_4$ (spinel sensu stricta; pure, stoichiometric, synthetic.) Cubic; a = 8.0832Å; Fd 3 m. Oxygen in approximately close packed arrangement, half as many tetrahedral as octahedral sites. Mg-O = 1.924 (4 equivalent oxygens), Mg occupies 97% of tetrahedral sites (Al = 3%), Mg occupies 4% of octahedral sites (Al = 96%).

Diopside ($CaMgSi_2O_6$; synthetic pure phase). Monoclinic; C 2/c; a = 9.746, b = 8.899, c = 5.251Å, β = 105.63°. Structure based on $(SiO_4)^{4-}$ tetrahedra bonded together by sharing 2 oxygens to form single chains (aligned along c). Chains bonded by Mg in 6-coordination and Ca in 6-coordination. Average Mg-O, 2.077 ± 0.031Å; 2 x O = 2.064, 2 x $O_2$ 2.115, 2 x $O_3$ 2.050Å.

Akermanite ($Ca_2MgSi_2O_7$; synthetic prephase studied.) Tetragonal; $P\bar{4}2,m$; a = 7.6344, c = 5.0513Å. Structure based on pairs of $(SiO_4)^{4-}$ tetrahedra sharing a single oxygen (borosilicate). Si-tetrahedra are bonded to Mg-, also in tetrahedral sites by sharing remaining oxygens. The structure can be considered as a 'framework' silicate. Ca occupies 8-fold interstitial sites. Average Mg-O = 1.915Å (4 equivalent oxygens). Forms complete solid solution with gehlerite $Ca_2Al_2SiO_7$ (to form melilites) which has both Al sites in 4-coordination. n.b. no octahedral sites occur in this mineral type.

$KMg_{0.5}Si_{2.5}O_6$ (Mg-leucite, synthetic.) End-member leucite (s.s) is $KAlSi_2O_6$ and is a framework silicate with all Al in 4-coordination; K is in 12-coordination interstitial sites. Mg-leucite is known only in the synthetic phase; the structure is not known but must be isostructured with $KAlSi_2O_6$-leucite since it has almost the same x-ray powder pattern. Thus Mg is part of the framework.

EXAFS and near-edge studies were also made on a range of glasses showing compositions of: akermanite, dropside, akermanite-gehlerite, Mg-leucite and others with forsterite components and also on basalt glass (natural). It is generally assumed that Mg is a network modifier (possibly 6-fold coordinated) and causes depolymerization of the framework leading to reduced viscosities of Mg-rich (basic) melts. The studies were intended to identify whether local structure was indeed consistent with 6-fold or 4-fold coordination for Mg. Table I presents a summary of the calculated EXAFS data.

Reference:

1. J R Smyth and D L Bish 'Crystal structures and cation sites of the rock-forming minerals. Allen & Unwin, 332 pp.

| Sample | EXAFS | | Crystallographic data | |
|---|---|---|---|---|
| | $R^a$ | $N^b$ | $R^a$ | $N^b$ |
| MgO crystal | 2.161 | 4.8 | 2.109 | 6 |
| Forsterite crystal | 2.142 | 4.2 | 2.113 | 6 |
| Pyrope crystal | ( 2.021 | 1.0 | 2.198 | 4 |
| | ( 2.349 | 1.2 | 2.343 | 4 |
| Spinel crystal | 2.097 | 4.4 | 1.922 | 4 |
| Diopside crystal | 2.173 | 4.4 | 2.081 | 6 |
| Diopside glass | 1.916 | 3.1 | | |
| Akermanite crystal | 1.929 | 4.6 | 1.915 | 4 |
| Akermanite glass | 2.043 | 4.5 | | |
| Leucite crystal | 1.957 | 3.5 | | |
| Leucite glass | 1.866 | 6.2 | | |
| Akerm./Gehler. glass | 2.116 | 5.0 | | |
| Anort./Forst. glass | 2.020 | 4.9 | | |
| Anort./Forst/$SiO_2$ glass | 1.960 | 3.7 | | |
| Basalt glass | 2.035 | 3.8 | | |

[a] Mg-O bond length in Å

[b] First shell coordination number

Comparison of EXAFS and Crystallographic data

# Mg K-Edge Absorption Spectra of Magnesium Oxide Species Formed in Mg-Exchanged Y-Type Zeolites

Tsunehiro Tanaka, Geng Zhang, Hiroyasu Suzuka,
Tsutomu Yamaguchi, Hideshi Hattori, Kozo Tanabe,
and Takanori Murata*

*Department of Chemistry, Faculty of Science, Hokkaido University, Sapporo 060.*
**Department of Physics, Kyoto University of Education, Fushimi-ku, Kyoto 612.*

Base catalyst is a promising one, which shows interesting behavior in many catalytic actions. In the present work, we have attempted to prepare a new base catalyst with shape-selective ability and characterize its active species by means of X-ray absorption spectroscopy.

The catalyst sample (MgO/MgY) was prepared by immersing Mg-exchanged Y-zeolite into a methoxyethanol solution of magnesium diethoxide, followed by calcination in air at 823 K. The catalyst prepared in this manner exhibited a certain basic properties elucidated by chemical reactions and desorption feature of carbon dioxide at various temperatures, suggesting that magnesium oxide (micro)crystal may be formed in/on Mg-Y-zeolite.

Soft X-ray absorption experiments have been carried out on beam line 7-A with UVSOR(Ring energy: 750 MeV) facilities.[1] A beryl two-crystal monochrometer was used. Energy calibration was made by using Al K-edge absorption. As reference materials, commercial $Mg(OH)_2$, $Mg(OEt)_2$, MgO, $Mg(NO_3)_2$, $Mg(HCO_3)_2$, and $MgCO_3$ were used.

Figure 1 shows the Mg K-edge absorption spectra of MgO, $Mg(OH)_2$ and the catalyst (MgO/MgY). The striking feature of the spectrum of MgO/MgY is that absorption curve in the region of XANES and NEXAFS is similar to that of MgO while in the EXAFS region the oscillation due to backscattering by environmental atoms is unclear. This indicates that a magnesium atom in MgO/MgY is located at similar site to that in MgO crystal and growth of crystallite is not sufficient in the catalyst sample. This is consistent with the X-ray diffraction result. At the present stage, we can not conclude whether or not the magnesium oxide species is formed in supercage of Mg-Y-zeolite. However, the formation of microcrystal of magnesium oxide or its amorphous crystal is very interesting although interaction between two kinds of metal oxides usually generates acid sites even if one of the oxides is basic.

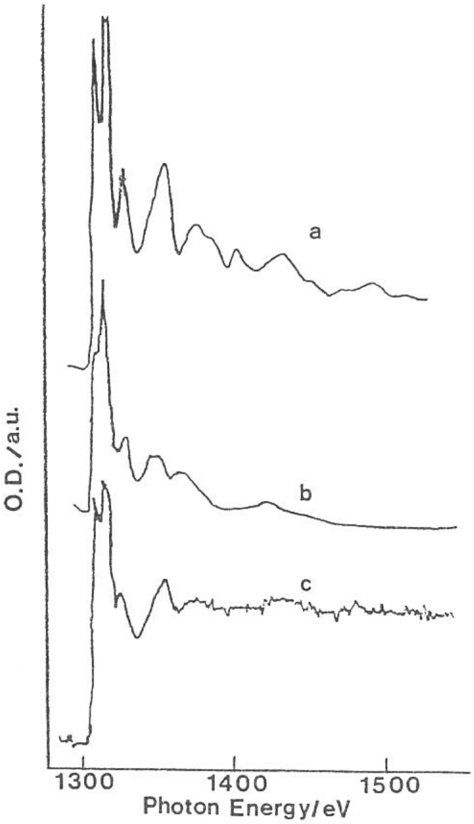

Figure 1 Mg K-edge Absorption spectra of (a) MgO, (b) $Mg(OH)_2$ and (c) MgO/MgY.

## Reference

1 T. Murata, T. Matsukawa, M. Mori, M. Obashi, S. Naoé, H. Terauchi, Y. Nishihata, O. Matsudo and J. Yamazaki, *J. Phys.*, 1986, *47*, C8-135.

# Al K-XANES and EXAFS Studies in Quasicrystals

Masahiro MORI, Tsutomu ISHIMASA, Katsutoshi USHIDA* and Tokuo MATSUKAWA**

College of General Education, Nagoya University, Chikusa, Nagoya 464
*Department of Applied Physics, School of Engineering,
Nagoya University, Chikusa, Nagoya 464
**College of General Education, Osaka University, Toyonaka, Osaka 560

It has been well known that fivefold axes of symmetry can not be present in crystals. Therefore, the appearance of fivefold symmetry was a noteworthy contribution to study any properties of such unknown new materials, including diffraction patterns. These are not crystalline in the conventional meaning, but maybe "quasicrystalline", being analogous to three-dimensional Penrose tiling as described by Mackay[1]. This above-mentioned state of materials differs from the ordinary crystalline state in the lattice periodicity; this state possesses no lattice periodicity. This means that the concept of the unit cell becomes meaningless. As the result, the conventional structure analysis of these quasicrystals may not be applicable and any clever methods to get these structures can not be found out until now. We have two aims to study K-edge absorption spectra of such peculiar quasicrystals. One is to get information of local structures. In this case,we have few ways to get their structures, and diffraction methods are helpless, but it is possible that the EXAFS experiment can be applied here. The other is to know electron states from XANES data.

We prepared some aluminum alloys; Al-Mn[2] and Al-Cu-Fe[3] alloys for quasicrystalline specimens, and Al for a standard one. Because of the stability of a quasicrystalline phase, we can not make the sample with suitable thickness for X-ray absorption experiments, nor can apply the evaporation method. We measured the photoelectric yield spectra instead of the absorption ones near Al K-edge by using double crystal monochromator at BL-7A soft x-ray beam line, UVSOR. It is well known the photoelectric yield emitted from a sample is directly proportional to its absorption coefficient. Single quartz crystals were used as monochromator crystals. Part of these experiments were done in the high vacuum ( less than $2.0*10^{-9}$ Torr), and, what were more, with using the clean surfaces obtained by filing.

Figure 1 shows XANES spectra of Al K-edge of quasicrystals and a pure aluminum at room temperature. All Al alloys have almost same Al K-edge energy. Spectrum (c) is the yield spectrum of a pure aluminum and is drawn to scale down by one fourth. Because this is very strong and has a more clear structure than the others. (a) is the yield spectrum of Al-Cu-Fe quasicrystals. This is the most structureless of the three, especially compared with (c). (b) from the Al-Mn quasicrystal is almost as same as (a). (b) has a slightly more clear structure than (a). This result seems depend on the fact that Al-Mn samples contain 10 or so percents of f.c.c. Al-Mn solid solution phase.

The quasicrystal does not have a clear structure in photoelectric yield spectra in the case of this energy resolution at least. The reason why its electron energy state is smooth is possibly that quasicrystals have some various sites of the nearest neighbor structures.

Data analysis of EXAFS is going on.

We are indebted to all staffs of the UVSOR facility, especially to M. Watanabe, O. Matsudo and K. Fukui for their continuous support and encouragement.

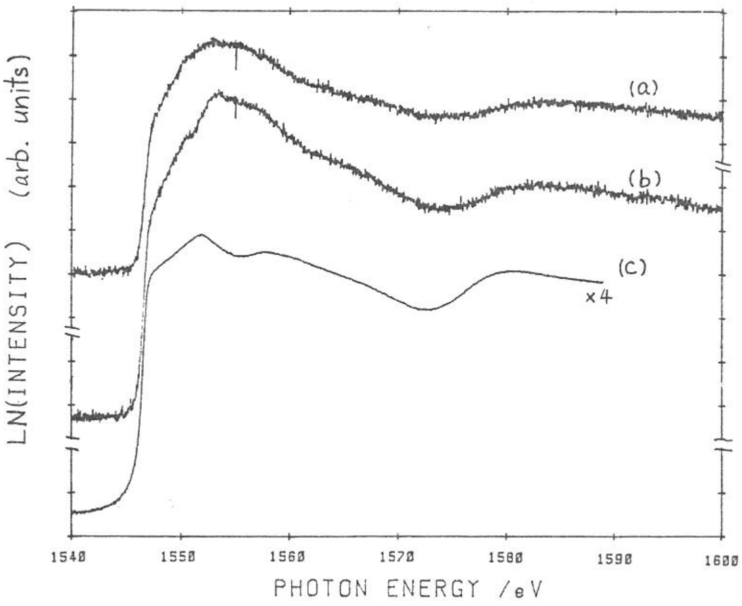

Figure 1. Photoelectric yield spectra of some aluminum alloys at room temperature drawm with the natural logarithm of intensity vs photon energy. (a) is the data of Al-Cu-Fe quasicrystals. (b) is from Al-Mn quasicrystals, and (c) is from pure Al.

References

1) A. L. Mackay, Physica 114A(1982)609

2) D. Shechtman, I. Blech, D. Gratias and J. W. Cahn, Phys. Rev. Lett., 53 (1984)1951

3) T. Ishimasa, Y. Fukano and M. Tsuchimori, Philos. Mag. Lett., 58(1988) 157

# LOCAL STRUCTURE OF AMORPHOUS $Si_xTe_{1-x}$ BY Si-K EXAFS

Keiji TSUNETOMO, Tatsumi SUGISHIMA
Takeshi IMURA and Yukio OSAKA

Department of Electrical Engineering, Hiroshima
University, Saijo, Higashi-Hiroshima, 724

## Introduction

Although most IV-VI crystals exist in 1:1 or 1:2 stoichiometries, $Si_2Te_3$ is the only crystal in the silicon-tellurium system. The crystalline $Si_2Te_3$ contains $Si_2$ units and each Si is tetrahedrally coordinated by 3 Te and 1 Si.1) In the context of amorphous chalcogenides, the distinction between chalcogenide crystal and its amorphous counterpart take on now significance. The silicon-tellurium system has a bulk-glass forming region from approximately 13 to 27 % silicon. The sputtering technique expands the glass forming region over almost all silicon concentrations.

We has investigated the local atomic structure of amorphous $Si_xTe_{1-x}$ by Si-K EXAFS.

## Experimental

Films of amorphous $Si_xTe_{1-x}$ alloy were prepared by rf sputtering of Si target upon which small pieces of Te were placed in radial array. The Te content in the film was controlled by the area ratio of the pieces of Te to the target. The film thickness was controlled for about 2μm, which gave a sufficient edge jump. About 1 μm thick polyester films were used for the substrates to reduce the X-ray absorption of the substrate. Typically, the pressure of Ar, the rf power and the substrate temperature $5 \times 10^{-3}$ Torr, 40W and 20 °C (water cooled), respectively. The chemical composition of films was determined by Rutherford backscattering spectroscopy at 165° direction for 2.5 MeV $He^+$ ion beam(≃10 nA) generated from a Van der Graff accelerator installed at Faculty of Engineering, Hiroshima University.

X-ray absorption spectra near the Si-K edge between 1.8 keV to 2.6 keV were investigated at 40 K in the X-ray beam line 7A of the Synchrotron Radiation facility at the Institute for Molecular Science. The radiation was monochromatized by a InSb(111) channel-cut crystal.

## Results and Discussion

Figure 1 shows an example of the EXAFS oscillation $\chi(k)$ of amorphous $Si_xTe_{1-x}$ film, vs. photo-electron wavenumber k.

Fourier transform of the spectrum integrated over the range from 2.5 $A^{-1}$ to 10 $A^{-1}$ of wavenumber are shown in Fig. 2. The first and second peak in the radial distribution function F(r) is due to the Si-Si and Si-Te pair. It must be noted that the peak of the Si-Si pair is clearly detected near x=0.36. If amorphous silicon-tellurium system is chemically ordered, the Si-Si pair in the film don't appear below x=0.33. Then, Figure 1 shows that the amorphous silicon-tellurium system is not chemically ordered and a large amount of Si-Si pair exist at x=0.36. This may be due to the fact that bulk-glass forming is not possible in the region x>0.27 and the crystalline $Si_2Te_3$ contain $Si_2$ units.

Te-K EXAFS on amorphous $Si_xTe_{1-x}$ have shown that amorphous $Si_xTe_{1-x}$ is not chemically ordered and the structure is well described by the random-bonding network in the region x>0.5, which is consist with the above-mentioned observation.

Reference

(1) K. Ploog, W. Stetter, A. Nowitzki and E. Schonherr: Mat. Res. Bull 11 (1976) 1145.

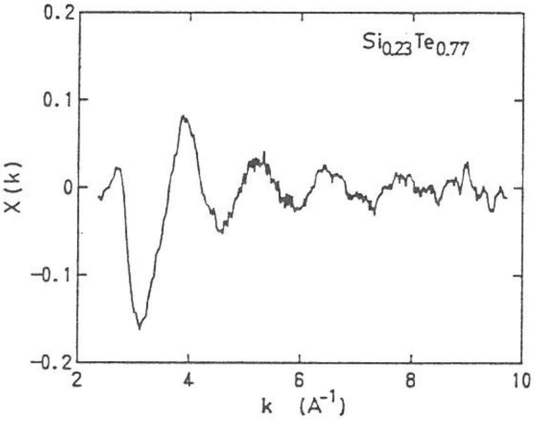

Fig. 1 EXAFS oscillation of amorphous $Si_{0.23}Te_{0.77}$.

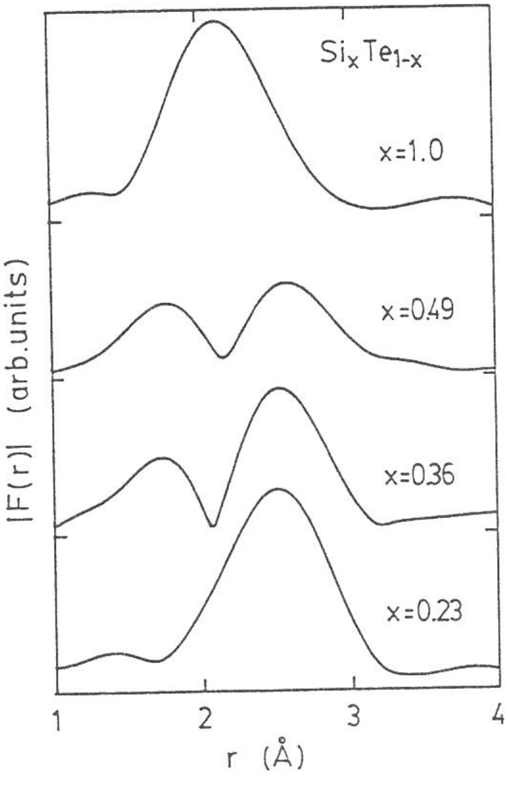

Fig. 2 Fourier transform of EXAFS for Si K-edge of amorphous $Si_xTe_{1-x}$.

# P-K EDGE ABSORPTION SPECTRUM OF POTASSIUM DIHYDROGENPHOSPHATE

Yasuo NISHIHATA and Hikaru TERAUCHI

School of Science, Kwansei Gakuin University, Nishinomiya 662

$KH_2PO_4$ (abbreviated to KDP) has been studied as a typical example of hydrogen-bonded crystal which undergoes ferroelectric phase transition. It has been known that the phase transition is triggered by an order-disorder rearrangement of the proton configuration. Recently, Tokunaga *et al.* [1] proposed the order-disorder model of phosphate ($PO_4$) dipoles in KDP from their Raman spectroscopic studies. They concluded that the momentary site symmetry of a $PO_4$ must be $C_2$ even far above the transition temperature $T_c$. We measure the EXAFS spectra near the P-K edge to examine the distortion of $PO_4$ tetrahedra directly.

The powder of KDP was put in collodion and the top clean part of the solution was spread on slide-glass. X-ray absorption spectrum of KDP in the collodion film peeled from the glass-plate was taken near the P-K edge by the use of the double crystal monochromator (DXM) constructed at BL-7A of UVSOR. The soft x-ray intensity monochromatized by InSb(111) plane (2d= 7.48Å) was monitored using an electron multiplier and the output current was lead into digital picoammeter. The obtained spectrum at room-temperature is shown in Fig. 1. Detailed analysis is now in progress.

Reference

[1] M. Tokunaga, Y. Tominaga, and I. Tatsuzaki, Ferroelectrics 63, 171 (1985).

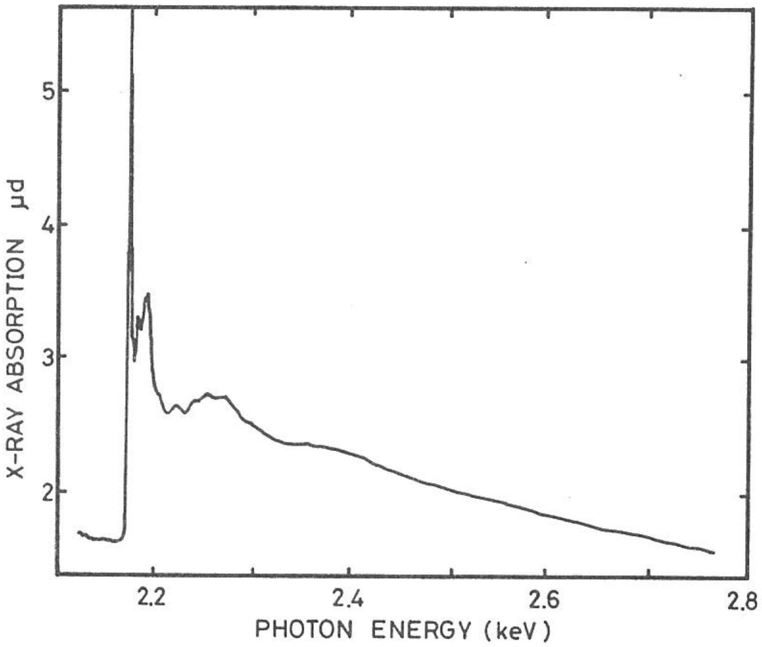

Fig. 1 X-ray absorption spectrum near the P-K edge of KDP at RT.

# PHOTOEMISSION STUDY OF SINGLE CRYSTAL $Bi_2Sr_2CaCu_2O_8$

Takashi TAKAHASHI[1], Hiroyoshi MATSUYAMA[1], Hitoshi FUJIMOTO[2]
Hiroshi KATAYAMA-YOSHIDA[1], Yutaka OKABE[1], Shoichi HOSOYA[3],
Kazuhiko SEKI[4], Masatoshi SATO[2], and Hiroo INOKUCHI[2]

[1]*Department of Physics, Tohoku University, Sendai 980*
[2]*Institute for Molecular Science, Okazaki 444*
[3]*Institute for Materials Research, Tohoku University, Sendai 980*
[4]*Department of Materials Science, Hiroshima University, Hiroshima 780*

Angle-resolved and resonant photoemission measurements have been performed on a single crystal $Bi_2Sr_2CaCu_2O_8$ [1]. Two energy bands with dispersion of 0.2-0.5 eV were observed in the vicinity of the Fermi-level and one of them intersects the Fermi level midway between the center and boundary of the Brillouin zone, giving a direct evidence for the existence of a Fermi surface. The Fermi-edge structure exhibits a resonant enhancement at the O 2s core-threshold, meaning a dominant O 2p nature of the Fermi-edge state. These results indicate the existence of the Fermi-liquid states with dominant O 2p nature in the high-Tc superconductor. The superconductivity could be driven by Cooper-pairing of the O 2p holes in the Fermi-liquid states, probably through the spin or charge fluctuation.

Photoemission measurements were performed with an angle-resolved photoelectron spectrometer at the beam line BL 8B2. A single crystal (Tc=85 K, 5x5x0.3 $mm^3$) was grown with the KCl-flux technique. The crystal has a smooth plane along which cleavage is very easy.

Figure 1 shows the "band structure" of $Bi_2Sr_2CaCu_2O_8$ determined by the present angle-resolved photoemission measurement. We find two bands in the vicinity of the Fermi level (bands A and B). Band B clearly intersects the Fermi level between the Γ and X(Y) points, showing the existence of a Fermi surface and the Fermi-liquid states. In the higher-binding-energy region, experimental bands are almost dispersionless in contrast with the highly dispersive feature of the calculated bands, indicating an effective renormalization due to the strong electron correlation. These experimental results provide a clear picture for the electronic structure of the high-Tc superconductor; the Fermi-liquid states in the vicinity of the Fermi level and almost localized states away from the Fermi level.

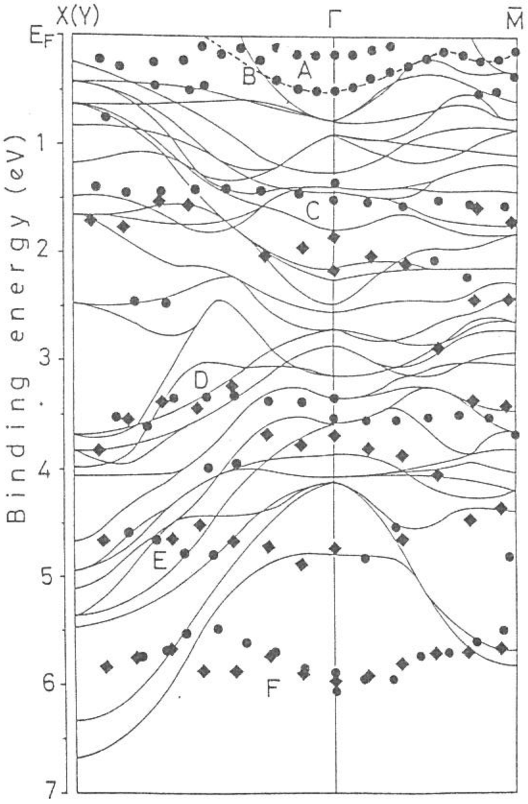

Fig. 1

Band structure of $Bi_2Sr_2CaCu_2O_8$ determined from the angle-resolved photoemission (circles and squares), compared with the band structure calculation by Freeman et al. (solid lines).

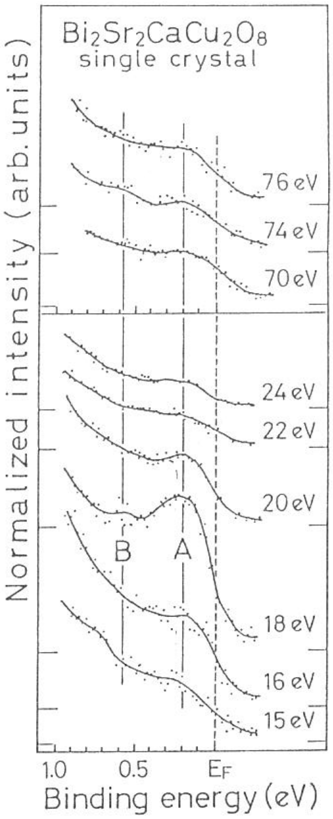

Fig. 2

Photoemission spectra in the vicinity of the Fermi level at the photon energies at the O 2s (lower) and Cu 3p (upper) core-thresholds.

Figure 2 shows the photoemission spectra in the vicinity of the Fermi-level, measured with photon energies at the O 2s and Cu 3p core-thresholds. We find a resonant enhancement of the Fermi-edge structure at the O 2s core thersold (~18 eV), but not at the Cu 3p core-thresold (~74 eV). This is a direct evidence for a dominant O 2p nature of the Fermi-liquid states in the high-Tc superconductor. The superconductivity could be driven by Cooper-pairing of the O 2p holes in the Fermi-liquid states through the spin or charge fluctuation.

This work was supported by a Grant-in-Aid for Scientific Research on Priority Area from the Ministry of Education, Science, and Culture.

[1] T. Takahashi, H. Matsuyama, H. Katayama-Yoshida, Y. Okabe, S. Hosoya, K. Seki, H . Fujimoto, M. Sato, and H. Inokuchi, Nature 334, 691 (1988).

# Reflection Spectra of Polydiacetylene with Direct $\pi$-Conjugation between Polymer Backbone and Side Groups

Kouichi ICHIMURA, Hachiro NAKANISHI,* Hiro MATSUDA,*
Masao KATO,* and Takayoshi KOBAYASHI

Department of Physics, Faculty of Science, University of
Tokyo, Hongo 7-3-1, Bunkyo-ku, Tokyo 113
*Research Institute for Polymers and Textiles, Tsukuba,
Ibaraki 305

One of the reasons why polydiacetylenes attract our interests is their large cubic optical susceptibilities due to the $\pi$-conjugation of the polymer backbones. Thus it is interesting to see how the susceptibilities are changed by a substitution of various kinds of side groups which have $\pi$-conjugation with backbones.

Poly-CPDO(poly-1-(N-carbazolyl)penta-1, 3-diyne-5-ol) is a new polydiacetylene and has carbazolyl side groups. Since the band gap of poly-CPDO is smaller than those of other known polydiacetylenes,[1) there must be $\pi$-conjugation between the polymer backbone and the side groups. So poly-CPDO is a good candidate which has larger cubic susceptibility than other polydiacetylenes.

In order to study basic optical properties of poly-CPDO we measured polarized reflection spectra of the single crystal at room and liquid helium temperatures by using synchrotron radiation of UVSOR. The light from the storage ring was monochromatized with a monochromator of Seya-Namioka mounting at BL7B.

Reflection spectra of poly-CPDO at room temperature for polarization of light E//b (a) and E⊥b (b) where b is the chain direction are shown in Fig. 1. At about the photon energies where peaks 2 and 3 are located there are also peaks in the case of other polydiacetylenes whose side groups include aromatic rings without having $\pi$-conjugation with polymer backbones.[2) Therefore the origin of these peaks are considered to be electronic transitions in carbazolyl rings of poly-CPDO. The reflection spectra of the polydiacetylenes which have phenyl rings in their side groups have peaks at about 7eV, and the peaks are attributed to the $\pi$-conjugation along the polymer backbones[2). Therefore peak B, which is located at 6.5eV, must be due to the electronic transition on the polymer backbone. Interestingly the photon energies of the peaks 2, 3, and B are lower than those of other polydiacetylenes with phenyl rings by about 1eV. This energy shift indicates $\pi$-conjugation between the backbone and the side groups of poly-CPDO. The same structures as broad bands denoted C are also observed in the case of the polydiacetylenes referred above.

Reflection spectra at liquid helium temperature (5.5±0.5K) are shown in Fig. 2, where (a) and (b) are for polarization E//b and E⊥b respectively. The spectrum (a) is almost the same as (a) observed at room temperature, but (b) is rather different from (b) in Fig. 1. It is possible that a phase transition of poly-CPDO single crystal occurs down to about 5K.

References
1) Matsuda, H. ; Nakanishi, H. ; Hosomi, T. ; and Kato, M. : Macromolecules 1988, 21, 1238-1240.
2) Tokura, Y. ; Oowaki, Y. ; Kaneko, Y.; Koda, T. ; and Mitani, T. : J. Phys. Soc. Jpn. 1984, 53(11), 4054-4063.

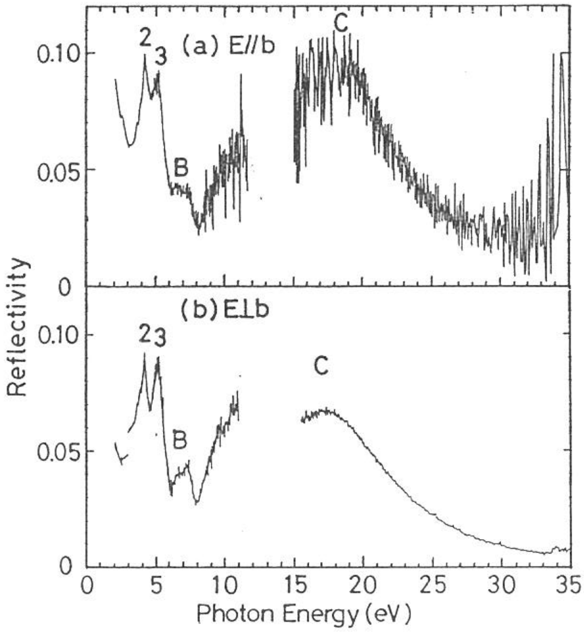

Fig. 1
Reflection spectra at room temperature with polarization of E//b (a) and E⊥b (b).

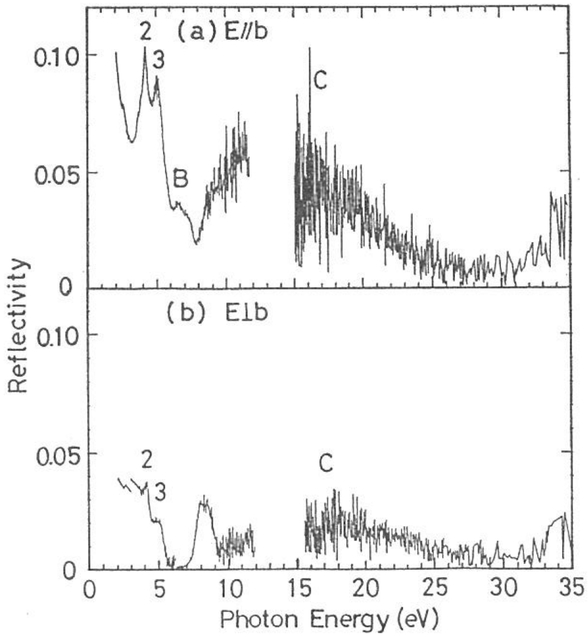

Fig. 2
Reflection spectra at liquid helium temperature (5.5±0.5K) with polarization of E//b (a) and E⊥b (b).

# OPTICAL SPECTRA OF POLYDIACETYLENE CRYSTALS AND ORIENTED-FILMS IN THE UV REGION

Tatsuo KANETAKE , Tatsuo HASEGAWA , Ken ISHIKAWA and Takao KODA
Department of Applied Physics, University of Tokyo,
Hongo, Bunkyo-ku, Tokyo 113

Polydiacetylenes (PDAs) are conjugated polymers obtained by solid-state polymerization of corresponding diacetylene monomers R-C≡C-C≡C-R', where R and R' are substitutional side-groups. These polymers have been attracting considerable interest, because of the typical quasi-one-dimensional character of the conjugated backbone π-electron system. In this study we have measured absorption and reflectance spectra of new class PDAs which have no phenyl-groups in the side-groups.

The samples which we had used for the measurements were PDA-$C_4UC_n$ [$R=R'=(CH_2)_4OCONH(CH_2)_{n-1}CH_3$] which did not have any phenyl groups or other groups with the conjugated π-electrons. Therefore the absorption structures at the visible and UV region are predominantly attributed to the conjugated backbone chains. They are also suitable for fabrication of highly oriented film by the vacuum deposition method$^{1)}$. Such oriented films are useful for the angle resolved photo-emission spectroscopy. We measured the reflectivity spectra of single crystal of PDA-$C_4UC_3$ and absorption spectra of monomeric and polymeric films of PDA-$C_4UC_5$, as the first step of the investigation of the π-electron structure of the backbone chain.

Figure 1 shows the polarized reflectivity spectra of a PDA-$C_4UC_3$ single crystal in the photon energy region of 1- 10 eV. Polarizations were parallel or perpendicular to the conjugated backbone chains. An intense reflection peak was observed at 2 eV. This reflection was strongly polarized along the chain direction and has been assigned to the $^1B_u$ exciton of $\pi$-$\pi^*$ transition. In higher energy region, there are two peaks which are also polarized along the chain direction. Assignment of these structures are discussed later with similar structure observed in PDA-$C_4UC_5$. The absorption spectra of monomeric and polymeric oriented films of PDA-$C_4UC_5$ are shown in FIg.2. Inspection of the figure shows that an absorption peak at about 7 eV decreases after polymerization while a peak at 9 eV increases.

We shall discuss the assignment of the individual structures observed in the reflectivity and absorption spectra by comparing these results with the spectra of PDA-PTS crystal reported before$^{2)}$. The most notable

difference between two polydiacetylenes is that additional absorption peaks observed in PDA-PTS in the 3-6 eV region is absent in PDA-$C_4UC_n$.
This difference is easily understood, if we assign these structure as due to phenyl groups in side-group of PDA-PTS. A peak at 7 eV has been assigned before to the $\pi$-$\pi^*$ transition of the in-plane carbon 2p $\pi$-electron in the triple bond(-C≡C-) of the backbone polymer chain. However since this structure decreases during polymerization, this assignment is seems to be questionable. We consider that the absorption peak of polymer is overlapping with that of the monomer, so that the absorption intensity decreases after polymerization. On the other hand, the absorption peak at 9 eV is likely assigned to side-chains, because it is not observed in PDA-PTS.

We are now planning to make more definite determination of the band structure of $\pi$-electron in the backbone chain by means of the angle-resolved photo emission spectroscopy. Such measurements become feasible experimentally using the highly oriented film of PDA-$C_4UC_n$ presently used.

**References**

1) T.Kanetake, K.Ishikawa, T.Koda, Y.Tokura and K.Takeda, Appl.Phys.Lett., 51(1987)1957.
2) Y.Tokura, T.Mitani and T.Koda, Chem.Phys.Lett.,75(1980)324.

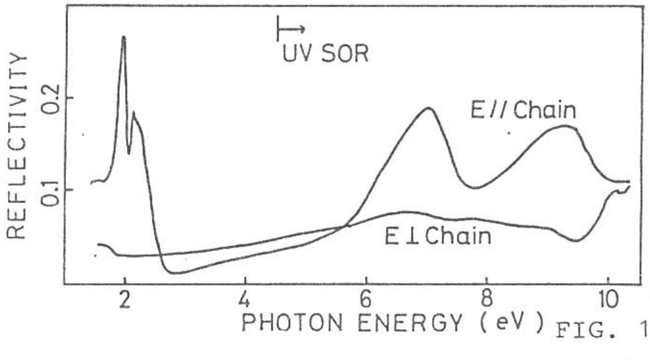

FIG. 1. Polarized reflectivity spectra of PDA-$C_4UC_3$ single crystal

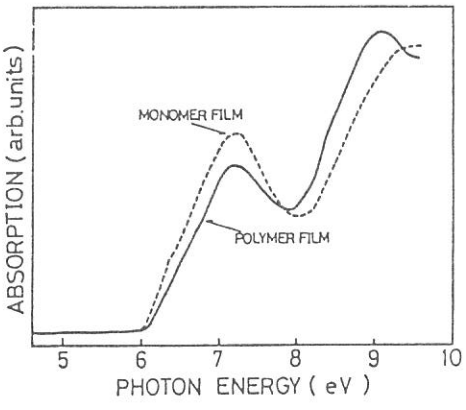

FIG. 2. Absorption spectra of monomeric and polymeric films of PDA-$C_4UC_5$

# FLUORESCENCE OF AROMATIC HYDROCARBON CRYSTALS. EXCITATION SPECTRUM AND MODULATION BY ELECTRIC FIELDS.

Ryuzi KATOH, Yoshinobu TAKEDA, Yasushi SHIMIZU,
Hiroyuki KOBAYASHI and Masahiro KOTANI

Faculty of Science, Gakushuin University
Mejiro, Tokyo 171

Aromatic compounds have generally very large absorption cross sections for VUV radiations and absorption is complete in a crystal of more than a few micron thickness. Associated with this strong absorption the reflection can also be large near the absorption peaks. Accordingly the correction for the reflection loss is important when some excitation spectrum (e.g., of fluorescence, photoconduction, etc.) is to be measured: The number of absorbed photons, rather than the number of incident photons, should be known for normalization purposes.

We have measured the reflection spectrum and the excitation spectrum of fluorescence with single crystals of perylene, p-terphenyl and anthracene in the wavelength region $\lambda \geqq 120$ nm. The measurements were made in a low-vacuum ($10^{-2}$-$10^{-3}$ Torr) chamber at BL1B. The intensity of the incident SR light was monitored with a photomultiplier set behind a glass plate coated with sodium salicylate. The reflected light from a sample specimen was measured with a similar detector. In fluorescence measurements the emission from the sample crystal was collected with fused quartz lenses and observed, after appropriate filtering, with a photomultiplier. A V-f converter was used to convert the dc output of a picoammeter into a train of pulses, which could be conveniently accumulated with a counter (Fig. 1). This constitutes an integrating system with a very long time constant and is useful unless the signal is very low, so that the photon counting is the only feasible detection method.

Modulation spectroscopy can be a very sensitive means to detect a state with a specific nature which is otherwise buried in other transitions of much larger cross sections. We have examined the proposal made by Y. Tokura that an insight can be gained into the relaxation of higher excited states through the observation of fluorescence modulation by an electric field (Y. Tokura, private communication. See also, KEK Report 86-10 "Future Prospect of the Research Study Using Intense and Bright Radiation in VUV and Soft X-ray Region", February 1987, p.12). We could reproduce essentially what Tokura et al. have observed with anthracene. The results are shown in Figs. 2 and 3. However, we observed that the modulation was strongly suppressed when 1 atm of argon was introduced into the sample chamber. This indicates that the modulation is not due to any relaxation of higher excited states in the solid, but quite probably due to the bombardment with electrons, emitted by VUV irradiation and accelerated by the applied field. It is possible that a small modulation observed in argon atmosphere is related to the energy relaxation in the solid. An experiment is being planned with an improved arrangement.

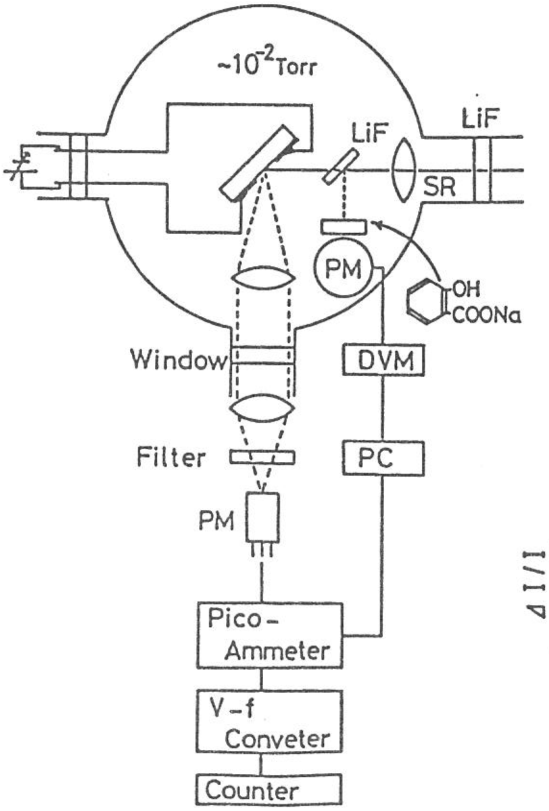

Fig. 1

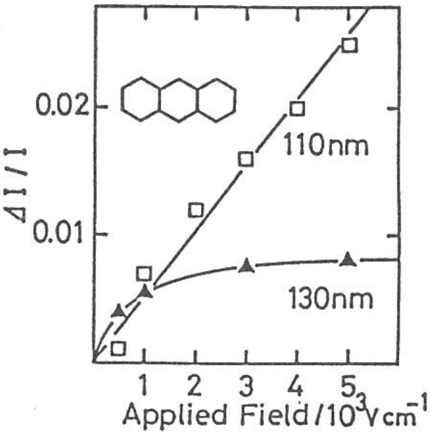

Fig. 2

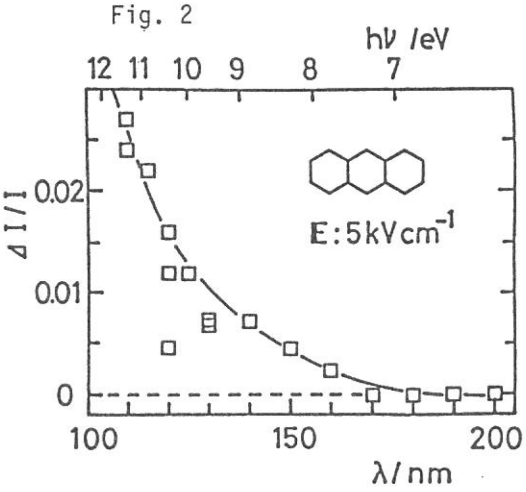

Fig. 3

# Fluorescence Excitation Spectra of Some Simple Alkenes in the Vacuum Ultraviolet Studied by UVSOR

Yoshihisa INOUE and Tadashi OKADA*

Basic Research Laboratory, Himeji Institute of Technology,
2167 Shosha, Himeji, Hyogo 671-22
*Faculty of Engineering Science, Osaka University,
Machikaneyama, Toyonaka, Osaka 565

**INTRODUCTION:** Photochemically, alkylated ethylenes are known to afford more than two photoproducts upon direct irradiation in the vacuum ultraviolet (VUV).[1] We have recently demonstrated that the relative ratio of individual photoproducts drastically varies depending upon the excitation wavelength employed, indicating intervention of distinctly different excited state for each photochemical process and slow mutual interconversion between the excited states involved.[2] On the other hand, the photophysical behavior of excited alkenes does not appear to be investigated extensively,[3] probably because they are extremely poor fluorescer. Hirayama and Lipsky have however succeeded in observing very weak fluorescence from a series of alkylated ethylenes excited at 185 nm in the vapor and/or liquid phases.[4]

In this study we have recorded the first excitation spectra of di-, tri-, and tetraalkylethylenes, which differ in shape substantially from their absorption spectra but provide a direct support for the assignment that the emissive state is $\pi$,R(3s) Rydberg rather than $\pi,\pi^*$ state. The anomalous wavelength-dependence of fluorescence quantum yields is further discussed in relation to the wavelength-dependent photochemical reactivity of the simple alkenes.

**RESULTS:** Since the intensity of monochromatic light from BL-7B through a 1 m Seya-Namioka monochrometer was extremely weak as compared with that of the radiation from conventional resonance lamps employed in refs. 2 and 4, we first examined 2,3-dimethyl-2-butene of most intense fluorescer among simple alkenes[4], using the time-resolved photon counting method. The shape of emission peak observed was practically identical to the pulse shape of the UVSOR irrespective of the excitation wavelength. The integrated emission intensity was measured at a 5 nm interval over a wavelength range 160-250 nm, and was plotted as a function of wavelength. The maximum fluorescence intensity was obtained by excitation at 229 nm, while the excitation at longer or shorter wavelengths results in an abrupt or gradual decline of florescence intensity.

Similar fluorescence measurements with 2-methyl-2-butene, trans-cyclooctene, and trans-2-octene were performed under comparable conditions to give much weaker emissions especially for the latter two dialkylethylenes. The observed maximum of the excitation spectrum was listed for each alkene in Table. Thus it was shown that the present system, utilizing the synchrotron radiation as a tunable light source in the VUV and the single photon counting method for detection, does work well in measuring excitation spectrum of very weak fluorescence whose quantum yield is as low as $10^{-6}$.

Table. Absorption and fluorescence excitation spectra of alkenes

| Alkene | Absorption(nm)[a] |  | Fluorescence excitation (nm)[b] |
|---|---|---|---|
|  | V-N($\pi,\pi^*$) | R-N($\pi$,R(3s)) |  |
| *trans*-2-Pentene | 180 | 201 | c) |
| *trans*-2-Octene | 179 | d) | 195 |
| *trans*-Cyclooctene | 197 | 205 | 214 |
| 2-Methyl-2-butene | 186 | 206 (216)[e] | 229 |
| 2,3-Dimethyl-2-butene | 187 | 218 (230)[e] | 229 |

[a] Ref. 3; gas-phase absorption maxima. [b] This work; peak intensity for neat liquid; accuracy: ±2.5 nm. [c] Not measured. [d] Not reported. [e] A.J. Merer and R.S. Mulliken, *Chem. Rev.*, **69**, 639 (1969).

**DISCUSSION:** Interestingly, the first excitation spectra of simple alkenes thus obtained differ substantially from their absorption spectra reported.[3-6] In Table 1, the reported absorption maxima for V-N and R-N transitions were comparatively listed along with the observed maximum of fluorescence excitation spectrum for each alkenes. Taking into account of the broad band width (5 nm) of the excitation light, the maximum of fluorescence excitation spectrum shows good agreement with the absorption maximum of R-N transition for each alkenes. Furthermore the relative intensity of fluorescence observed upon excitation at 185, 214, and 229 nm nicely coincides with the quantum yield reported.[4] These results unequivocally provide definitive evidence in support of the tentative assignment of the emissive state to $\pi$,R(3s) Rydberg rather than $\pi,\pi^*$ excited state.

From the photochemical point of view, it is crucial that the relative fluorescence intensity coincides again with the relative ratio between the carbene- and 1,3-hydrogen-shift-derived products. This verifies the long-proposed mechanism that the "carbene" arises from the $\pi$,R(3s) Rydberg state,[1,2] in which the cation-radical like electronic configuration around the molecular core promotes the alkyl shift to the cation center.

**ACKNOWLEDGMENT:** This work was performed mostly at the UVSOR, Institute for Molecular Science. We are grateful of the technical support of Drs. M. Watanabe, K. Fukui, and T. Kasuga at the UVSOR.

## REFERENCES

1 For reviews, see: P.J. Kropp, *Org. Photochem.*, **4**, 1 (1979); M. G. Steinmetz, *ibid.*, **8**, 67 (1987).
2 Y. Inoue, T. Mukai, and T. Hakushi, *Chem. Lett.*, **1983**, 1665.
3 M.B. Robin, "Higher Excited States of Polyatomic Molecules," Vol. 2 (Academic, New York, 1975) Chap. 4; Vol. 3 (Academic, Orlando, FL, 1985) Chap. 10.
4 F. Hirayama and S. Lipsky, *J. Chem. Phys.*, **62**, 576 (1975).
5 L.C. Jones, Jr., and L.W. Taylor, *Anal. Chem.*, **27**, 228 (1955).
6 M.B. Robin, R.R. Hart, and N.A. Kuebler, *J. Chem. Phys.*, **44**, 1803 (1966).

# EXCITATION TRANSFER IN LIQUID CYCLOALKANES

Tadashi OKADA, Masaaki HAGIHARA, and Kenji KAMATA

Department of Chemistry, Faculty of Engineering Science,
Osaka University, Toyonaka, Osaka 560

Many authors have reported the effective excitation transfer reaction from solvent excited states to the solute molecules in hydrocarbon liquids. Most of the experiments have involved steady state measurement of the yield of solvent or solute fluorescence in the presence and absence of a quencher. Although some experiments have been performed using pulsed irradiation, the mechanism for the production of solute excited states in alkane solution has not yet been fully elucidated.

We have measured the time dependences of the solvent and solute, anthracene, fluorescence in liquid cyclohexane and trans-decalin at room temperature as functions of the solute concentration and excitation wavelength. The observed results are summarized as follows. The decay curve of solvent fluorescence detected by using a bandpass filter having a maximum transmission at 214 nm was analyzed successfully as a single exponential. when the solution was excited by VUV radiation a growth of the excited state of anthracene was observed at nanosecond to subnanosecond time region. The rise time of the anthracene fluorescence was considerably faster compared to the decay time of the solvent fluorescence. An example of anthracene fluorescence is shown in Fig. 1.

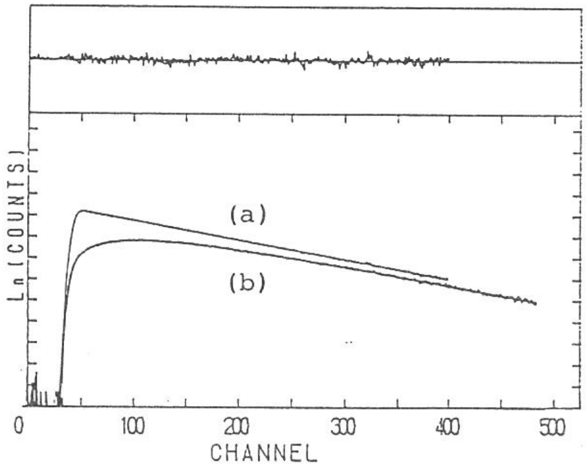

Fig. 1. Time dependence of the anthracene fluorescence in trans-decalin excited at (a) 339 nm and (b) 150 nm. [anthracene]=1.6 $10^{-3}$ M. 47.85ps/channel

We assume tentatively the reaction scheme of eq 1 for the analysis of the obtained results.

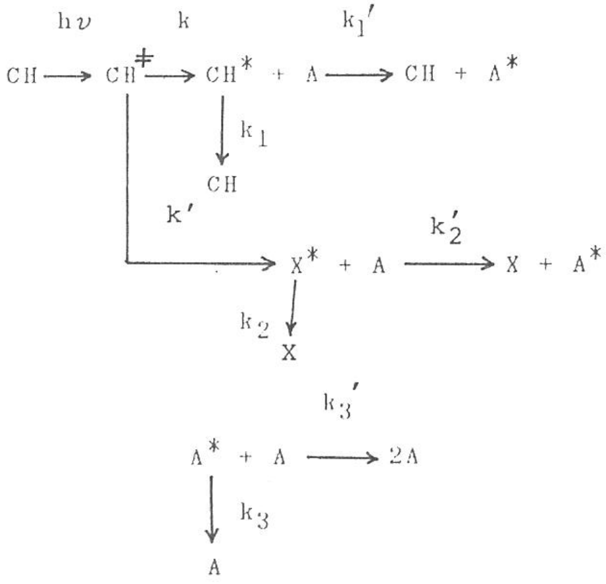

(1)

where $CH^{\ddagger}$, $CH^*$, and $A^*$ are higher excited state of solvent, fluorescent state of solvent, and excited single state of anthracene, respectively. $X^*$ is nonfluorescent energy donor of which the chemical species is not clear. The formation of $CH^*$ and $X^*$ is assumed to be attained in the excitation pulse width (ca. 450 ps FWHM). The following equations for anthracene fluorescence decay curve under excitation by VUV radiation can be derived.

$$A^*(t) = a_1\exp(-t/\tau_1)+a_2\exp(-t/\tau_2)+a_3\exp(-t/\tau_3) \qquad (2)$$

$$\tau_1^{-1} = k_1+k_1'[A],\ \tau_2^{-1} = k_2+k_2'[A],\ \tau_3^{-1} = k_3+k_3'[A] \qquad (3)$$

The bimolecular rate constant, $k_2'$, in decalin seems to depend on the excitation wavelength. In Table I the rate constants of eq 1 in cyclohexane and trans-decaline solutions excited at 170 nm is presented.

Table I. Kinetic parameter of eq 1 obtained by excitation wavelength at 170 nm

| | $k_1$ / $10^8 s^{-1}$ | $k_1'$ / $10^{10} M^{-1} s^{-1}$ | $k_2$ / $10^9 s^{-1}$ | $k_2'$ / $10^{11} M^{-1} s^{-1}$ | $k_3$ / $10^8 s^{-1}$ | $k_3'$ / $10^9 s^{-1}$ |
|---|---|---|---|---|---|---|
| cyclohexane | 13.5 | 5 | 2.8 | 15 | 1.9 | 8 |
| trans-decalin | 3.45 | 2.1 | 0.8 | 0.6 | 1.9 | 5.2 |

# PHOTOIONIZATION THRESHOLD AND PHOTOIONIZATION YIELD OF SUPERCRITICAL XENON DOPED WITH TMAE (TETRAKIS-DIMETHYLAMINOETHYLENE) AS A FUNCTION OF XENON DENSITY

Kazumichi NAKAGAWA, Arisato EJIRI, *Richard A. Holroyd,
#Shinzou KUBOTA, +Kazuie KIMURA and Masaru NISHIKAWA

Department of Pure and Applied Sciences, University of Tokyo, 3-8-1 Komaba, Meguro-ku, Tokyo 153, Japan
*Department of Chemistry, Brookhaven National Laboratory, Upton, New York 11973, U.S.A.
#Rikkyo University, Nishi-Ikebukuro 3, Tokyo 171, Japan
+The Institute of Physical and Chemical Research, Wako, Saitama 351, Japan

Xenon fluid is known to dissolve large molecular weight solutes such as polypropylene glycol (molecular weight ~4000)[1] via the cluster-assisted dissolution mechanism[2]. Recently doped supercritical rare gas systems have drawn attention of high energy physicists[4] because of (a)high electron mobility and (b)large photoionization quantum yield in these systems owing to decrease in ionization threshold of dopants and high dopant concentration attainable in supercritical fluids. From the interest on the possibility of using these systems in high energy particle detectors, we measured density dependence of photoionization threshold energy $I_f$ and photoionization yield of supercritical xenon doped with TMAE (tetrakis-dimethylaminoethylene) (TMAE/Xe system).

Extra pure TMAE[5] prepared at the Brookhaven Laboratory was used. Measurements were performed at BL7B of UVSOR. Experimental set-up used was the same as that reported in Ref.[6] except for usage of parallel plate electrodes instead of gold film electrode. Measurements of absolute intensity of incident light was performed in order to obtain the photoionization quantum yield. Optical path length of the cell is 10 mm.

Fig. 1 shows photoconductivity excitation spectra at 300 K of pure vapor TMAE and TMAE-doped supercritical xenon. From the 5/2-th power law analysis[7] on the vapor phase TMAE spectrum, the vapor phase ionization potential of TMAE was determined to be 5.39 eV, which is in good agreement with the value 5.36 eV reported by Nakato et. al.[8]. $I_f$ values determined by the same procedure are shown in Fig. 2.

Photocurrent of ~72 pA was observed in TMAE/Xe system at xenon density of $7.5 \times 10^{21} \mathrm{cm}^{-3}$ for incident light intensity of $2.3 \times 10^{9}$ photons/second at 200nm (bandwidth ~1 nm) under electric field of 240 volts/cm. With these values and the absorbance ( 0.646 at 200 nm ) recorded simultaneously, photoionization quantum yields of the system was calculated to be ~0.26 (electrons/absorbed photon) at 200 nm. The value in the fluid is quite large if one considers the density. Quantum yield of vapor TMAE obtained similarly was ~0.35 at 190 nm, which is sufficiently close to that (~0.3) reported by Holroyd et. al.[9].

Density dependence of $I_f$ values are compared with the calculated values by $I_f=Ig+Vo+P$ (Eq.1)[7] utilizing the gas phase ionization potential of TMAE (Ig=5.39 eV), the experimental values of conduction band energy Vo of xenon fluids reported by Reininger et. al.[10] and polarization energy P calculated from the Born charging formula with bulk dielectric constant and with the ionic radius R=0.32 nm for $TMAE^+$ ion[5,8]. As clearly seen in Fig. 2, Eq. 1 reproduces the experimental results quite well. It is to be noted that $I_f$ values vary smoothly at low densities and no abrupt decrease of $I_f(N)$ is observed. This is in contrast with the observation in anthracene-doped xenon[3], suggesting that photoionization in TMAE/Xe system is not strongly influenced by the cluster formation.

References: [1]P.M.Renzepis et al., Nature 293,165(1981). [2]G.L.Rößling et al., Ber.Bunsenges.Phys.Chem.87,882(1983). [3]K.Nakagawa et al., Chem. Phys.Lett. 147,557(1988). [4]S.Kubota, private communication. [5]R.A. Holroyd et al., J.Phys.Chem. 89,4244(1985). [6]K.Nakagawa et al., Chem. Phys.Lett.(in press). [7]R.A.Holroyd et al., J.Chem.Phys. 79, 483(1983). [8]Y.Nakato et al., Bull.Chem.Soc.Jpn. 45,1299(1972). [9]R.A.Holroyd et al. Nucl.Inst. and Meth. A261,440(1987). [10]R.Reininger et al., Phys.Rev. B28, 4426(1983).

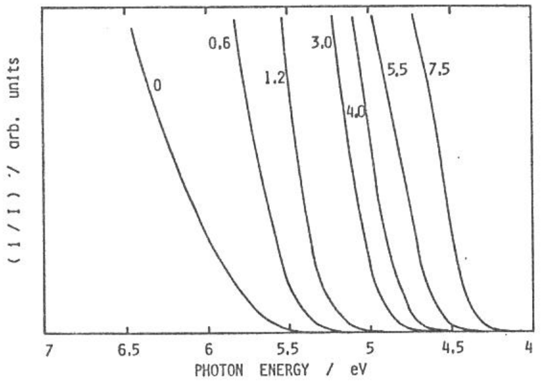

Fig.1. Photoconductivity excitation spectra near the threshold of pure vapor TMAE and TMAE-doped super-critical xenon at each xenon density in the unit of $10^{21}cm^{-3}$.

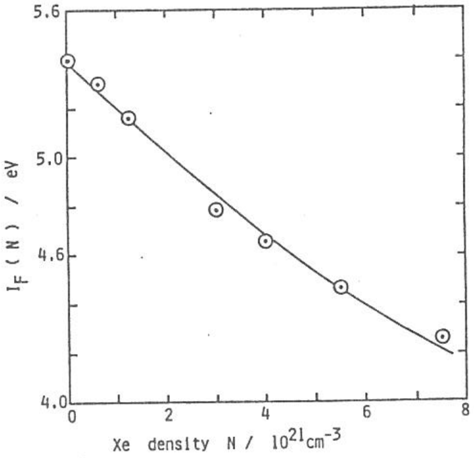

Fig.2. $I_f$ versus xenon fluid density N. Solid line shows the result of calculation (see text).

# EFFECT OF XENON DENSITY ON STRUCTURES IN PHOTOCONDUCTIVITY EXCITATION SPECTRA OF SUPERCRITICAL XENON DOPED WITH ANTHRACENE+)

Kazumichi NAKAGAWA, Arisato EJIRI, Masaru NISHIKAWA and *Kazuie KIMURA

Department of Pure and Applied Sciences, University of Tokyo, 3-8-1
Komaba, Meguro-ku, Tokyo 153, Japan
*The Institute of Physical and Chemical Research, Wako, Saitama 351, Japan

Recently, Holroyd et al.[1] studied photoconductivity excitation spectra of several hydrocarbon liquids doped with anthracene(A) and suggested that the photoconductivity structure observed above the first ionization potential of A, are due to molecular Rydberg transitions of A without energy shift from the vapor phase values because of close correspondence to the vapor-phase Rydberg transitions assigned by Koch et al.[2]. This suggestion seems to contradict strongly many studies which conclude that Rydberg transitions shift in high pressure gases and in condensed phases[3,4]. In this work, we measured photoconductivity excitation spectra of supercritical xenon doped with anthracene (A/Xe(N) system) as a function of density N in attempt to examine whether the structures do or do not shift with change in xenon density. The origin of the structures is also discussed.

A heavy-walled photoconductivity cell having a gold film electrode (thickness ~15nm) evaporated inside the entrance quartz window was used. Monochromatic light beam from a Seya-Namioka monochromator on BL7B of the UVSOR was used with bandwidth of 0.8 nm. Xenon density N (in the unit of $10^{21}cm^{-3}$) was controlled from 3.0 to 8.0 by adjusting the pressure from 62 to 99 bar at 300 K. Liquid 2,2-dimethylbutane was also used as a solvent (A/DMB system) in order to confirm that our experimental set-up can reproduce the structures observed by Holroyd et al.[1, 5].

Fig. 1 shows photoconductivity excitation spectra measured at 300 K. Values of photoconductivity threshold $I_f$ of A/Xe(8) system (curve (b)) determined by the empirical 5/2-th power law[6] is 6.15 eV, which is nearly the same as that for A/DMB system(curve (a)), 6.14 eV. It is noteworthy that the photoconductivity structures for both systems are almost identical, which means that the nature of the interaction between A and the host medium is essentially the same for both systems.

The energy values for the structures in the A/Xe(N) spectra are plotted against N in Fig. 2. Curve $I_f$ shows density dependence of $I_f(N)$ values[7]. Curves 1 to 4 are drawn in parallel to the $I_f$ curve in such a manner as to let the largest number of points be on a single curve. As seen from the figure, curves 1 to 4 reproduce very well the density dependence of the energy positions of the structures. Thus it is reasonable

---

+) To be appeared in Chem. Phys. Lett. (in press).

to interpret that energy shift of the structures are due to the same mechanism which gives rise to the shift in the photoconductivity threshold $I_f(N)$.

Since the shift in $I_f$ values are caused by medium polarization for positive ions and also electrons, the electronic states from which the photoconductivity structures originate are of spatially extended nature. There are three possibilities;

1. Rydberg states converging to the second ionization potential of anthracene with energy shift P(N)+Vo(N) at each density N.
2. Vibrational levels of anthracene ion populated through autoionization of neutral superexcited states ($S^{**}$) of A as suggested by Tweeten et. al.[8] on the basis of the agreement of photoconductivity structures to the vibrational progression observed in the photoelectron spectrum of anthracene vapor.
3. Rydberg states converging to the first ionization potential of A without shift[1], which is in apparent agreement with the recent observation of absorption spectra of NO in fluid argon in the lower density region[9].

References: [1]R.A.Holroyd, J.M.Preses, E.H. Böttcher and W.F.Schmidt,J.Phys.Chem.88,744(1984). [2]E.E.Koch, A.Otto and K.Radler, Chem.Phys.Lett. 21, 501(1973). [3]e.g. Chr.Füchtbauer and H.-J. Reimers, Z.Phys. 97,1(1935). [4]R.Reininger, I.T. Steinberger, S.Bernstorff, V.Saile and P.Laporte, Chem. Phys. 86,189(1984). [5]R.A.Holroyd and K. Nakagawa(unpublished data). [6]R. A.Holroyd, J.M. Preses and N.Zevos, J.Chem.Phys. 79,483(1983). [7]K. Nakagawa, A.Ejiri, K.Itoh and M.Nishikawa, Chem. Phys.Lett. 147,557(1988). [8]D.W.Tweeten and S.Lipsky (to be published). [9]E.Morikawa, A.M. Köhler, R.Reininger and V.Saile, J.Chem.Phys. 89, 2729(1988).

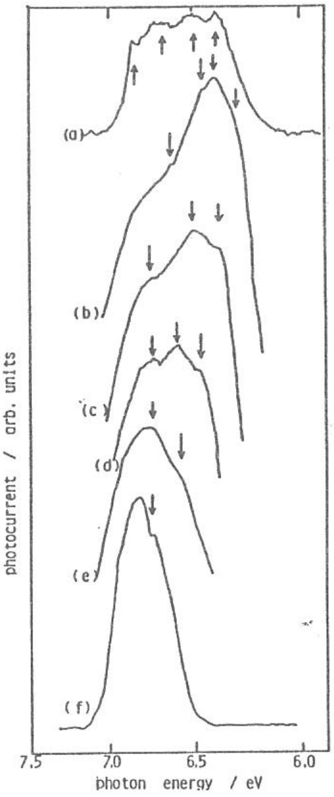

Fig. 1. Photoconductivity excitation spectra at 300 K for anthracene/ liquid 2,2-dimethylbutane (a) and anthracene/ supercritical xenon at xenon density of 8.0(b), 6.6(c), 5.4 (d), 4.3(e), 3.6(f) x $10^{21} cm^{-3}$. Arrows mark position of structures.

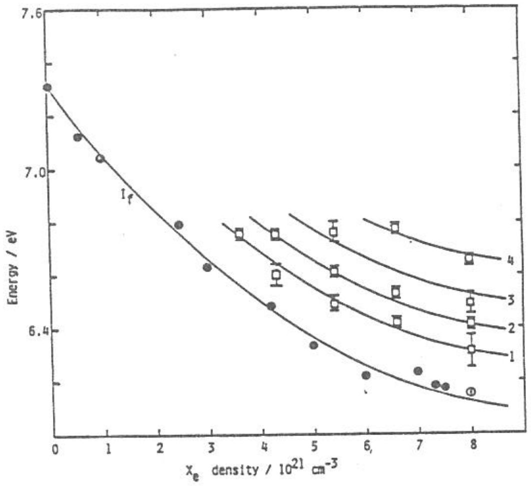

Fig. 2. A plot of enrgies of photoconductivity structures (□) vs. xenon density. Curve $I_f$ shows density dependence of photoconductivity threshold (●). See text for curves 1 to 4.

# ANGLE-RESOLVED PHOTOEMISSION FROM ORIENTED THIN FILMS OF STEARONE WITH SYNCHROTRON RADIATION : PART II BINDING ENERGY CALIBRATION OF PHOTOEMISSION SPECTRA

N. UENO, K. SEKI*, N. SATO**, H. FUJIMOTO***, K. SUGITA

and

H. INOKUCHI***

Department of Image Science and Technology,
Faculty of Engineering, Chiba University, Yayoi-cho, Chiba 260

*Department of Materials Science, Faculty of Science,
Hiroshima University, Hiroshima 730

**Department of Chemistry, College of Arts and Sciences,
The University of Tokyo, Komaba, Meguro, Tokyo 153

***Institute for Molecular Science, Myodaiji, Okazaki 444

In our previous report [1], we mentioned that there was an unclarified binding energy shift in the photoemission spectra of stearone depending on the photon energy. Recently we found that this energy shift was the result of incorrect calibration of the PGM monochromator.

Here, we present the corrected spectra in Fig. 1 and recalculated energy band dispersion in Fig. 2. In Fig. 2, the experimental results for n-$C_{36}H_{74}$ [2,3] and LB-films of Cd-arachidate [2] are also shown for comparison. The energy axes for n-$C_{36}H_{74}$ and Cd-arachidate are slightly shifted to fit the deep-lying $B_1$ band at k=0. The dotted curves are the experimentally-expected dispersion for $A_1$ and $B_1$ bands.

## References

1) N. Ueno, K. Seki, N. Sato, H. Fujimoto, K. Sugita, and H. Inokuchi, UVSOR Activity Report 66 (1987).
2) K. Seki, N. Ueno, U. O. Karlsson, R. Engelhardt, and E. E. Koch, Chem. Phys. 105, 247 (1986), and references therein.
3) H. Fujimoto, T. Mori, H. Inokuchi, N. Ueno, K. Sugita and K. Seki, Chem. Phys. Lett., 141, 485 (1987).

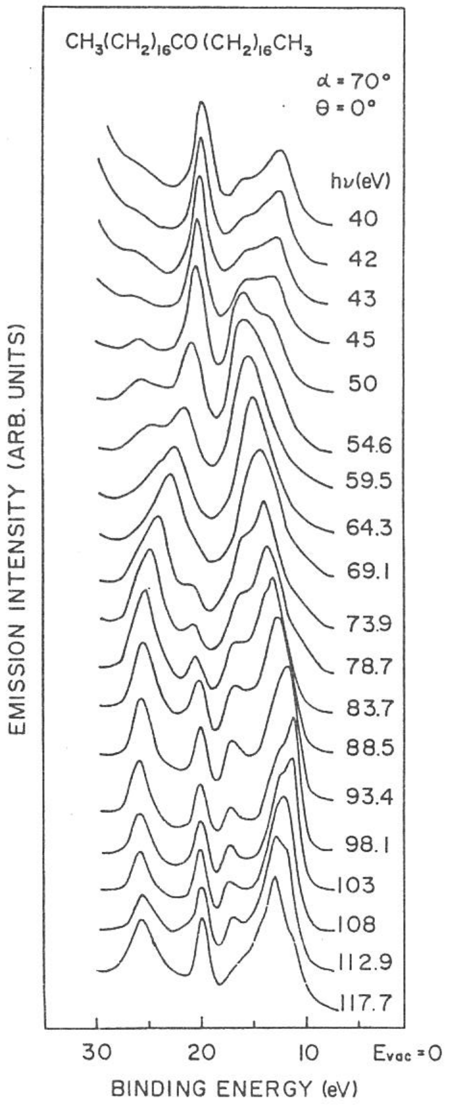

Fig. 1 Photon energy dependence of normal-emission photoelectron spectra of stearone (corrected).

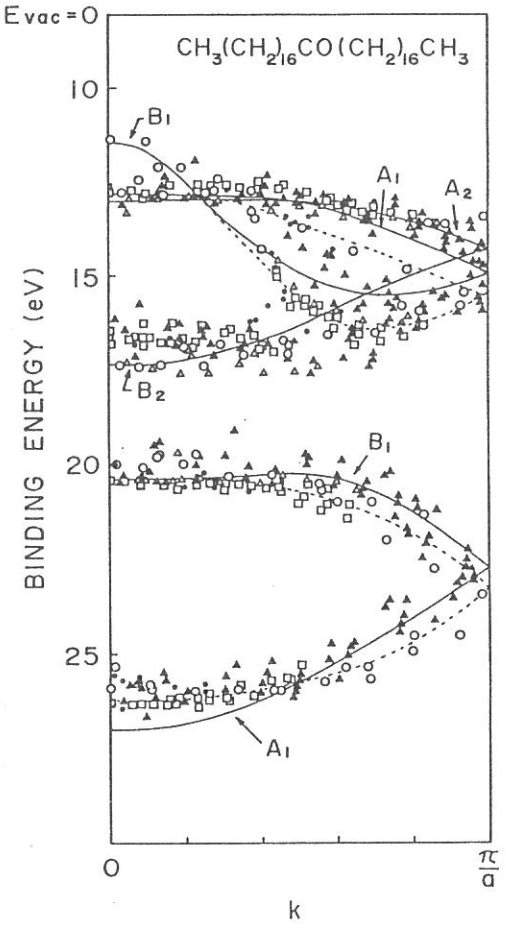

Fig. 2 Energy-band dispersion of stearone(•,○). The results for n-$C_{36}H_{74}$ (△)[2](▲)[3] and LB-films of Cd-arachidate (□)[2] are also shown for comparison.

# PHOTOELECTRON SPECTROSCOPY OF POLY(DIMETHYLSILOXANE)

Tomei SUGANO, Kazuhiko SEKI, Toshiaki OHTA,
Hitoshi FUJIMOTO,* and Hiroo INOKUCHI*

Department of Materials Science, Faculty of Science, Hiroshima
University, Hiroshima 730
*Institute for Molecular Science, Myodaiji, Okazaki 444

Recently, Si containing polymers attract much interest due to their unique electronic and electric properties. We have started a systematic study of the electronic structure of these polymers, and already reported the uv and X-ray photoelectron spectroscopy of poly(dimethylsilylene (PDMS) $\leftarrow Si(CH_3)_2 \rightarrow_n$ [1] and poly(methylphenylsilylene) $\leftarrow SiCH_3(C_6H_5 \rightarrow_n$ [2]. Here we report the UV photoelecteron spectra of polydimethylsiloxane (PDMSO) $\leftarrow O-Si(CH_3)_2 \rightarrow_n$, which is known to be a good insulator.

The liquid sample of mean molecular weight of 4940 was obtained from Chisso Co. The specimen for the UPS measurements was prepared by spin coating of a few drops of 0.2 w/w $CH_2Cl_2$ solution onto Cu or Mo substrates. The liquid film sample did not flow down even for a vertical setup of the substrate surface due to its high viscosity. The photoelectron spectra were measured on the angle-resolved photoemission system of BL8B2 in the photon energy range of 20-120 eV.

In Fig. 1(a), we show the photoelectron spectrum at 103.5 eV. The spectrum measured at other photon energies showed similar spectral features. For comparison, in Fig. 1(b)-(d) we also show the reported UPS spectra of related compounds: PDMS [1], disiloxane, and $SiO_2$. The correlation derived from these data according to the following discussion is summarized in Fig. 2.

Among the compounds in FIg. 1, PDMS shows the lowest ionization threshold (5.9 eV), which is derived from Si-Si bonds. PDMSO has no such bonds, and its ionization threshold, as determined precisely by independent measurements by a retarding field analyzer, is 8.5 eV. Such large value is similar to other good insulators such as polyethylene (8.5 eV) [3] and poly(tetrafluoroethylene) (10.6 eV) [4]. The peak A is ascribed to the O2p lone pairs as in the case for disiloxane [5] and $SiO_2$ [6].

The peaks B and D are assigned to the states derived from the SiC bonds and Si3s levels, from the comparison with the PDMS spectrum. Due to the inductive effect of electron-withdrawing O atoms, these states are expected to be shifted to higher binding energy in going from PDMS to PDMSO. The peaks B and D are at a little higher energies than the features of PDMS assigned to these states, respectively. The peak D may contain contribution from the O2p orbitals, as in the case of disiloxane and $SiO_2$.

The peak C is assigned to the states from the $CH_3$ groups, which appears at the same energy in PDMS. They will not be much affected by the introduction of the O atoms. Finally, the peaks E and F are easily assigned to the C2s and O2s levels, which agree with those of similar peaks seen in the spectra of PDMS and $SiO_2$, respectively.

The present results clearly show that the electronic structure of PDMS is drastically changed by inserting oxygen atoms to form PDMSO. The sigma conjugation of PDMS is broken by the O atoms. This change is comparable to the large change from poly(p-phenylene) to poly(p-phenylene oxide), where the pi-coinjugation is broken by the O atoms [7].

## References

[1] K. Seki, T. Mori, H. Inokuchi, and K. Murano, Bull. Chem. Soc. Jpn., 61, 351 (1988).

[2] K. Takeda, M. Fujino, K. Seki, and H. Inokuchi, Phys. Rev. B36, 8129 (1987).

[3] M. Fujihira and H. Inokuchi, Chem. Phys. Lett., 17, 554 (1972).

[4] H. Tanaka, K. Seki, T. Ohta, H. Fujimoto, and H. Inokuchi, unpublished.

[5] H. Bock, P. Mollere, G. Becker, and G. Fritz, J. Organomet. Chem. 61, 113 (1973).

[6] T. DiStefano and D. E. Eastman, Solid State Commun., 9, 2259 (1971).

[7] G. Crecelius, J. Fink, J. J. Ritsko, M. Stamm, H.-J. Freund, and H. Gonska, Phys. Rev., B28, 1802 (1983).

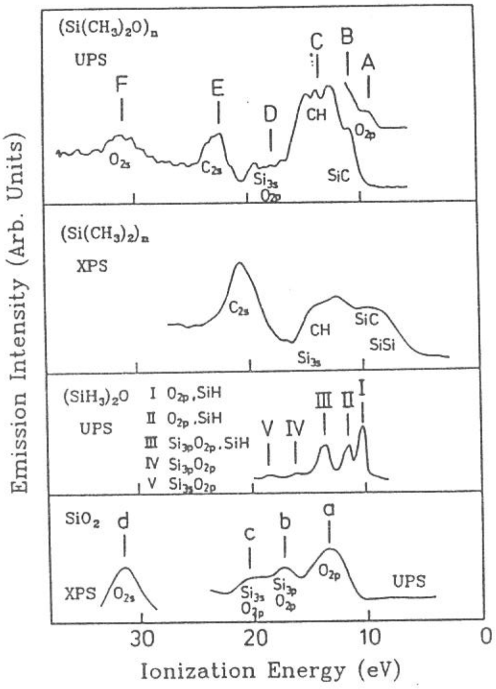

Fig. 1. Photoemission spectra of
(a) poly(dimethylsiloxane) (PDMSO),
(b) poly(dimetjylsilylene) (PDMS)[1],
(c) disiloxane [5] and (d) $SiO_2$ [6]

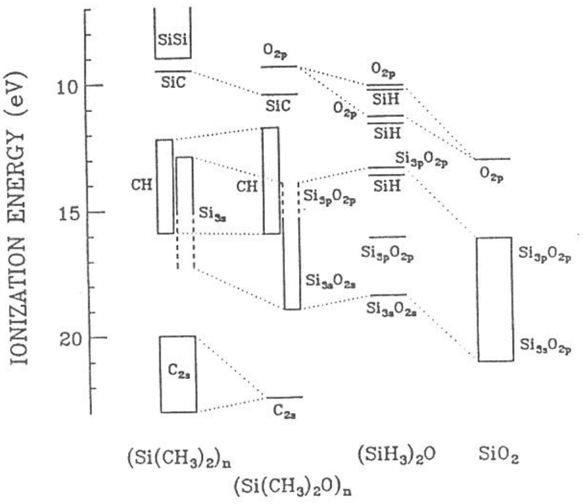

Fig. 2. Correlation of ionization energies of photoelectron bands in Fig. 1.

# PHOTOEMISSION SPECTRA OF NAPHTHACENE THIN FILMS

Naoki SATO, Nobuo UENO,* Hitoshi FUJIMOTO,** Kazuhiko SEKI,***
Kazuyuki SUGITA,* and Hiroo INOKUCHI**

*Department of Chemistry, College of Arts and Sciences,*
*University of Tokyo, Komaba, Meguro, Tokyo 153*
**Department of Image Science and Technology, Faculty of*
*Engineering, Chiba University, Chiba 260*
***Institute for Molecular Science, Myodaiji, Okazaki 444*
****Department of Materials Science, Faculty of Science,*
*Hiroshima University, Hiroshima 730*

The electronic structure of solid naphthacene has often been studied using photoemission spectroscopy (see, *e.g.*, ref. 1), since naphthacene is classified to a typical organic semiconductor. The vapor pressure of naphthacene is not so high as its thin films should be held on a cooled substrate in UHV for making photoemission measurements. Their photoemission spectra are observed to be rich in features in the valence electron region as compared with those for other organic materials. Such results make this material feasible to a study of the electronic structure in some detail.

In this work, VUV photoemission spectra of naphthacene thin films were measured in a wide range of photon energy, *i.e.* 30 - 103 eV, for the purpose of studying their electronic structure in connection with the molecular arrangement in the solid state. The results can effectively be compared with those obtained from the measurement in the photon energy range 10 - 45 eV by Yannoulis, *et al.*.2)

Naphthacene films of 20 - 60 nm thickness were slowly vacuum-deposited onto a Mo substrate at room temperature and *in situ* measurements of their photoemission spectra were made, using the angle-resolved UPS (ARUPS) system3) installed at the beam line BL8B2 of the UVSOR. The films prepared in the way above are known to be polycrystalline with nearly upright orientation of the planar naphthacene molecules or with *ab*-plane of the unit cell in a crystallite parallel to the substrate surface.

Fig. 1 depicts ARUP spectra of a naphthacene thin film as a function of polar angle $\theta$ for the emission of the electrons excited by *s*-polarized ($\alpha$ = 0°) light at a photon energy of 31 eV, where $\alpha$ is the polar angle for the incident light. For comparison, $\theta$ dependence of the spectra was also measured with predominantly *p*-polarized ($\alpha$ = 70°) light. These results are in good agreement with those by Yannoulis, *et al.*[2] This indicates that molecules are oriented almost perpendicularly also in the sample film.

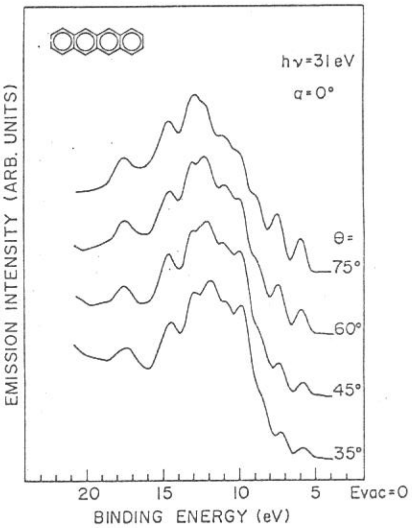

**Fig. 1.** $\theta$-dependence of the UPS spectra.

Fig. 2 shows photon energy dependence of normal emission ($\theta$ = 0°) spectra of the naphthacene film obtained at $\alpha$ = 70°. Seventeen features are observed in the valence band region: they extend over a binding energy range from 5.8 eV to 22 eV under the vacuum level. No features demonstrate any shifts on the abscissa, whereas a drastic change has been observed in their relative intensities for the wide range of the photon energy. This will be explained predominantly by the photon energy dependence of photoionization cross sections which is different in the valence molecular orbitals and, in addition, by angular distributions of electrons emitted from the oriented molecules. To elucidate these, further studies both experimental and theoretical are still in progress.

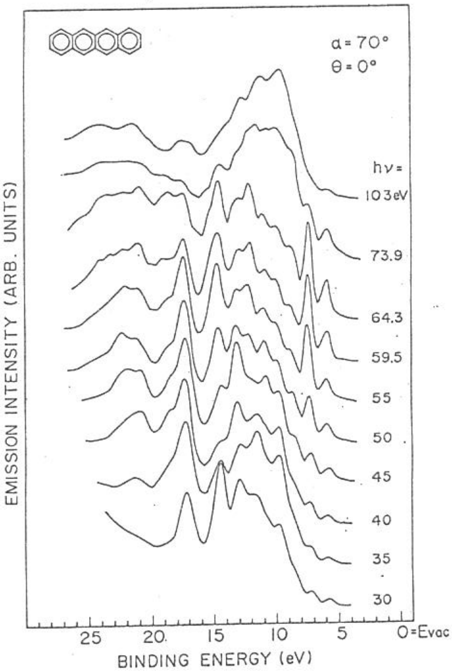

**Fig. 2.** $h\nu$-dependence.

1) K.Seki, H.Inokuchi & Y.Harada, *Chem.Phys.Lett.* 20(1973)197.
2) P.Yannoulis, E.E.Koch & M.Lähdeniemi, *Surf.Sci.* 192(1987) 299.
3) K.Seki, H.Fujimoto, T.Mori & H.Inokuchi, *UVSOR Act.Rep.* (1986)11.

# Angle-resolved photoemission from oriented Thin Films of Poly-Fluoroaluminium Phthalocyanine.

M. Fahy, H. Fujimoto, A. Dann, H. Hoshi, Y. Maruyama,
H. Inokuchi and M. Willis*

*Institute for Molecular Science, Myodaiji, Okazaki 444.*
**Department of Chemistry, University of Nottingham,*
*Nottingham, UK.*

Phthalocyanines, whilst they have been known for many years, still represent one of the best materials for future applications [1]. They are among the most stable organic materials known, both chemically and thermally and can be sublimed to form high quality thin films. Many workers have measured the UPS spectra of phthalocyanine materials [2]. However, agreement between MO calculations and experiment is generally quite poor and there is some disagreement on the assignment of the UPS peaks. The technique of ARUPS using synchrotron radiation on an oriented sample should enable a more in depth investigation to be carried out. Unfortunately most phthalocyanines do not easily form oriented thin films or crystals large enough for ARUPS measurements. However, recent work using molecular beam epitaxy (MBE) techniques have shown it is possible to get a highly oriented thin film of poly-fluoroaluminium phthalocyanine (fig.1) on a KBr crystal substrate [3]. The oriented and polymeric nature of the sample make it an ideal material to study.

Preliminary experiments have revolved around preparing an oriented sample in the preparation chamber of the UPS. Films need to be prepared and measured in-situ because PcAlF strongly adsorbs oxygen. When a 100A PcAlF was sublimed, in-situ, on KBr (1A/minute, $10^{-8}$torr) a good quality film was obtained but a UPS spectrum could not be measured because of charge-up of the sample. Coating with a further 5A of gold had no effect. To try to prevent charge-up a PcAlF film prepared in the MBE system on a KBr substrate was mounted on electrically conducting cohesive tape and then the KBr was dissolved off with water. This, it was hoped, could then act as a conducting, epitaxial, substrate for future depositions in the UPS. Unfortunately the water used to remove the KBr in some way affected the conducting properties of the tape and the quality of the film. Hence the measured spectra were distorted by charge up and signal from the substrate.

UPS spectra were taken for a film of PcAlF prepared in-situ (1A/minute, $10^{-8}$Torr) on a polycrystalline molybdenum substrate. The spectra were taken with an incident angle of 60° at normal emission with incident energies of 110eV and 40eV (figures 2 and 3 respectively). In figure 3 the spectrum measured at $h\nu$=40eV is compared to those obtained for $PcH_2$ and PcCu by Battye [2]. The similarities are clear suggesting that in this region the spectrum is due mainly to orbitals associated with the Pc ring. The peak labeled A is due to the molecular $\pi$ orbital. The peak B is associated with the non-bonding N loan pair orbitals. C and D are predominantly C 2p in character. The region to slightly higher energy of D is dominated by 4 strongly binding $\sigma$ orbitals which can form co-ordinative bonds with the central metal. When $h\nu$=110eV it is hard to distinguish structure apart from the large peak from an Al core level. The position of peaks due to the fluorine and the effect of polymerisation is not clear at present.

Future work will involve investigating the higher energy region and using oriented samples to obtain the energy band dispersion.

References:
1 J. Simon and J-J. Andre, Molecular Semiconductors, Springer-Verlag (1985).
2 F. Battye, A Goldmann and L. Kasper, Phys. Stat. Sol. (b) 80, 425 (1977).
3 A. Dann, H. Hoshi, Y. Maruyama, T. Inabe and M. Willis, Bunshi Kouzo Sougou Tourondai (Tokyo 1988) 1C04.

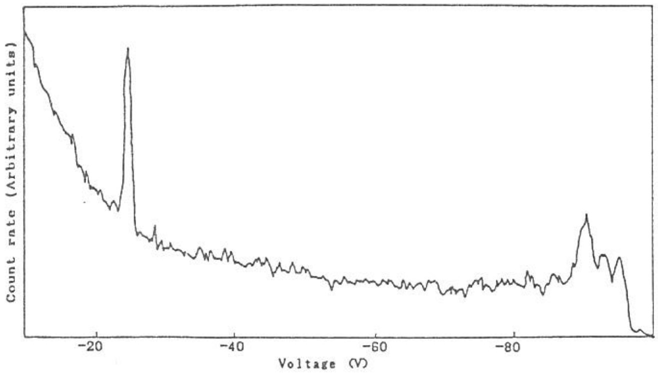

Figure 2: UPS spectrum of PcAlF with $h\nu$=110eV.

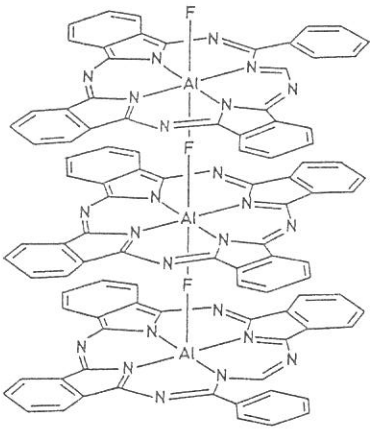

Figure 1: The structure of PcAlF.

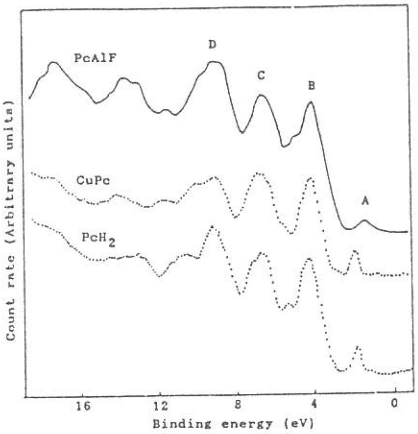

Figure 3: Comparison of UPS spectrum of PcAlF with $h\nu$=40eV with spectrums for $PcH_2$ and CuPc as measured by Battye et al [4] using $He^{II}$ radiation ($h\nu$=40.8eV).

# CHARACTERIZATION OF LB FILMS CONTAINING OLIGOTHIOPHENES BY ULTRAVIOLET PHOTOELECTRON SPECTROSCOPY

H.Nakahara, J.Nakayama, M.Hoshino, K.Fukuda,
H.Fujimoto*, U.Nagashima*, H.Inokuchi* and K.Seki**

Department of Chemistry, Faculty of Science,
Saitama University, Urawa 338,
*Institute for Molecular Science, Myodaiji, Okazaki 444,
**Department of Material Science, Faculty of Science,
Hiroshima University, Hiroshima 730.

Though conducting thin films of polythiophenes have been widely investigated, the molecular arrangements were scarecely controlled. Previously, using several oligothiophenes the molecular organization in LB films has been reported from consideration of the surface pressure - area isotherms for the monolayers in relation to the molecular structures such as the size and geometry.1) It has been clarified that the rod-like molecules with a sufficient molecular length can be incorporated with a well-defined alignment in mixed monolayers of fatty acids, whereas this is not the case for the bent molecules with $\alpha$-$\beta$ linkages. In this work, we characterize the LB films containing oligothiophenes by the ultraviolet photoelectron spectroscopy (UPS) in addition to the polarized electronic spectra.

Oligothiophenes and the related compounds used in this work are listed in Table 1, together with their melting points and the absorption maxima in chloroform solution. These were prepared as described previously1) and purified by recrystallization from hexane or chlorobenzene, or by sublimation.

Figure 1 shows the polarized electronic absorption spectra obtained with 45° incidence for the LB film of $T_5$ mixed with Cd stearate (1:2 in a molar ratio) compared with the solution spectrum. The visible band in the solution exhibits a blue shift in the LB film and the polarized spectra for the film shows a significant dichroism, indicating the almost vertical orientation of the long-axis of the $T_5$ molecule.

Figure 2 shows the UPS spectra of the LB film (5 layers) containing $T_5$ mixed with Cd stearate, in various angle ($\theta$) of the photoemission with the 60° incidence ($\alpha$) of the photon ($h\nu = 45$ eV) compared with that of the vacuum-deposited film. The bands A and B below $E_b = 5$ eV assigned to the $\pi$ bands are relatively intensified with increasing of the angle $\theta$. This fact reflects the vertical orientation of $T_5$ molecule in the LB film.

Comparing the UPS spectra for the LB film of Cd stearate embedding $T_5$ with those for the pure Cd stearate film ($h\nu$ = 60 eV), the $\pi$ bands can be apparently observed in the lower binding energy ($E_b$) region, as shown in Fig.3. For $T_4$ molecules embedded in the LB film of Cd stearate, any $\pi$ bands couldn't appear in the lower $E_b$ region because of the insufficient molecular length. $T_7$ and $T_8$ molecules cannot yet be well organized in the LB films because of an experimental difficulty due to their little solubility in organic solvents.

REFERENCE

1) H.Nakahara, J.Nakayama, M.Hoshino and K.Fukuda, Thin Solid Films, 160, 87 (1988).

Table 1. Oligothiophenes used in this work.

| | | m.p. / °C | $\lambda_{max}$ /nm (CHCl$_3$ soln) | Abbr. |
|---|---|---|---|---|
| I. | 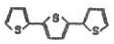 | 95 - 96 | 252, 354 | $T_3$ |
| II. | 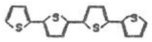 | 213-214 | 390 | $T_4$ |
| III. | 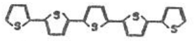 | 252-254 | 416 | $T_5$ |
| IV. | 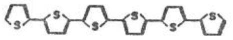 | 300 | 438 | $T_6$ |
| V. |  | 282-283 | 460 | $T_3VT_3$ |
| VI. |  | 326-328 | 440 | $T_7$ |
| VII. | 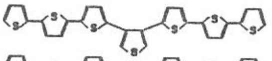 | 203 | 370 | $T_3T^{\beta}T_3$ |
| VIII. | 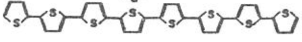 | 364 | — | $T_8$ |

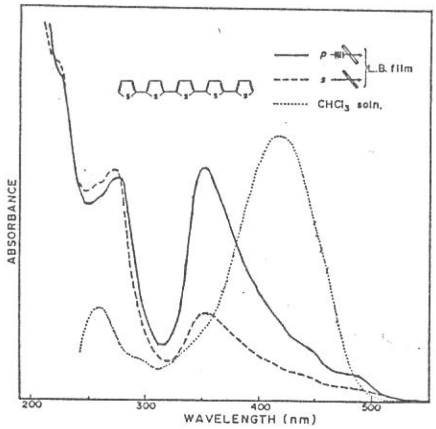

Fig.1. Polarized electronic spectra for hte LB film of $T_5$ mixed with Cd stearate, as compared with the solution spectrum.

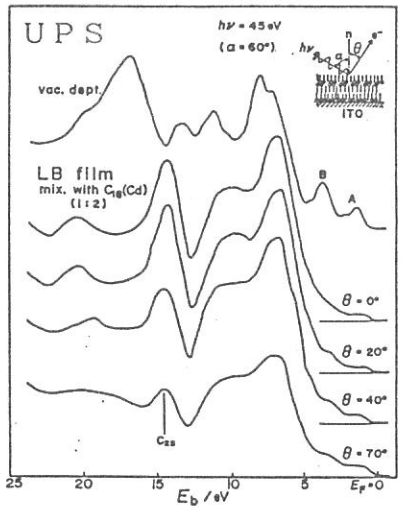

Fig.2. Angular dependence of UPS spectra of the LB film containing $T_5$ ($h\nu$ =45eV).

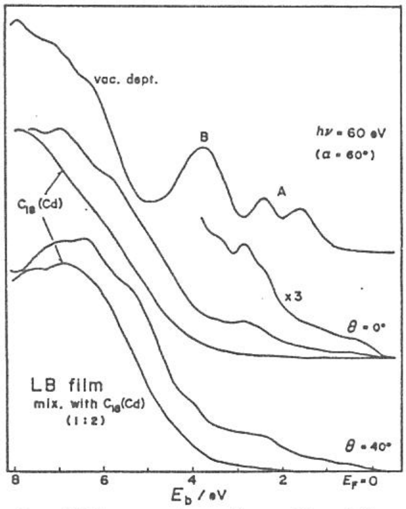

Fig.3. UPS spectra for the LB film of Cd stearate embedding $T_5$, as compared with those for the pure Cd stearate film.

# ULTRAVIOLET PHOTOEMISSION STUDY OF POLYTHIOPHENE OLIGOMERS (II)

H. Fujimoto, K. Seki,* U. Nagashima, H. Nakahara,**
J. Nakayama,** M. Hoshino,** K. Fukuda,** and H. Inokuchi

*Institute for Molecular Science, Myodaiji, Okazaki 444*
**Department of Materials Science, Faculty of Science,*
*Hiroshima University, Hiroshima 730*
***Department of Chemistry, Faculty of Science,*
*Saitama University, Urawa 338*

We have reported previously on the effect of irregularity on $\pi$-electron systems by the ultraviolet photoelectron spectroscopy (UPS) for several oligothiophenes.1,2) It is shown that the $\beta$ linkage significantly affects the electronic structure of the polythiophene system, confirming that the control of polymerization is important for achieving good conductivity.

Here we report the results of the UPS study on the $\alpha$-linked oligothiophenes, $\alpha_4$-$\alpha_8$, containing 4-8 thiophene rings. Our purpose is to investigate the dependence of the electronic structure on the number of thiophene rings and to confirm that $\alpha_7$ is a good model for polythiophene.

Thin films of 30-50 nm thickness were prepared by *in situ* vacuum evaporation in the preparation chamber and subsequently transferred to the main chamber.3) UPS spectra were measured for the normal emission from a sample surface with the incident angle of the light beam of 60°.

Figure 1 shows the orbital energies of $\alpha_n$ calculated by MNDO method.4 Thiophene $\alpha_1$ has two $\pi$-orbitals; one extends on the $\alpha$ carbons and the other has almost no contribution from $\alpha$-$C_{2p}$ orbitals. Therefore, one of them splits into bonding and antibonding $\pi$-bands in $\alpha_n$ and becomes the widely dispersive $\pi$-band in polythiophene, while the other forms a nonbonding $\pi$-band.

Figures 2-4 show the UPS spectra of oligothiophenes. The calculated orbital energy by MNDO (vertical line) and the Gaussian broadened theoretical UPS spectrum (broken line) are also shown. The peak at $E_b$=3.5 eV is the above mentioned nonbonding $\pi$-band and almost independent of the number of thiophene units. In the lower binding energy part ($E_b$=0.7-3 eV), several peaks are observed and become broader with unit number n of $\alpha_n$. At n≧7, a continuous $\pi$-band, which corresponds to the delocalized $\pi$-band,is observed in this region.

In summary, we could observed the $\pi$-band growing with increasing the unit number and compare with the calculated orbital energy by MNDO. The agreement between the observed and calculated spectra is very well, particularly in the $\pi$-region.

References

1) H. Fujimoto, U. Nagashima, H. Inokuchi, K. Seki, H. Nakahara, J. Nakayama, M. Hoshino, and K. Fukuda, *J. Chem. Phys.*, **89**, 1198 (1988).

2) H. Fujimoto, K. Seki, U. Nagashima, H. Nakahara, J. Nakayama, M. Hoshino, K. Fukuda, and H. Inokuchi, *UVSOR Activity Report*, **15**, 68 (1987).

3) K. Seki, H. Fujimoto, T. Mori, and H. Inokuchi, *UVSOR Activity Report*, **14**, 11 (1986).

4) U. Nagashima, H. Fujimoto, H. Inokuchi, and K. Seki, *J. Mol. Struct.*, in press.

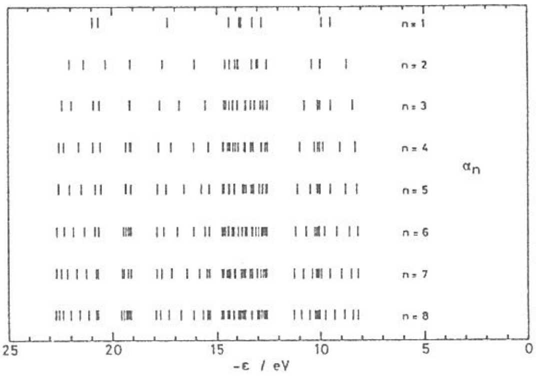

Fig.1 Calculated orbital energy by MNDO.

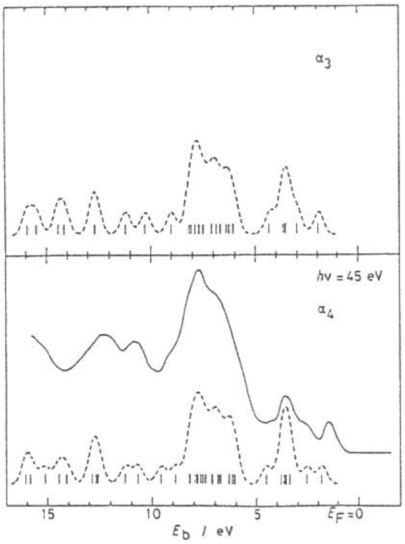

Fig.2 UPS spectra of $\alpha_3$ and $\alpha_4$. The orbital energy and Gaussian broadened UPS spectra are also shown.

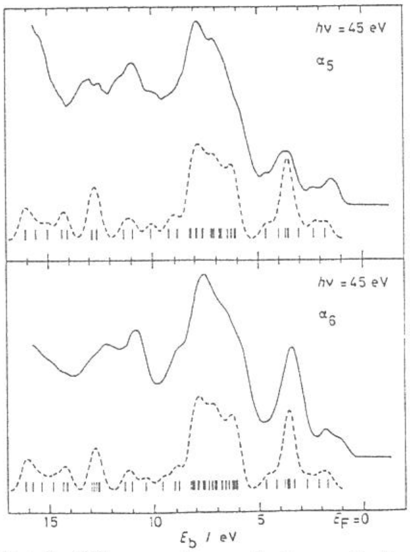

Fig.3 UPS spectra of $\alpha_5$ and $\alpha_6$.

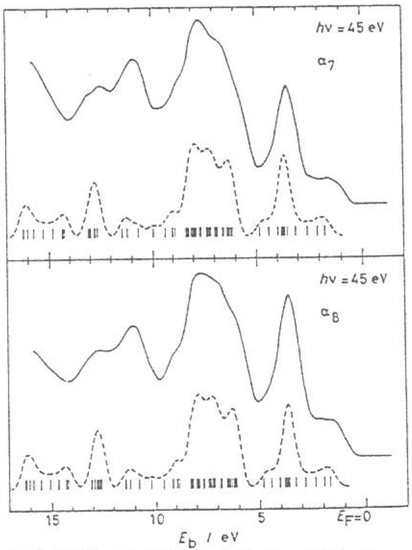

Fig.4 UPS spectra of $\alpha_7$ and $\alpha_8$.

# Photo-induced $CN^-$ Production on KCl with Undulator Light

Hideyuki NAKAGAWA, Toshiki DEGUCHI, Hiroaki MATSUMOTO,
Takeshi MIYANAGA[*], Masami FUJITA[**], Kazutoshi FUKUI[***]
and Makoto WATANABE[***]
Department of Electrical and Electronis Engineering,
Fukui University, Fukui 910
[*] Department of Physics, Faculty of Education,
Wakayama University, Sakaedani, Wakayama 640
[**] Maritime Safety Academy, Wakaba, Kure 737
[***] Institute for Molecular Science, Myodaiji, Okazaki 444

Bazhin et al.1) have found that a prominent molecular luminescence spectrum, containing some ten regularly spaced vibrational bands in the range 3.3 - 5.8 eV, is produced on some alkali halide crystals by bombardment with light ions ($H^+$ and $He^+$). Further studies2,3) on this luminescence have proved that the molecular bands are identical to the vibrational bands observed in certain alkali halide crystals doped with $CN^-$-ions4,5).

The same molecular luminescence bands have been observed on the KCl crystal with irradiation of undulator light (semi-monochromatic extreme ultraviolet light at 31.5 nm) and their fundamental behaviors, such as dose- and temperature-dependence, have been reported previously6). In the present study, the growth of the $CN^-$ luminescence bands, accordingly the growth of the $CN^-$-centers, have been investigated on the KCl crystal by varying environment gas species and gas pressure.

Figure 1 shows an emission spectrum obtained at RT on KCl which was freshly cleaved in vacuum and irradiated for 6 h with undulator light (UL) in the $8x10^{-7}$ torr $CO_2$ gas atmosphere. Measurements were made with a spectral band pass of 1.2 nm (0.02 eV at 5 eV). Nine well-defined molecular bands are situated with an equi-interval of about 0.25 eV in the region from 3.5 to 5.8 eV. These bands are identical to those observed in the KCl:$CN^-$ system5). The separation energy is referred to the stretching vibrational one of the ground state $CN^-$-ions. These emission bands could not be observed with non-irradiated KCl and enhance their intensity with increase of the irradiation dose. Thus, some photo-induced chemical reaction certainly occurs to create the $CN^-$-ions on the KCl crystal from the environment gas species.

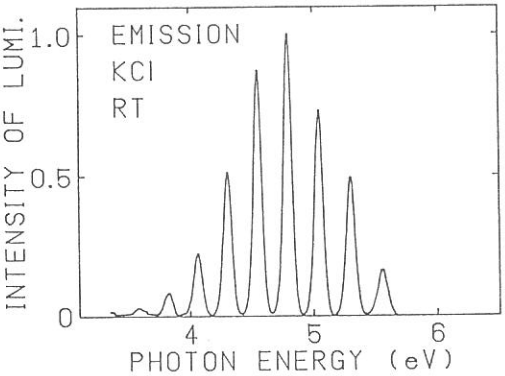

Fig.1 Emission spectrum of KCl irradiated for 6 h with undulator light in the $8x10^{-7}$ torr $CO_2$ gas.

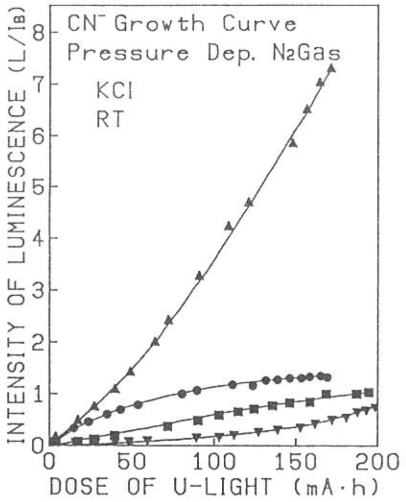

Fig.2 Growth curves of $CN^-$-centers on KCl irradiated in $N_2$ gas.

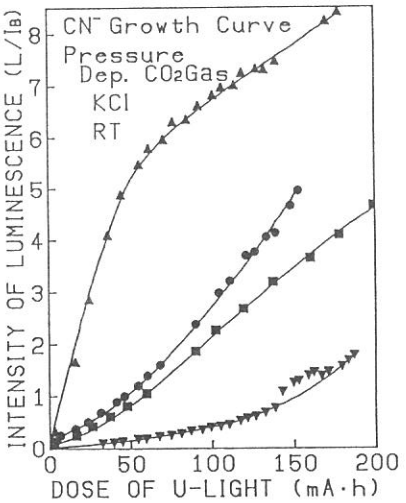

Fig.3 Growth curves of $CN^-$-centers on KCl irradiated in $CO_2$ gas.

Gas pressure:
▼ --$2\times10^{-9}$, ■ --$2\times10^{-8}$, ● --$1\times10^{-7}$, ▲--$8\times10^{-7}$ torr.

Figures 2 and 3 give the $CN^-$ growth data obtained at RT with KCl under UL-irradiation in the $N_2$ and $CO_2$ atmospheres. Measurements were made for the atmospheric gas pressure of $2\times10^{-9}$ ( ▼ ), $2\times10^{-8}$ ( ■ ), $1\times10^{-7}$ ( ● ) and $8\times10^{-7}$ ( ▲ ) torr. The intensities of the $CN^-$-luminescence, L, are normalized with electron beam current in the storage ring, $I_B$, and the value of the integrated beam current with respect to irradiation time is used as a measure of the irradiation dose. In the figures is plotted the peak intensity of the 5.07 eV band as a function of the irradiation dose. It is obvious from the figures that the $CN^-$-luminescence enhances its intensity with increase of the UL-dose and that the growth rate of the $CN^-$-centers become rapid as increasing atmospheric $N_2$ or $CO_2$ gass pressure. This indicates that the $CN^-$-centers are formed on KCl from the $N_2$ and/or $CO_2$ molecules with the aid of UL-irradiation. Though details of the $CN^-$ formation mechanism are not so clear at present, it would be supposed from the present experiments that the $CN^-$ production process consists of three steps, that is, photo-dissociation of source species such as $N_2$ and $CO_2$, chemical synthesis to form CN-radicals and photo-induced surface reaction to implant them as the $CN^-$-centers on/in the KCl crystal.

1) A.I.Bazhin et al.: J. Chem. Phys. 65 (1976) 3897.
2) W.A.Metz, E.W.Thomas: Nucl. Instrum. & Methods 194 (1982) 505.
3) D.Cherry et al.: Nucl. Instrum. & Methods B13 (1986) 533.
4) E.von der Heyden, F.Fischer: Phys.Status Solidi b69 (1975) 63.
5) M.Mendenhall et al.: Chem. Phys. Lett. 147 (1988) 59.
6) H.Nakagawa et al.: UVSOR 15 (1987) 56.

# FABRICATION OF ORGANIC THIN FILM BY SR-CVD

H. Yamada, M. Nakamura, H. Katoh, T. Hayakawa, S. Morita and S. Hattori
Dept. of Electronics, Nagoya Univ. Furocho, Chikusaku, Nagoya 464

Chemical vapour deposited film can be usually obtained through an excitation process of vapour monomer using photo, heating, ion beam, electron beam and plasma as the exciting sources. As a new CVD technology, Synchrotron Radiation Chemical Vapour Deposition (SRCVD) was investigated using BL8A line. Generally, photo-CVD have been conducted using UV wavelength which can be effectively absorbed in the vapour monomers. For SRCVD, the wavelength region shorter than 200 A are utilized for the film deposition. In this paper, the fundamental investigation on the direct pattern formation was performed using styrene monomer gas. The influences on the gas pressures and substrate temperature as CVD parameters were examined. If the direct fine pattern formation can be realized, it is expected that SRCVD can be a new dry resist coating manner in place of plasma polymerization for a vacuum lithography. The separate processes both the deposition and exposure are unified to be the single process by a simultaneous progress, resulting in a reduction of process number.

The styrene monomer gas was introduced from the back side of sample holder. Gas pressure was arranged by controlling the monomer flow rate from 0.15 to 0.5Torr. The dependence of substrate temperature was investigated at RT and 0 C. In the irradiation area at a diameter of about 4 mm, SRCVD was practically performed on Si substrate. The irradiation for SRCVD was conducted by opening the valve after an arrangement of monomer gas pressure. Practically, the deposition was conducted under the direct irradiation without X-ray filters at an electron energy of 750MeV. For the direct pattern formation, Ni mesh having the size of about 20x20 um$^2$ was set just before Si substrate. Influence of the gap between the mesh mask and substrate on the pattern profile was examined. The molecular structure of deposited styrene and film thickness were measured by IR and Tally-Step, respectively. The pattern profile was checked by an optical microscope.

Styrene film was deposited for the both the irradiated and unirradiated areas. Remarkably, the deposition advanced at the higher rate for an irradiated area than for an unirradiated area. The features of deposition rate on Si substrate are shown in Fig. 1 as a function of monomer gas pressure. By separating from the irradiation area, the deposition rate was extremely decreased. The film formation at an unirradiated area is considered to be due to the diffusion of styrene radicals excited in an irradiation area. The dependence on the substrate temperature is shown in Fig. 2. The gas pressure was kept at the constant pressure of 0.5 Torr during the deposition. By cooling the substrate, the deposition rate was remarkably enhanced for an irradiated area. However, it was almost unchanged for an irradiated area. It is considered for an irradiated area that the deposition rate could be enhanced by the increasing number of styrene radical adsorbed on the substrate due to the cooling. For an unirradiated area, it is expected that the deposition rate could not be increased because the diffusivity of styrene radical generated in an irradiation area became small with a drop of substrate temperature. In fact, the film deposition was observed after an irradiation time of a few seconds with cooling the substrate. The styrene film for an irradiated area could not be almost solved in benzene solvent, while that for an unirradiated area was easily developed in the same solvent. It was found that SRCVD of styrene was undergone accompanying with the reaction of crosslinking which can be induced by SR direct irradiation. Photographs of direct fine pattern formation which could be obtained by the direct irradiation through Ni mesh pattern are shown in Fig. 3. The terms of (a), (b) and (c) indicate Ni mesh pattern, the direct pattern formation at g=2mm and the direct pattern formation at g=0.2mm, respectively. When the pattern formation was performed at g=2mm, it was observed that the pattern profile was warped in a comparison with the original Ni mesh pattern. At g=0.2mm, the pattern profile could be successfully attained at the same profile as the original pattern. The warp of pattern profile was considered to be caused by the increasing spread of irradiated shape in proportion to the gap length. As a result, it is considered to be possible that the direct fine pattern formation can be successfully performed by the deposition method using the collimated SR irradiation.

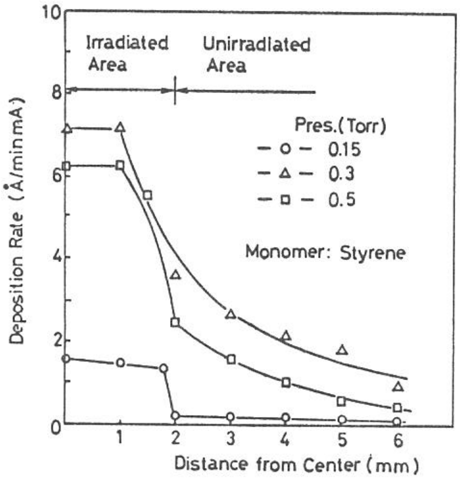

Fig. 1 Deposition rate as a function of monomer gas pre..

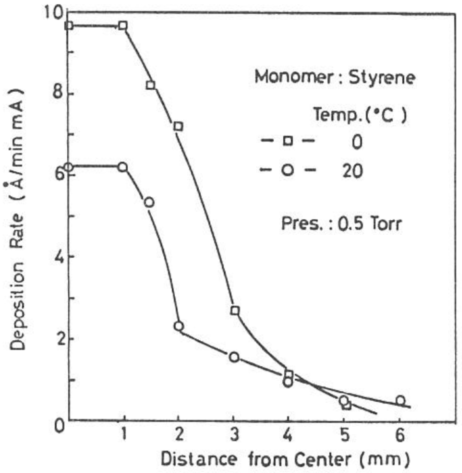

Fig. 2 Deposition rate as a function of substrate temp..

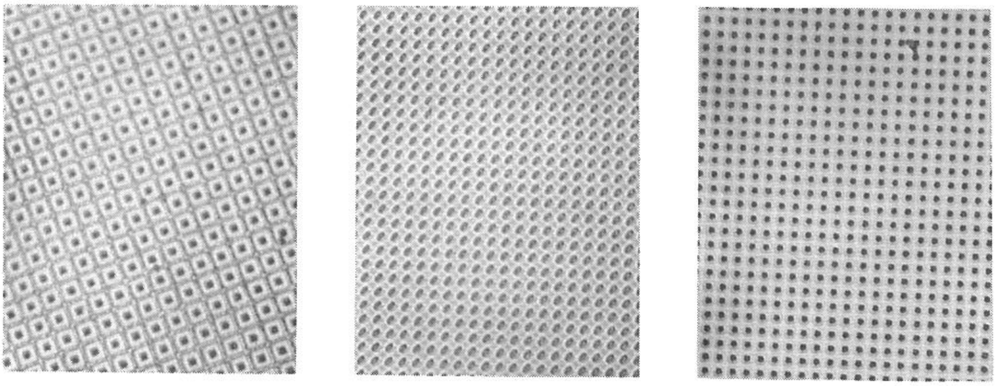

(a) Nimesh (b) g=2mm (c) g=0.2mm

Fig. 3 Photographs of as-deposited styrene pattern

# Synchrotron Radiation-Assisted Etching of Semiconductor Materials. II. Polycrystalline Silicons Using Undulator Light.

Kosuke SHOBATAKE, Haruo OHASHI,* Nobuo HAYASAKA**, Hiroshi KUME*** and Atsunari HIRAYA

Institute for Molecular Science, Myodaiji, Okazaki 444
* Visiting graduate student from Toyohashi University of Technology
** Sponsorial Research Fellow from VLSI Research Center, Toshiba Corporation, Komukai Toshiba-cho, Saiwai-ku, Kawasaki 210 JAPAN.
*** Graduate School of Natural Sciences, Niigata University, Niigata 920-21 Japan

Synchrotron radiation-assisted surface reactions of solid semiconductor have recently attracted attention from the viewpoint of the understanding of their mechanisms and the development of surface fabrication techniques.[1,2] So far the wavelength range of the synchrotron radiation (SR) used for this purpose has been limited to the unfiltered light or filtered light with thin metal films. In this study the photo-assisted etching reactions of various polycrystalline Si surfaces are studied using undulator light as a light source. For most of the present experiments we have used the undulator light from the beam line BL3A1 for the gap lengths 70 mm (14.2 nm) and 33 mm (wavelength of the 1st order light: 25.1 nm). We have measured the pressure and wavelength dependences of the etch rates of polycrystalline Si samples with $Cl_2$ gas.

**Experimental** Briefly the experiments are done using the modified surface photochemistry apparatus, stationed on the

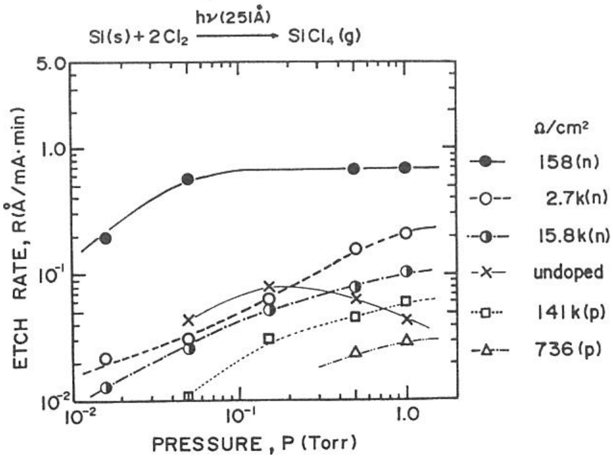

Figure 1. Etch rate vs. $Cl_2$ pressure for the SR-assisted etching reaction of polycrystalline Si surfaces.

undulator beam line BL3A1, which was hitherto installed on the beam line BL8A. The modified apparatus has one more differential pumping chamber than the former one.[1] The undulator light is irradiated on a sample attached on the sample manipulator in the reaction chamber filled with an etchant gas, whose pressure ranges from 0.016 to 1.0 Torr. The etch rate (in the units of Å/mA stored current•min) is determined by measuring the change in the sample thickness using an thickness measurement apparatus (Nikon model NFM-5) relative to the integrated irradiated SR for a given pressure of etchant gas.

**Results and Discussion**

Figure 1 shows the etch rates versus $Cl_2$ pressure for all six polycrystalline samples, three P-doped n-type, two B-doped p-type, and undoped poly-Si samples for the undulator light at 25.1 (at a gap length of 33 mm with an Al filter) and 14.2 nm. The pressure dependence of the etch rate differs quite a lot from one sample to another, ie as the electron density in the Si sample is varied. The undoped sample shows quite a different pressure dependence from other samples.

In Fig. 2 is illustrated the etch rate as a function of sheet resistance for the $Cl_2$ pressure of 0.5 Torr. The abscissa is scaled such that the free electron density decrease, ie. for the n-type poly-silicon samples the sheet resistance increases in the logarithmic scale and for p-type polysilicon samples the sheet resistance decreases as the resistance decrease relative to the undoped poly-silicon. We find that the etch decreases with decreasing the free electron density.

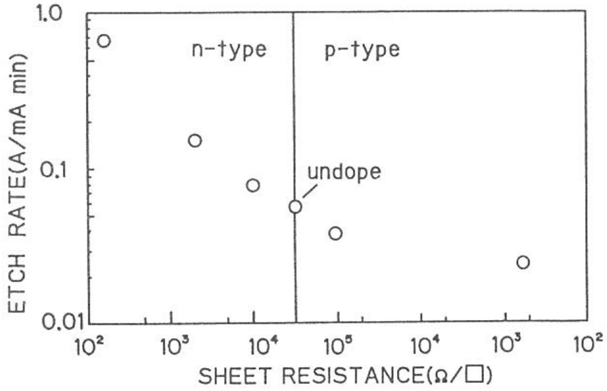

Figure 2. Etch rate of poly-Si surface vs. its sheet resistance for SR-assisted etching reaction using $Cl_2$ gas at 0.5Torr as an echant.

**References**

1] N. Hayasaka, A. Hiraya, and K. Shobatake, Jpn. J. Appl. Phys. **26**, L1110 (1987).

2] T. Urisu and H. Kyuragi, J. Vac. Sci. Technol. **B5**, 1436 (1987).

# Synchrotron Radiation-Assisted Etching of $SiO_2$ With $SF_6$ as an Etchant Using Undulator Light.

Kosuke SHOBATAKE, Haruo OHASHI,* Nobuo HAYASAKA**, Hiroshi KUME*** and Atsunari HIRAYA

Institute for Molecular Science, Myodaiji, Okazaki 444
* Visiting graduate student from Toyohashi University of Technology
** Sponsorial Research Fellow from VLSI Research Center, Toshiba Corporation, Komukai Toshiba-cho, Saiwai-ku, Kawasaki 210 JAPAN.
*** Graduate School of Natural Sciences, Niigata University, Niigata 920-21 Japan

Synchrotron radiation-assisted surface reactions of $SiO_2$ have recently been studied by Urisu and Kyuragi, who have found the importance of the surface excitation effect as the rate determining step.[1] In the present study the photo-assisted etching reaction of $SiO_2$ surface is studied using undulator light as a light source and normal synchrotron light. For most of the present experiments we have used the undulator light from the beam line BL3A1 for the gap lengths 70 mm (14.2 nm) and 33 mm (wavelength of 25.1 nm for the first order light). We have measured the pressure and wavelength dependences of the etch rates of $SiO_2$ with $SF_6$ gas. The experimental procedures are described in the preceding report.

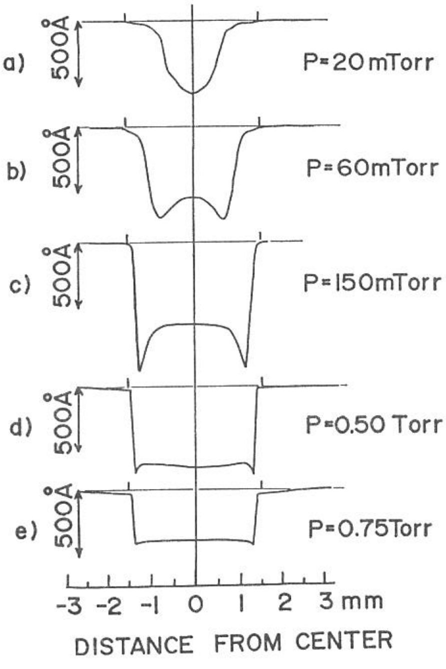

Figure 1. Cross sectional profile of the etched surface of $SiO_2$ for different $SF_6$ pressure P.

## Results and Discussion

The important information to understand how the etching reaction proceeds would be in the cross sectional profile of the obtained surface. Figure 1 shows the cross sectional profiles of the $SiO_2$ surfaces etched by irradiating the unfiltered normal SR from BL8A beam line for different $SF_6$ pressures using the film thickness measuring apparatus (Nikon Model NFM-5). The diameter of the last channel was 3mm and the distance between the end of the channel and the sample was 9 mm. It is noted that (i) almost only the SR-irradiated $SiO_2$ surface area is etched, however (ii) the cross sectional profile differs quite a lot with the $SF_6$ pressure; (iii) the profiles obtained at higher pressures support the mechanism that the etch rate is proportional to the irradiated light intensity, while those at lower pressures imply that the etch rate is strongly dependent on the F atom concentration formed in the photodissociation reaction preceding by the etching reaction. It is interesting to note that the cross sectional profile differs a lot especially when the $SF_6$ pressure is very low. The etch rate has been determined for the etched depth at the center of the irradiated area, but if the average depth (estimated by the etched volume divided by the irradiated area) is adopted, at lower pressures the etch rate must be smaller than the presently estimated value.

In Figure 2 is plotted the etch rate of $SiO_2$ by $SF_6$ against the $SF_6$ pressure for the undulator light at 25.1 (at a gap length of 33 mm with an Al filter) and 14.2 nm. A similar pressure dependence has been also obtained, when unfiltered undulator light is irradiated upon the $SiO_2$ sample. It is noted that the pressure dependence of etch rate reflects the light intensity profile irradiated upon the $SiO_2$ surface through 4.9 cm $SF_6$ gas path length implying that surface excitation is a very important step in the reaction. The rate of F atom production gives somewhat different pressure dependence from that of the irradiated light upon the surface. From the results shown in two figures one may conclude that the etching reaction done with the undulator light is not dependent upon the F atom formation rate since the F atom concentration is high, but is limited by the light intensity irradiated upon $SiO_2$ surface.

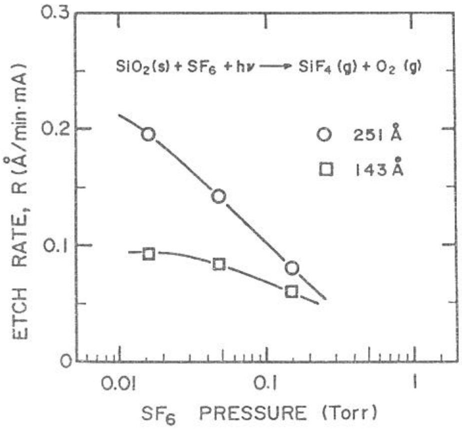

Figure 2. Relative etch rate as a function of $SF_6$ pressure for undulator light wavelengths, 14.2 and 25.1 nm.

**Refenence**

1] T. Urisu and H. Kyuragi, J. Vac. Sci. Technol. **B5**, 1436 (1987).

# DEGRADETION OF HYDROGENATED AMORPHOUS SILICON FILMS INDUCED BY IRRADIATION OF SYNCHROTRON RADIATION

Akira Yoshida, Yoji Saito, and Katsushi Inoue
Toyohashi University of Technology, Toyohashi 440

Hydrogenated amorphous silicon (a-Si:H) is a useful material for low cost solar cells, but the degradation induced by visible light illumination, the Staebler-Wronski effect[1], has been reported by various researchers.

In this study[2], we have examined the degradation phenomena in a-Si:H films induced by irradiation of vacuum ultra violet (VUV) light from synchrotron radiation (SR).

The samples were prepared by rf glow discharge decomposition of silane gas diluted with 10% hydrogen. Undoped a-Si:H films with the thickness of about 0.7 μm were deposited onto Corning 7059 glass substrates at 250°C.

First, we also examined the degradation of the a-Si:H films induced by intense illumination of visible light from tungsten halogen lamp, in order to compare with those by SR light. Figure 1 shows the dependence of $\sigma_{ph}$ of the films on the intensity of illumination ranged from 100 to 200mWcm$^{-2}$ as a function of the irradiation time t, where $\sigma_{ph}$ is the value of photoconductivity of the films when the power of illumination is 50mWcm$^{-2}$. The initial value of $\sigma_{ph}$ is about 2X10$^{-4}$Scm$^{-1}$. From this figure, $\sigma_{ph} \propto t^{-1/3}$, then $\sigma_{ph}$ approaches to several percents of the initial value with increase of t, and $\sigma_{ph}$ is approximately proportional to the illumination intensity with the minus 0.6 power. These behaviors are almost explained by the indirect bond-breaking model[3].

Figure 2 shows the dependence of $\sigma_{ph}$ of the films on $I_b$ as a function of the irradiation time t of SR light, where $I_b$ is the electron beam current in the UVSOR storage ring. The intensity of the light increases linealy with the beam current (about 9.8mWcm$^{-2}$ per unit mA). In this figure, $\sigma_{ph}$ rapidly decreases in a few seconds, and is proportional to $t^{-1}$. Moreover, it is found that $\sigma_{ph}$ is nearly proportional to $I_b^{-1}$ for the same t. These facts are different from those for the conventional degradation induced by the illumination of visible light, and they cannot be explained by the previous indirect bond-breaking model.

Then, we propose a direct bond-breaking model. Based on this model, we obtain the results of $\sigma_{ph} \propto t^{-1}$ and $\sigma_{ph} \propto L^{-1}$. Therefore, the direct bond-breaking process is a principal mechanism of the degradation in a-Si:H induced by SR light irradiation.

References

1 D.L.Staebler and C.R.Wronski, Appl.Phys.Lett. 31, 292(1977).
2 Y.Saito, K.Inoue and A.Yoshida, J.Appl.Phys., in press.
3 M.Stutzmann, W.B.Jackson, and C.C.Tsai, Phys.Rev.B 32, 23(1985).

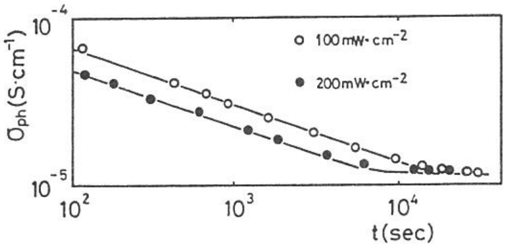

Fig.1 Dependence of photoconductivity on the power of visible light illumination as a function of irradiation time

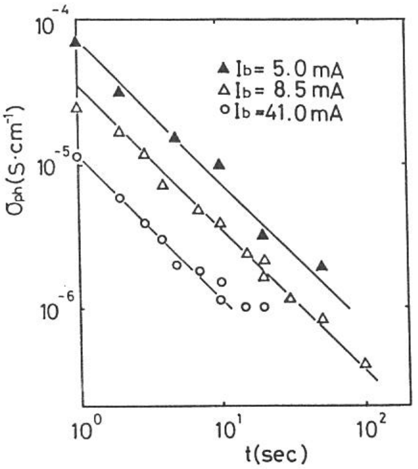

Fig.2 Dependence of photoconductivity on the beam current of SR as a function of irradiation time

# REFLECTIVITY MEASUREMENTS OF CAVITY MIRRORS FOR VUV-XUV LASERS

Kou KUROSAWA, Yasuo TAKIGAWA* and Wataru SASAKI

Department of Electronics, University of Osaka Prefecture,
Mozu-Umemachi, Osaka 591

*Department of Solid State Electronics, Osaka Electro-Communication University, Hatsumachi, Neyagawa, Osaka 572

In order to obtain high output power with the rare gas excimer lasers, the development of damage-resistant cavity mirrors is the most important aspect to be solved. Thin films of Al evaporated in high vacuum have the highest reflectivity even in the VUV region, but the damage threshold is very low, on the order of about $0.1J/cm^2$.[1] Dielectric multilayer mirrors have not been developed for the VUV and XUV wavelength regions. In comparison to these mirrors, the mirrors using bulk materials have a higher damage threshold, although their reflectivities are limited by the intrinsic optical properties of the materials.[2]

In the present study, we report reflectivities of SiC, Si, W, Cr, $SiO_2$, and $MgF_2$ measured at beam line BL1B of the UVSOR facility and the possibility of cavity mirrors for Kr(146nm), Ar(126nm), and Ne( 80nm) excimer lasers. The SiC mirror was fabricated by CVD deposition onto a graphite substrate and then by mechanically polished. The $SiO_2$ mirror is an ordinary qaurtz glass. The others are the respective single crystals. Among these mirrors, the $MgF_2$ one shows transmissivity above 115nm and thus is used as the output coupler for Ar and Kr excimer lasers, although the damage threshold is not high enough for their high power operation. The surface profiles were observed with the laser interferometric technique using a digital optical profiler (Wyco Corp., Tucson, AZ). The rms surface roughness were estimated with a statistical method for 1024 surface elements along lines 1.3mm in length. The estimated values for these mirrors were less than 1nm.

The obtained reflection spectra are shown in Figs. 1-3. The SiC mirror shows relatively high reflectivity more than 30% in the range between 60nm and 200nm. In the case of the Cr mirror, its reflectivity is as high as more than 60% in the visible region, keeps the value higher than 50% down to 170nm and then shows a considerable decline. It should be noted that this is the first observation of reflection spectrum of a Cr single crystal in such wide wavelength region. For the case of the $SiO_2$ mirror, there exist four distinct features below 120nm which are assigned to Si-O bonds. The reflectivity of Si falls down to almost 0% at 70nm, while that of the W mirror still keep more than 20% down to 60nm. The reflection specturm of the $MgF_2$ mirror shows a feature like that in $SiO_2$. It may be assigned to Mg-F bonds. In Table I are listed the reflectivities at three individual wavelengthes of the rare gas excimer lasers together with their melting points and also the output energy per pulse of the Ar excimer laser when the respective reflectors are used with a combination with the $MgF_2$ output coupler. The mirrors of Si, $SiO_2$ and $MgF_2$ that have relatively low melting points have been observed serious damages on the mirror surfaces. The SiC, W and Cr mirrors have relatively high reflectivity in the VUV-XUV regions and high melting points, and thus they have the possibility to be used as the reflectors for the high power rare gas excimer lasers.

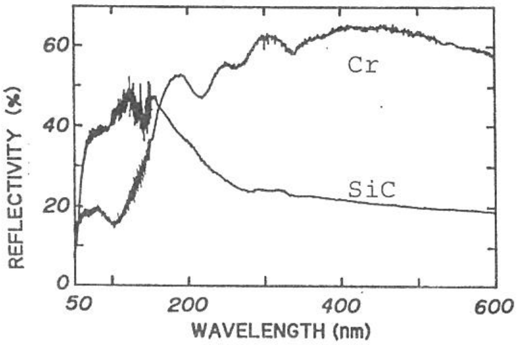

Fig.1 Reflection specta of SiC and Cr mirrors.

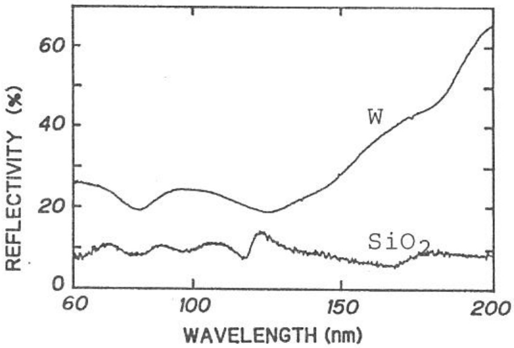

Fig.2 Reflection spectra of W and $SiO_2$ mirrors.

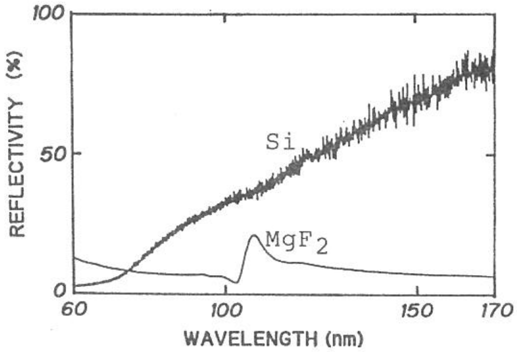

Fig.3 Reflection spectra of Si and $MgF_2$ mirrors.

References
[1]Y. Uehara et. al.: Opt. Lett., 9, 539(1984).
[2]K. Takeuchi et al.: Rev. Laser Eng., 16, 691(1988).

Table I. Characteristics of cavity mirrors for the rare gas excimer lasers.

| Material | Reflectivity(%) | | | Melting point | Output |
|---|---|---|---|---|---|
| | Kr(146nm) | Ar(126nm) | Ne(80nm) | (°C) | (mJ) |
| SiC | 42 | 45 | 38 | 2200 | 80 |
| Si | 66 | 52 | 15 | 1420 | 33 |
| Cr | 32 | 22 | 19 | 1900 | >20 |
| W | 26 | 19 | 20 | 3382 | |
| $SiO_2$ | 7 | 14 | 11 | 1720 | 20 |
| $MgF_2$ | 8 | 8 | 10 | 1260 | -- |

# OPTICAL PROPERTIES OF $SiO_2$ AND $MgF_2$ CAVITY MIRRORS IRRADIATED BY HIGH POWER VUV LASER

Yasuo TAKIGAWA, Kou KUROSAWA* and Wataru SASAKI*

Department of Solid State Electronics, Osaka Electro-Communication University, Hatsumachi, Neyagawa, Osaka 572

*Department of Electronics, University of Osaka Prefecture, Mozu-Umemachi, Osaka 591

An electron-beam pumped Ar excimer laser emitts an intense coherent radiation of more than 1 MW at 126nm of the vacuum ultraviolet wavelength region.[1] A quartz glass reflector is usually used with a combination of a $MgF_2$ output coupler for the cavity mirrors. After several shots of laser operation the clear beam patterns have been observed on the mirror surfaces. The degradation of the output power for the successive shots is considered to be due to the mirror damages. In order to characterize the irradiation damages, we measure the transmission and reflection spectra of the $MgF_2$ and $SiO_2$ mirrors before and after the Ar excimer laser irradiation with the UVSOR.

Figure 1 shows the transmission spectra of the $MgF_2$ mirror before (solid line) and after (dashed line) the laser irradiation. The transmissittance falls off just above the fundamental absorption. On the other hand, the reflection spectra (Fig. 2) show a slight degradation over the whole wavelength region measured here while their spectral patterns remain unchanged. The transmission and reflection spectra of the $SiO_2$ mirror are shown in Figs. 3 and 4, respectively. By the laser irradiation the transmittance shows a considerable decline just above the fundamental absorption edge of 145nm, which is almost the same trend as the $MgF_2$ mirror. However, the reflection spectrum shows a considerable change by the laser irradiation. Before the irradiation there appear four distinct reflectivity peaks below 120nm which are assigned to Si-O bonds. After the irradiation they almost disappear and furthermore the reflectivity shows the maximum value around 200nm. The reflection spectrum above 120nm is very similar as that of Si single crystal except for the absolute value. On the basis of these results of $SiO_2$, we can safely say that the Si-O bonds are broken in the surface layer of the $SiO_2$ mirror by the high power Ar excimer laser radiation. The bond breaking results in the appearance of Si. This is verified by XPS and EPMA measurements.[2] In the case of the $MgF_2$ mirror, the surface is considered to be roughened by the irradiation, which results in the degradation in the reflectivity and transmittance.

References

[1]W. Sasaki et al.: Rev. Laser Eng., 14, 370-377(1986).
[2]Y. Takigawa et al.: to be submitted.

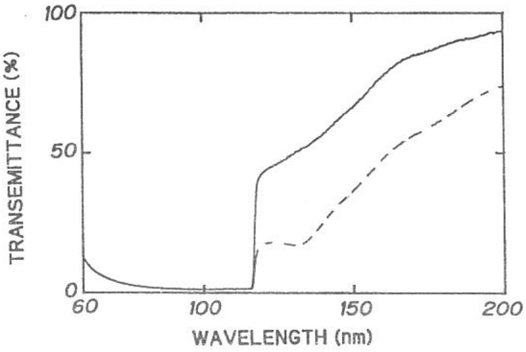

Fig.1 Transmission spectra of $MgF_2$ mirror before (solid line) and after (dashed line) the laser irradiation.

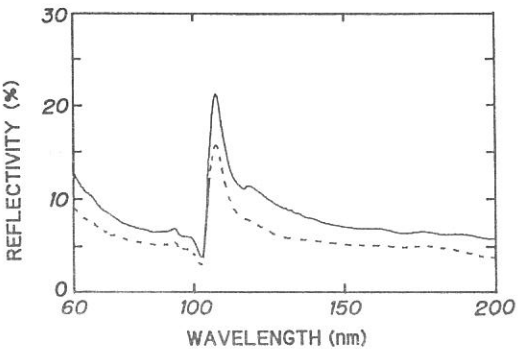

Fig.2 Reflection spectra of $MgF_2$ mirror before (solid line) and after (dashed line) the laser irradiation.

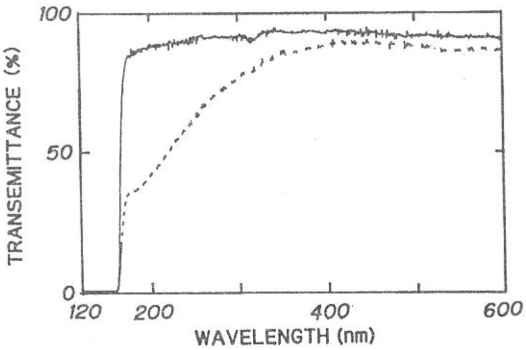

Fig.3 Transmission spectra of $SiO_2$ mirror before (solid line) and after (dashed line) the laser irradiation.

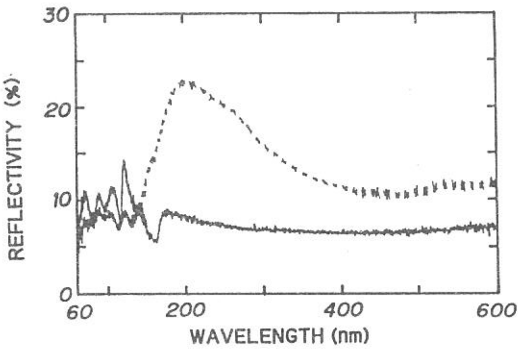

Fig.4 Reflection spectra of $SiO_2$ mirror before (solid line) and after (dashed line) the laser irradiation.

# Characterization of multilayer reflector in 40-150A region

Makoto SAKURAI, Koujun YAMASHITA*, Masayuki OHTANI*, Kazuo TANAKA**, and Masataka KADOH**

Institute of Plasma Physics, Nagoya University, Nagoya 464-01
*Department of Physics, Osaka University, Toyonaka 560
**Institute of Laser Engineering, Osaka University, Suita 565

The multilayer reflector is promising optical component to realize high reflectivity for soft x-ray region near normal incidence condition. Then, the development of multilayer reflector makes it possible to fabricate normal incidence x-ray telescope and x-ray laser mirror in the wavelength region of 40-300A. We measured reflectivities of multilayer reflectors with the monochromatized synchrotron radiation in 40-150A region on BL5B.

The beam line consists of plane grating monochromator (PGM) and calibration chamber. Co-axial rotational stage which enables the reflectivity measurement is installed in the calibration chamber. The rotation axis can be made pallarel or perpendicular to that of grating, or parallel to the direction of SR. Two kind of measurement are possible; the measurement with continuous wavelength scanning at fixed scattering angle ( $\lambda$ scan), and with continuous angular scanning at fixed wavelength ( $\theta$ scan). At present experiment, rotation axis is perpendicular to that of grating. The reflectors and detector are mounted on co-axial stage. We used two kind of detectors; secondary electron multiplier with BeCu photocathode and proportional counter with polypropylene window.

Fig. 1 shows the reflectivity of a multilayer reflector (Mo/Si, 2d=225 A) measured by the electron multiplier ( $\lambda$ scan mode). The spectra are normalized with direct beam intensity (fig. 2). The detector was located in specular geometry. The diffraction peak is clearly observed at the position predicted from the Bragg condition. Since the direction of polarization is perpendicular to the sample surface, the reflectivity diminishes near $45^\circ$. Fig. 3 shows the variation of reflected photon intensity with incident angle from a multilayer ( Ni/C, 2d=114 A) for several wavelength ($\theta$ scan). It was measured by proportional counter. The highest peak in each spectrum corresponds to Bragg reflection except for $\lambda$ = 40 A, while associating peaks are possibly due to interference effect of multilayers.

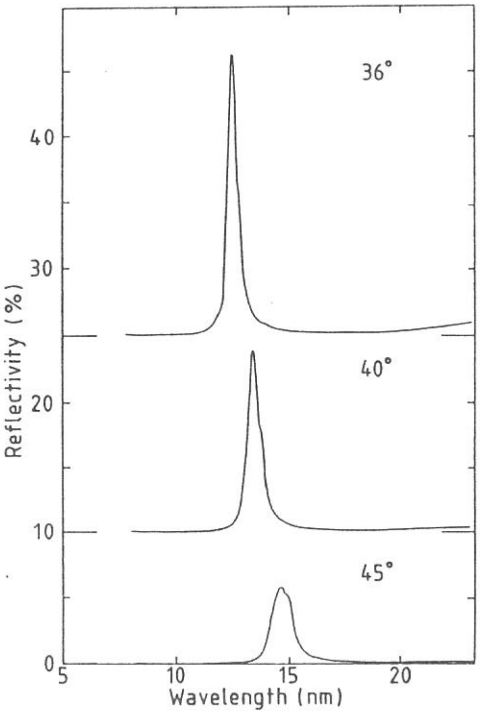

Fig. 1 Reflectivities of Mo/Si for various incident angles.

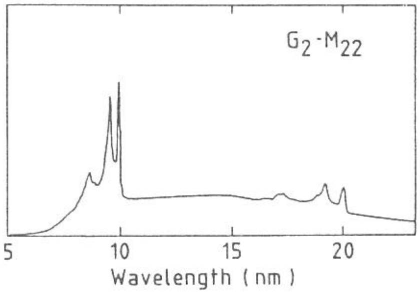

Fig. 2 Intensity distribution of direct beam measured with electron multiplier (BeCu).

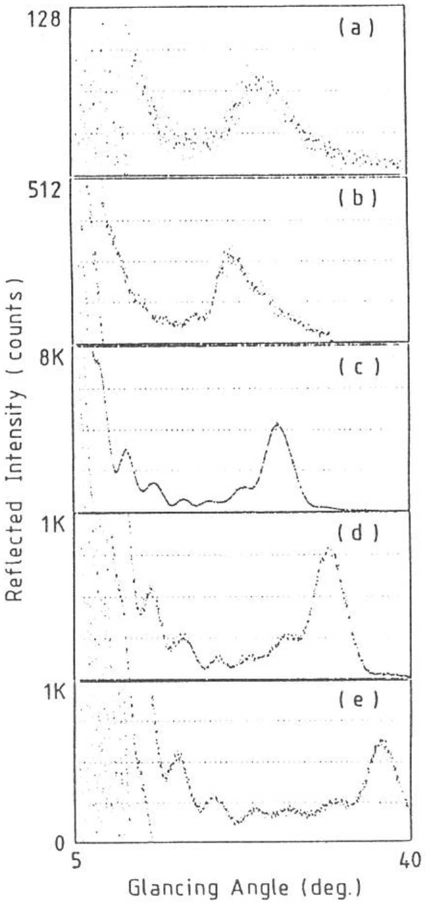

Fig. 3 Reflected intensity distribution of Ni/C for various incident wavelength; (a) 40 A, (b) 47 A, (c) 54 A, (d) 61 A, and (e) 68 A.

# VUV Microscope with Free-Standing Zone Plates at UVSOR

Hiroshi Kihara[1], Yoshio Shimanuki[2], Kenzo Kawasaki[2], Norio Watanabe[3], Mieko Taniguchi[3], Hirotsugu Tsuruta[4], Yoshinori Nagai[5], Yutaka Watanabe[6], and Shigetaro Ogura[6]

1) Jichi Medical School, School of Nursing, Minamikawachi, Tochigi 329-04, Japan
2) Department of Oral Anatomy, School of Dental Medicine, Tsurumi University, Tsurumi 2-1-3, Yokohama 230, Japan
3) Department of Physics, Faculty of Science, Nagoya University, Nagoya 464, Japan
4) Department of Materials Sciences, Faculty of Science, Hiroshima University, Hiroshima 730, Japan
5) College of General Education, Azabu University, Fuchinobe, Sagamihara, Kanagawa 229, Japan
6) Canon Research Center, CANON INC., Morinosato-Wakamiya 5-1, Atsugi, Kanagawa 243-01, Japan

In our previous paper [1], results for VUV microscopy (beam line 6A2) with a plane-grating monochromator and a masked zone plate were reported, which showed that resolution was 2-3 microns, as expected from the width of the outermost ring of the zone plate.

As a next step, observations were done with two zone plates; condenser and micro-zone plates. Original fabrication procedures of the zone plates were reported elsewhere [2]. It was improved in several points. The present characteristics are: n=312, f=150 mm at 8 nm light, $dr_n$=0.93 µm, and Au thickness = 2 µm with a central mask of 0.2 mmϕ as a condenser zone plate. The same dimensional zone plate without masks was used as a micro zone plate.

For this experiment, beam line 8A was used. Experimental set-up is shown in Fig. 1. At the most upstream point, a pinhole (PH1) and a condenser zone plate(CZP) was set. With PH1 and CZP, a parallel beam of 1 mmϕ diameter was selected. CZP was placed 4678 mm behind the source (0.8 mmϕ), which was focused at 208 mm apart form CZP. The source image was 36 umo. A pinhole (PH2) of 36 umo was selected to compromize the resolution and the image brightness. Samples were placed a little distant from PH2. The distance between PH2 and the sample was set at 12.5 mm to keep it as short as possible. The second zone plate (MZP) was set at 226.5 mm distant from PH2, as all the incoming photons are available for imaging. Detectors (MCP with double layers or films) were located 2863.5 mm from MZP, which has a magnification ratio as 13.4. In case of MCP observation, obtained images were monitored on fluorescent screen, which was usually averaged with SIT camera by accumulation.

With these set-ups, we have tested imagings of Cu #1000 mesh as a standard sample. In Fig. 2, its image is shown. It was taken with a pinhole of 100 µ with Minicopy film of 5 min exposure time.

Next, we tested several biological specimens such as diatoms, ground sections of tooth and bones, and nerve tissues. At 6.0 nm, samples mounted on a Collodion film supported with Cu #200 mesh could be observed. In Fig. 3, an image of diatoms, which was taken with MCP (double layers) and SIT camera, is shown as an example.

## Acknowledgement

The authors are grateful for the help and encouragements from Prof. M. Watanabe, K. Fukui, O. Matsudo and other staffs of the Institute for Molecular Sciences. The authors also appreciate continuous encouragement form Profs. N. Kato and F. Oosawa. Use of MCP and SIT camera was realized by a kind offer of Hamamatsu Photonics, which is also greatly appreciated. This work was supported by a grant in aid from the Ministry of Education, Research and Science in Japan.

## References

1. H. Kihara, Y. Shimanuki, K. Kawasaki, Y. Watanabe, S. Ogura, H. Tsuruta, and Y. Nagai: In "X-ray Microscopy II" (Ed. by D. Sayer, M. Howells, J. Kirz and H. Rarback), pp.164-167, Springer-Verlag, Berlin (1988).
2. Y. Nagai, Y. Nakajima, Y. Watanabe, S. Ogura, K. Uyeda, Y. Shimanuki, and H. Kihara: In "X-ray Microscopy" (Ed. by P. C. Cheng and G. J. Jan), pp. 263-288, Springer-Verlag, Berlin (1987).

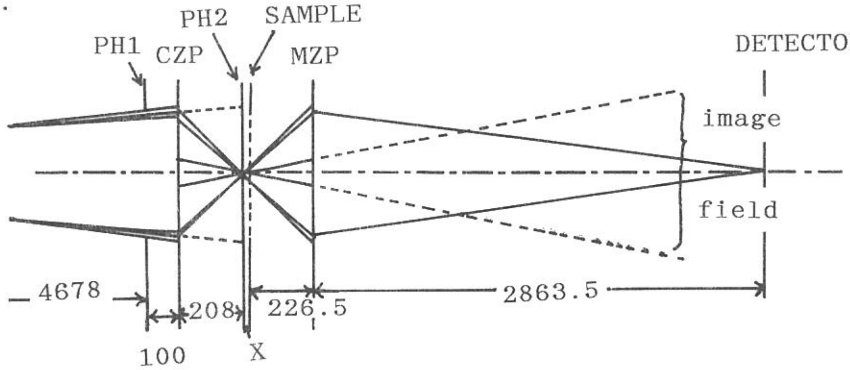

Fig. 1. A diagram of the VUV microscope with two zone plates without a monochromator. PH1; pinhole 1 (1mmϕ), ZP1; condenser zone plate with a central mask, PH2; pinhole 2 (34 μ), ZP2; micro zone plate without a central mask.

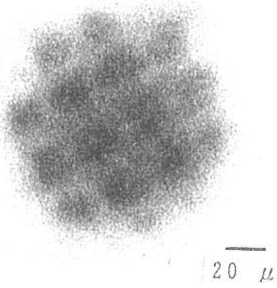

Fig. 2. Cu #1000 mesh pattern taken with minicopy film. 13.4 -fold magnification. 5 min, 6.0 nm.

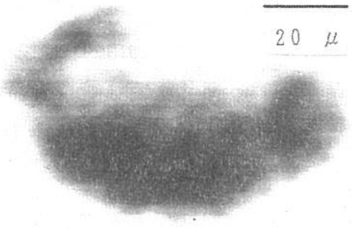

Fig. 3. Diatom image. The sample was placed on collodion membrane supported with Cu #200 mesh. 6.0 nm. The image on the fluorescent screen of MCP with double layers was monitored with SIT camera for accumulation ( 4 sec).

# EFFECT OF PRESSURE ON THE INTERACTION-INDUCED FAR-INFRARED ABSORPTION OF LIQUID CARBON DISULFIDE

Yoshitaka FUJITA, Tetsuhiko OHBA and Shun-ichi IKAWA

Department of Chemistry, Faculty of Science, Hokkaido University,
Sapporo 060

Far-infrared absorption of non-dipolar liquids is caused by a transient dipole moment induced through molecular collisions. Its integrated intensity and band profile tell about how the molecules interact and move in the liquid state. Effect of pressure on these spectral properties should give an important clue to the mechanism of the interaction process. Recently, we have measured the far-infrared absorption of liquid carbon disulfide as a function of pressure by use of a far-infrared spectrometer at BL6A1. The integrated intensity and the peak frequency increased about 45% and 17%, respectively, as the pressure increased from 1 bar to 1.8 kbar.

A high pressure cell used is shown in Fig. 1. The body of the cell is made of SUS-630 and the windows are hyper-pure silicon crystals of 10 mm diameter and 10 to 14 mm thicknesses which provide a thickness of a sample in the 2 - 10 mm range. The effective aperture of the cell is 4 mm and its optical path length including windows is 30 mm. Alignment of the cell set in the sample compartment of the spectrometer was performed with a 1 mW He-Ne laser beam, the silicon windows being pulled out.

Figure 2 shows observed spectra at several pressures. Integrated intensities, A($cm^{-2}$), calculated in the 20-230 $cm^{-1}$ range and frequencies of the band maxima, $\nu_m$($cm^{-1}$), were plotted against pressure in Fig. 3. Both A and $\nu_m$ increase linearly with increasing pressure.

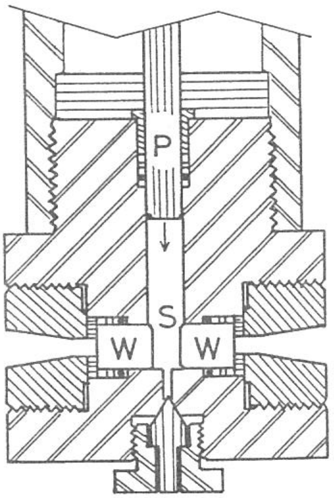

Fig. 1 High pressure cell.
P:piston, W:windows, S:sample.

Following an electric multipole theory,[1] the far-infrared absorption of liquid carbon disulfide is attributed to the quadrupole-induced dipole moment and the absorption intensity as a function of pressure is given by

$$A(p) = cF(p)\rho(p)\langle m_z^2\rangle_p, \qquad (1)$$

$$\langle m_z^2\rangle_p \propto \langle \sum_j{}' [P_3(\cos\Omega_{ij})]^2 / r_{ij}^8 \rangle_p, \qquad (2)$$

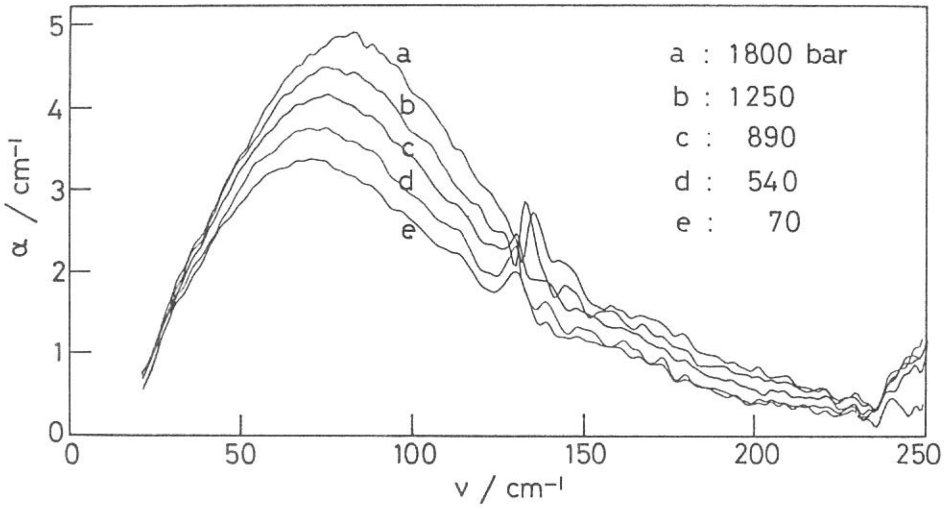

Fig. 2 Far-infrared spectra of liquid carbon disulfide at several pressures.

where c is a constant, F(p) the internal field factor, $\rho(p)$ the number density, and $m_z$ the transient dipole moment induced on a molecule by the quadrupole moments of the surrounding molecules. Pressure dependence of F and $\langle m_z^2 \rangle$ can be approximately estimated from $\rho$ values obtained by the Tait-Tamman equation.$^{2)}$ Calculated values of A(p) are plotted by a broken line in Fig.3, being scaled to the intensity at 1 bar. The theoretical result roughly reproduces the experimental slope. A detailed analysis is now in progress.

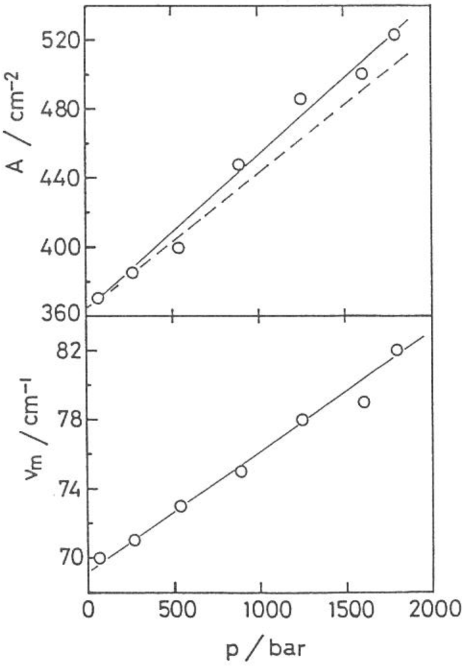

Fig. 3 Effect of pressure on the integrated intensity A and peak frequency $\nu_m$ of far-infrared absorption of liquid carbon disulfide. The broken line indicates the calculated pressure dependence of A by Eq. (1).

References

1). T.I. Cox and P.A. Madden, Mol. Phys. 39, 1487 (1980).

2). N.S. Isaacs, Liquid Phase High Pressure Chemistry (Wiley, Chichester, 1981), Chap. 2.

# Far-Infrared Absorption in Nickel- and Copper Microcrystals

Shōsuke Mochizuki(1) and Kimihiro Ishi(2)

1) Department of Physics, College of Humanities and Sciences,
Nihon University, 3-25-40 Sakurajosui, Setagaya-ku, Tokyo 156
2) Research Institute for Scientific Measurements, Tohoku
University, 2-1-1 Katahira, Sendai 980

The interaction of metal microcrystals with electromagnetic radiation has been interest for more than ten years because of the quantum size effect on the conduction electrons and the anomalous far-infrared absorption. We measured the far-infrared absorption of nickel and copper microcrystals embedded in polyethylen in the temperature range from 15 K to room temperature at BL6A1 beam line by using the far-infrared measuring system.

Fig. 1 shows the absorption coefficient of nickel microcrystals embedded into polyethylen at a filling factor 0.01. The microcrystals had an average diameter of 21 nm. The absorption coefficient K is very small at low frequencies, bends up near 45 $cm^{-1}$, and increases nearly linearly at high frequencies. It is found that a temperature change produces a relatively small change in the far-infrared absorption of nickel microcrystals.

Fig. 2 shows the absorption coefficient of the copper microcrystals embedded into polyethylen at a filling factor 0.01. The microcrystals had an average diameter of 50 nm. The absorption coefficient increases with frequency and shows the strong saturation. This absorption has also a weak temperature dependence.

These far-infrared absorptions observed at present investigation can be qualitatively understood by examining the roles of the induced electric dipole absorption and the induced magnetic dipole absorption of the conduction electrons in metal microcrystals with some impurities introduced during the gas-evaporation process.

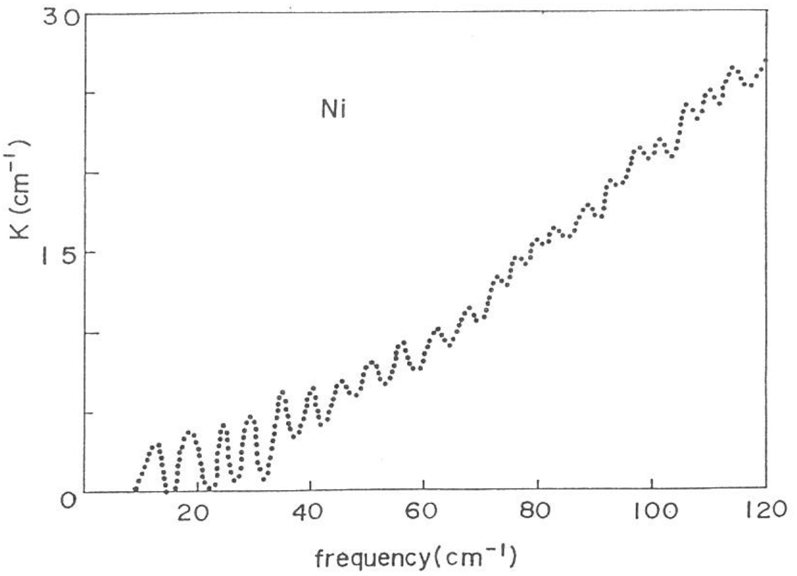

Fig. 1

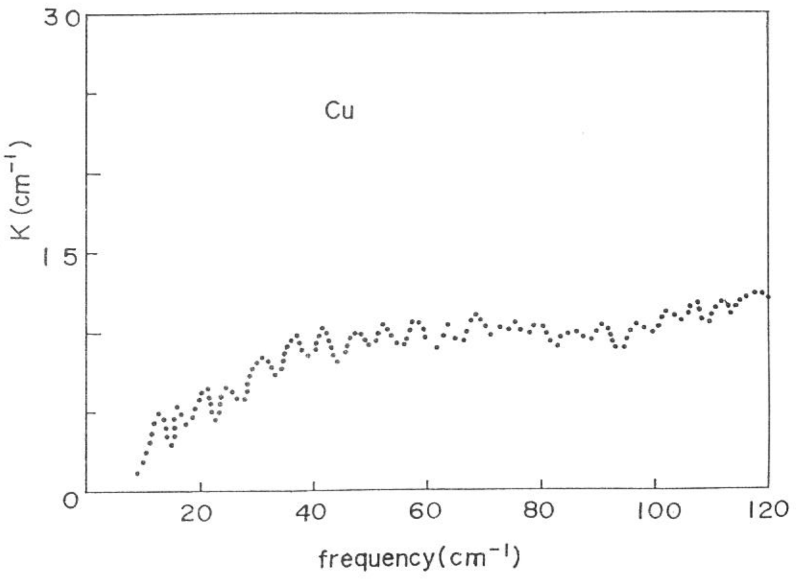

Fig. 2

# FAR-INFRARED AND MILLIMETER WAVE SPECTROSCOPY OF SUPER IONIC CONDUCTORS $RbAg_4I_5$ AND $KAg_4I_5$

Teruyoshi AWANO, Takao NANBA* and Mikihiko IKEZAWA**

Department of applied Physics, Tohoku Gakuin University,
Tagajo 985
*Department of Physics, Tohoku University, Sendai 980
**Research Institute for Scientific Measurements, Tohoku University, Sendai 980

Alkali silver iodide super ionic conductors $RbAg_4I_5$ and $KAg_4I_5$ have the high ionic conductivity at temperatures above 122 K ($RbAg_4I_5$) or 139 K ($KAg_4I_5$).[1] These crystals belong to the $O^7$ of the space group at temperatures above 208 K ($RbAg_4I_5$) or 194 K ($KAg_4I_5$) and each unit cell contains four molecules.[2,3]

Absorption band which is caused by diffusive motion of $Ag^+$ ions is expected to appear in the spectral region of several wave numbers. Many studies of light scattering have been made.[4,5] But far-infrared and millimeter wave absorption has not been studied in detail because of experimental difficulties.[6]

We have measured reflectivity spectra of $RbAg_4I_5$ and $KAg_4I_5$ single crystals in the spectral region from 5 to 200 $cm^{-1}$ at temperatures between 15 K and 300 K, and calculated optical constants by the Kramers-Kronig analysis.

Electrical conductivity spectra of $RbAg_4I_5$ and $KAg_4I_5$ are shown in Fig. 1 and Fig. 2. At 15 K, 68 ($RbAg_4I_5$) or 70 ($KAg_4I_5$) absorption bands were observed. These absorption bands appeared

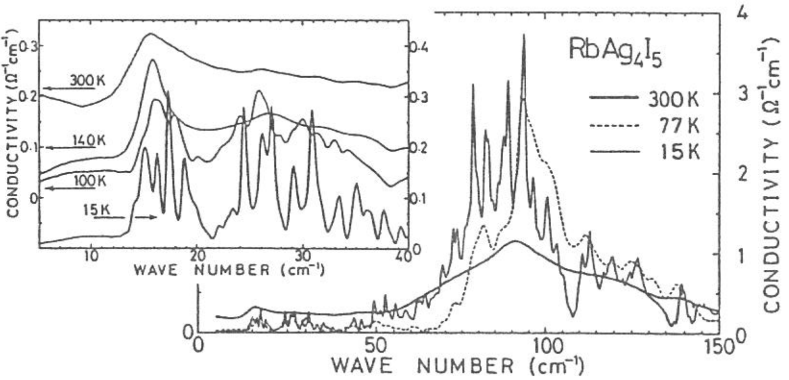

Fig. 1
Electrical conductivity of $RbAg_4I_5$ calculated from the reflectivity spectrum.

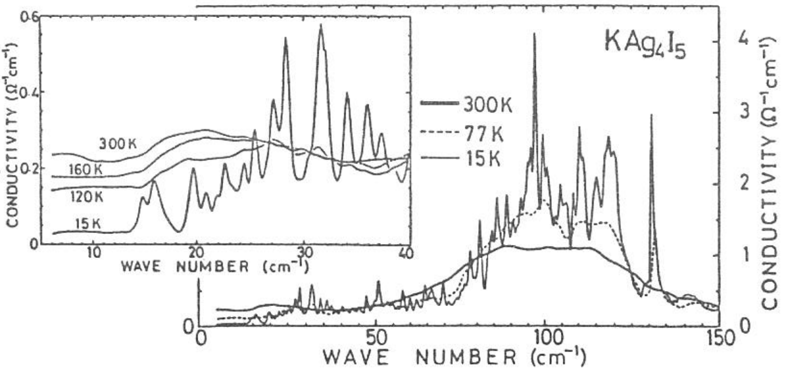

Fig. 2
Electrical conductivity of $KAg_4I_5$.

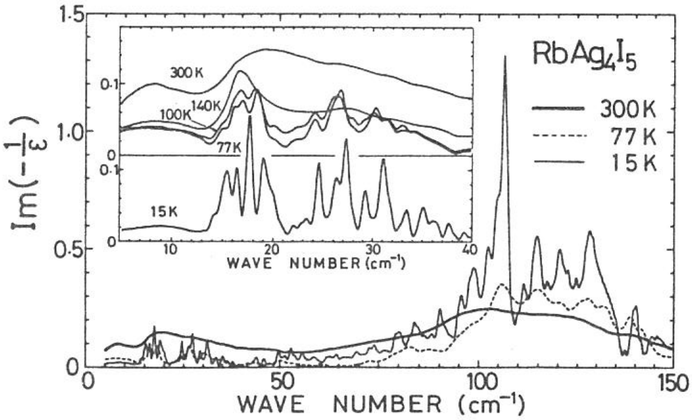

Fig. 3
Energy loss function of $RbAg_4I_5$ calculated from the reflectivity spectrum.

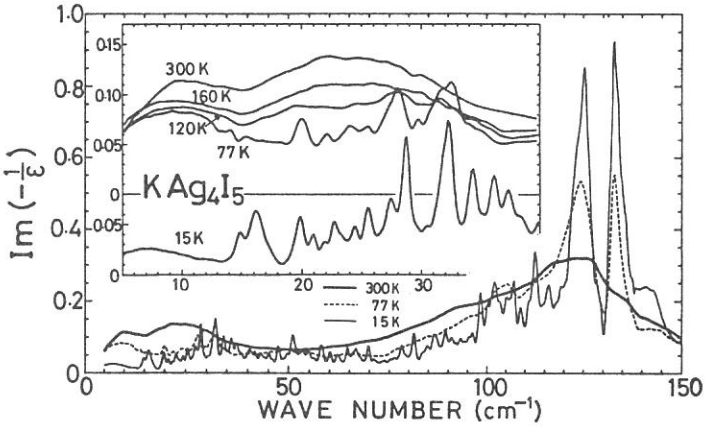

Fig. 4
Energy loss function of $KAg_4I_5$.

at temperatures below the transition temperature. Broad bands observed at 300 K correspond to the absorption struture at low temperatures. In the spectral region below 10 cm$^{-1}$, increase of the conductivity toward the low energy side was observed at 300 K. This increase disappeared at low temperatures and seems to be due to the diffusive motion of Ag$^{+}$ ions.

Energy loss function spectra of $RbAg_4I_5$ and $KAg_4I_5$ are shown in Fig. 3 and Fig. 4. A broad peak was observed near 8 cm$^{-1}$ in each crystal. This peak is considered to be due to ionic plasmon.

## References

1) B. B. Owens and G. R. Argue: Science **157**, 308 (1967)
2) S. Geller: Science **157**, 310 (1967)
3) S. Geller: Phys. Rev. B **14**, 4345 (1976)
4) D. A. Gallagher and M. V. Klein: Phys. Rev. B **19**, 4282 (1979)
5) E. Cazzanelli, A. Fontana, G. Mariotto and F. Rocca: J. Phys. C**6**, 190 (1981)
6) K. Funke and H. J. Schneider: Solid State Ionics **13** 335 (1984)

# THE CHANGE IN THE PHONON SPECTRUM OF KI AND RbI DUE TO THE B1-B2 PHASE TRANSITION

Takao NANBA and Makoto WATANABE*

Department of Physics, Faculty of Science, Tohoku University,
Sendai 980

*Institute for Molecular Science, Myodaiji, Okazaki 444

It is known that alkali halide crystals except cesium halide crystals undergo a phase transition from the B1 phase (rock salt structure) at the standard condition to the B2 phase (cesium chloride structure). However, the direct observation of the change in the optic phonon spectrum of alkali halides due to the pressure-induced phase transition has not been reported because of its Raman inactive character.

Using the transmission measurement system under high pressure in the far infrared region completed at the beam line BL6A1, we measured the change in the optic phonon spectrum of KI and RbI with pressure at room temperature.

Fig. 1 shows the change in the transmission spectrum of KI with pressure. The thickness of the evaporated film of KI was 2 $\mu$m. The applied pressure is given at each spectrum. A dot vertical line at 1.8 GPa shows the critical pressure of the B1-B2 phase transition for KI. A sharp dip which corresponds to the TO phonon absorption is shown by a downward arrow at each curve in the figure. The dip at 130 cm$^{-1}$ appearing in each spectrum is due to the absorption of the crystalline quartz filter of the detector.

The energies of the TO phonon of KI are plotted as the function of the pressure in Fig. 2. The TO phonon energy was observed to show a blue shift in the two phases with the increase in pressure. The sudden decrease of the TO phonon energy in the spectrum at 2.15 GPa from that at 1.7 GPa corresponds to the phase transition.

Fig.3 shows similar plot for RbI with that for KI given in Fig.2. The critical pressure for the B1−B2 phase transition for RbI is 0.34 GPa. The sudden decrease in the TO phonon energy beyond 0.34 GPa corresponds to the phase transition.

From the measurement of the shift of the TO phonon energy with pressure, the mode gruneisen parameters of KI and RbI in the two phases were found. They are $\gamma_{TO}^{B1}=1.70$ and $\gamma_{TO}^{B2}=2.70$ for KI, and $\gamma_{TO}^{B1}=3.28$ and $\gamma_{TO}^{B2}=2.53$ for RbI, respectively.

Fig.1 Transmission spectra of the evaporated film of KI under high pressure (right).

Fig.2 The observed peak energy of the TO phonon of KI versus pressure (down).

Fig.3 The observed peak energy of the TO phonon of RbI versus pressure (right down).

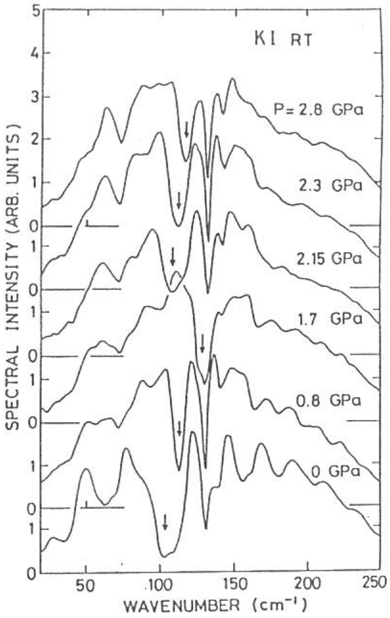

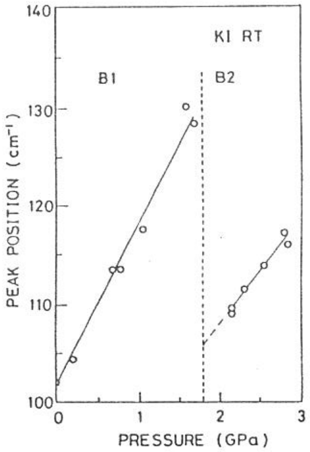

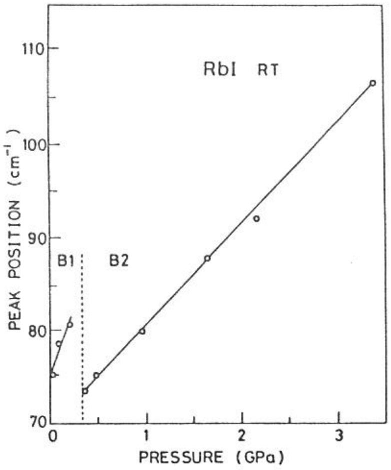

# APPENDIX

## ORGANIZATION

### *Staff*

Director

| | | |
|---|---|---|
| Katsumi | KIMURA | Professor |

Light Source Group

| | | |
|---|---|---|
| Toshio | KASUGA | Associate Professor |
| Hiroto | YONEHARA | Research Associate |
| Toshio | KINOSHITA | Engineer |
| Masami | HASUMOTO | Engineer |

Beam Line Group

| | | |
|---|---|---|
| Makoto | WATANABE | Associate Professor |
| Atsunari | HIRAYA | Research Associate |
| Kazutoshi | FUKUI | Research Associate |
| Kusuo | SAKAI | Section Chief Engineer |
| Osamu | MATSUDO | Unit Chief Engineer |
| Jun-ichiro | YAMAZAKI | Engineer |
| Eiken | NAKAMURA | Engineer |

Secretary

| | |
|---|---|
| Kayoko | MATSUDA |

### *Guest Scientist*

| | | |
|---|---|---|
| Shun-ichi | NAOE | Adjunct Associate Professor<br>from Kanazawa Univ.<br>(April 1987 - March 1989) |

### *Representative of Beam Lines*

| | | | |
|---|---|---|---|
| BL2A | Kosuke | SHOBATAKE | Dept. Molecular Assemblies |
| BL2B2 | Katsumi | KIMURA | Dept. Molecular Assemblies |
| BL3B | Inosuke | KOYANO | Dept. Molecular Assemblies |

| | | | |
|---|---|---|---|
| BL8B2 | Hiroo | INOKUCHI | IMS |
| Others | Makoto | WATANABE | UVSOR |

*Steering Committee (April 1988 - March 1990)*

| | | | |
|---|---|---|---|
| Toshio | KASUGA | IMS | |
| Katsumi | KIMURA | IMS | Chairman |
| Inosuke | KOYANO | IMS | |
| Norio | MORITA | IMS | |
| Tadayoshi | SAKATA | IMS | |
| Kosuke | SHOBATAKE | IMS | |
| Makoto | WATANABE | IMS | |
| Shun-ichi | NAOE | IMS and Kanazawa Univ. | |
| Jun-ichi | CHIKAWA | Nat. Lab. High Energy Phys. | |
| Junji | FUJITA | Nagoya Univ. | |
| Yoshihiko | HATANO | Tokyo Inst. Tech. | |
| Yoshio | NAKAI | Kyoto Univ. | |
| Tadashi | OKADA | Osaka Univ. | |
| Kazuhiko | SEKI | Hiroshima Univ. | |
| Shigemasa | SUGA | Univ. of Tokyo | |

## JOINT STUDIES (fiscal year 1988)

| | |
|---|---|
| Special Project | : 3 |
| Cooperative Research | : 15 |
| Use of Facility | : 80 |
| Users' Meeting | : 1 |
| Workshop on Beam Dynamics and Free Electron Laser | : 1 |
| Users' Time | : 42 Weeks |

## LIST OF PUBLICATIONS (1988)

1) *"Longitudinal Active Damping for UVSOR Storage Ring"*

T.Kasuga, M.Hasumoto, T.Kinoshita and H.Yonehara

Jpn. J. Appl. Phys. **27** (1988) 100.

2) *"Interatomic Radiative Transition of a Valence Electron to Inner Core : Luminescence from Cs-Halides and RbF at Room Temperature"*

S.Kubota, J.Ruan, S.Sakuragi, M.Itoh and S Hashimoto

J. Lumi. **40/41** (1988) 149.

3) *"Auger-Free Luminescence due to Interatomic Transitions of Valence Electrons into Core Holes in* $BaF_2$*"*

M.Itoh, S.Hashimoto, S.Sakuragi and S.Kubota

Solid State Commun. **65** (1988) 523.

4) *"Investigation of Fragmentation Processes Following Core Photoionization of Organometallic Molecules in the Vapor Phase"*

S.Nagaoka, S.Suzuki and I.Koyano

Nucl. Instrum. Methods Phys. Res. **A266** (1988) 699.

5) *"Vacuum System for UVSOR Storage Ring"*

T.Kasuga, H.Yonehara, T.Kinoshita and M. Hasumoto

Proc. IEEE Particle Accelerator Conf., Washington, D.C., (IEEE, 1987) p.1672.

6) *"Absorption Spectra of* $PbI_2$ *Layered Crystals 2-100 eV Range"*

T.Hayashi, K.Toyoda and M.Itoh

J. Phys. Soc. Jpn. **57** (1988) 1861.

7) *"Time-Resolved Synchrotron Spectroscopy of Exciton Fluorescence in Anthracene Single Crystals"*

T.Mitani, T.Yamanaka, M.Suzuki, T. Horigome, K.Hayakawa and I.Yamazaki

J. Lumi. **39** (1988) 313.

8) *"Synchrotron Radiation Wavelength Dependence on Self Development of Plasma Polymerized Resists"*
H.Yamada, T.Satoh, S.Itoh, M.Nakamura, S.Morita and S.Hattori
J. Appl. Polym. Sci. **42** (1988) 157.

9) *"Ultraviolet Photoemission Study of Oligothiophenes : The Effect of Irregularity on π-Electron Systems"*
H.Fujimoto, U.Nagashima, H.Inokuchi, K.Seki, H.Nakahara, J.Nakayama, M.Hoshino and K.Fukuda
J. Chem. Phys. **89** (1988) 1198.

10) *"Observation of Interatomic Radiative Transition of Valence Electrons to Outermost-Core-Hole States in Alkali Halides"*
S.Kubota, M.Itoh, J.Ruan S.Sakuragi and S.Hashimoto
Phys. Rev. Lett. **60** (1988) 2319.

11) *"Photoconductivity Threshold of Supercritical Xenon Fluids Doped with Anthracene as a Function of Fluid Density"*
K.Nakagawa, A.Ejiri, K.Itoh and M.Nishikawa
Chem. Phys. Lett. **147** (1988) 557.

12) *"XANES and EXAFS Studies on K-Shell Absorption in $K_{1-x}Na_xCl$ Solid Solutions"*
T.Murata, T.Matsukawa and S. Naoe
Solid State Commun. **66** (1988) 787.

13) *"Electronically Stimulated Desorption of Neutral and Ionic Species from Lithium Fluoride Surfaces"*
T.Yasue, A.Ichimiya, Y.Yamada, T.Gotoh, Y.Kawaguchi, M.Kotani, S.Ohtani, Y.Shigeta, S.Takagi, Y.Yazawa and G.Tominaga
Nucl. Instrum. Methods Phys. Res. **B34** (1988) 357.

14) *"Evidence from Angle-Resolved Resonant Photoemission for Oxygen-2p Nature of the Fermi-Liquid States in* $Bi_2CaSr_2Cu_2O_8$*"*

T.Takahashi, H.Matsuyama, H.Katayama-Yoshida, Y.Okabe, S.Hosoya, K.Seki, H.Fujimoto, M.Sato and H.Inokuchi

Nature **334** (1988) 691.

15) *"Suppression of Longitudinal Coupled-Bunch Instability by Decoupling Method"*

T.Kasuga, H.Yonehara, M.Hasumoto and T.Kinoshita

Jpn. J. Appl. Phys. **27** (1988) 1976.

16) *"Cationic Core Excitons in NaBr and* $MgBr_2$*"*

T.Matsukawa, S.Naoe, T.Murata and M.Mori

J. Phys. Soc. Jpn. **57** (1988) 2916.

17) *"Bunch Lengthening in Single-Bunch Mode of UVSOR Storage Ring"*

H.Yonehara, T.Kasuga, M.Hasumoto and T.Kinoshita

Jpn. J. Appl. Phys. **27** (1988) 2160.

18) *"Far-Infrared Absorption of Silicon Crystals"*

T.Ohba and S.Ikawa

J. Appl. Phys. **64** (1988) 4141.

19) *"Photoabsorption Spectra and Photodissociation of* $S_2Cl_2$ *in the Vacuum Ultraviolet"*

I.Tokue, A.Hiraya and K.Shobatake

Chem. Phys. Lett. **153** (1988) 346.

20) *"Fabrication and Focal Test of a Free-Standing Zone Plate in the VUV Region"*

H.Kihara, Y.Shimanuki, K.Kawasaki, Y.Watanabe, S.Ogura, H.Tsuruta and Y.Nagai

*X-Ray Microscopy II* (Springer, 1988), p.164.

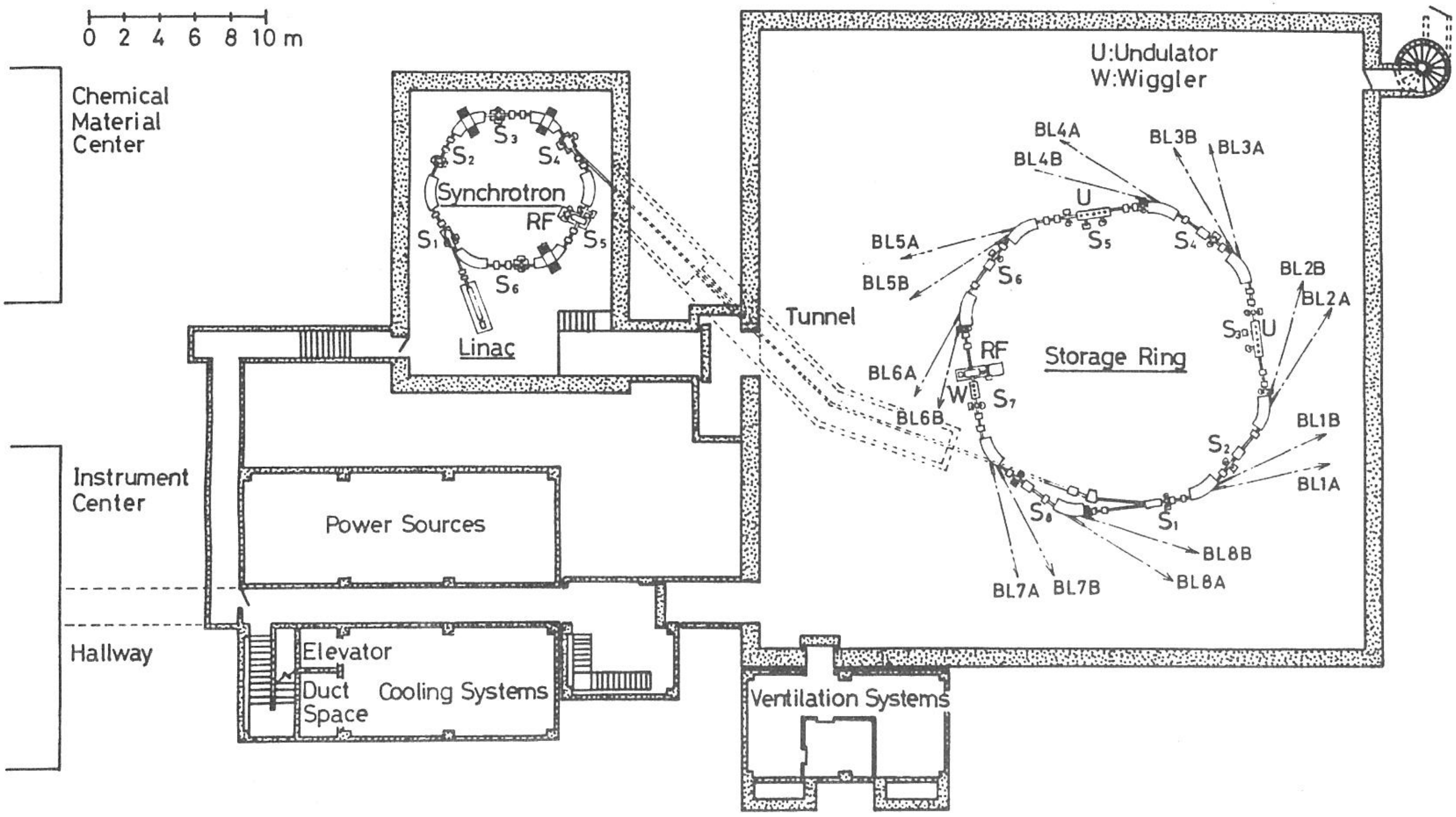

Plan view of the basement of the UVSOR Facility.

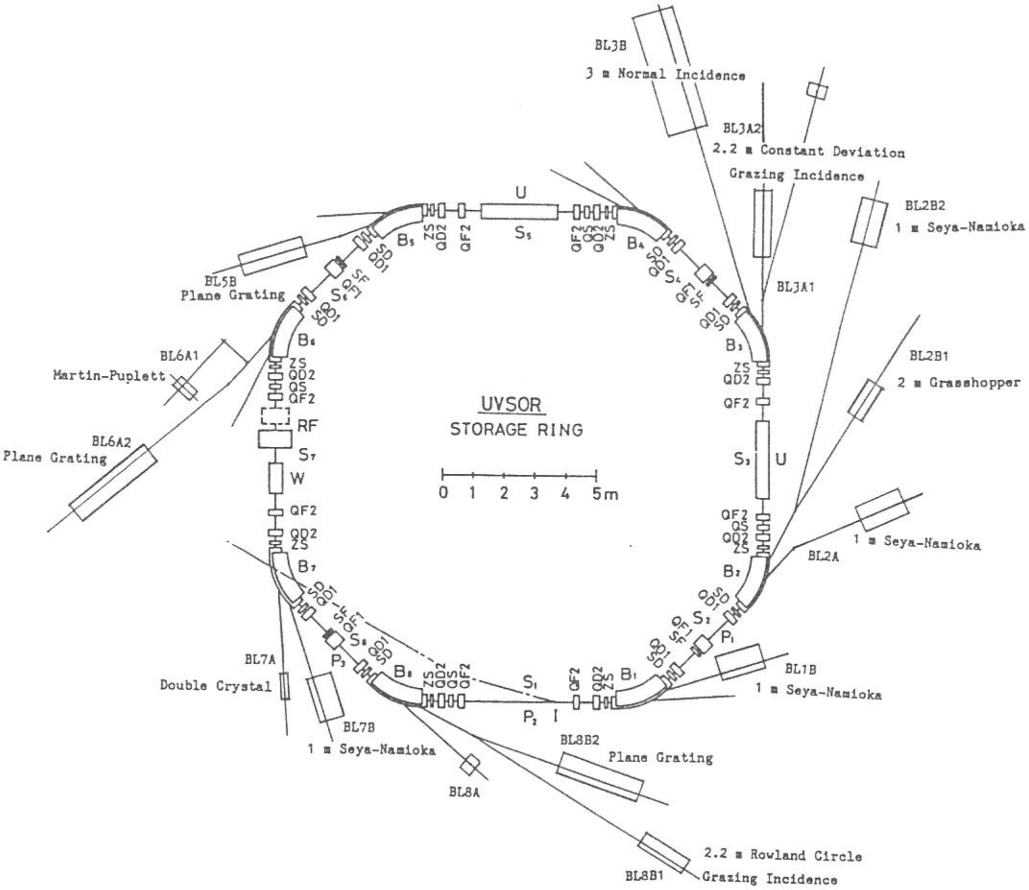

The UVSOR storage ring and the beam lines.

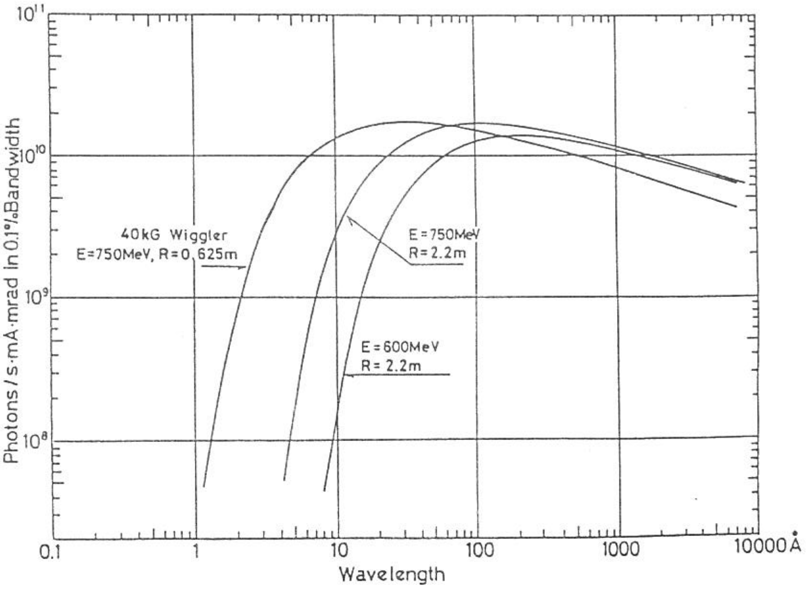

Intensity distribution of the UVSOR radiation.

## LOCATION

Ultraviolet Synchrotron Orbital Radiation (UVSOR) Facility, Institute for Molecular Science (IMS) is located at Okazaki. Okazaki (population 290,000) is 260 km southwest of Tokyo, and can be reached by train in about 3 hours from Tokyo via New Tokaido Line (Shinkansen) and Meitetsu Line.

Address is as follows.
UVSOR Facility
Institute for Molecular Science
Myodaiji, Okazaki 444, JAPAN

Telephone : 0564-54-1111 (IMS), ex. 3400-3409 (UVSOR)
Fax : 0564-54-2254 (IMS)
Telex : 4537475 KOKKEN J (IMS)

EDITORS : M. Watanabe and K. Fukui